

**MULTI OBJECTIVE CONCEPTUAL DESIGN OPTIMIZATION OF AN
AGRICULTURAL AERIAL ROBOT (AAR)**

**A THESIS SUBMITTED TO
THE GRADUATE SCHOOL OF NATURAL AND APPLIED SCIENCES
OF
MIDDLE EAST TECHNICAL UNIVERSITY**

BY

SEGAH ÖZDEMİR

**IN PARTIAL FULFILLMENT OF THE REQUIREMENTS
FOR
THE DEGREE OF MASTER OF SCIENCE
IN
AEROSPACE ENGINEERING**

SEPTEMBER 2005

Approval of the Graduate School of Natural and Applied Sciences.

Prof. Dr. Canan ÖZGEN
Director

I certify that this thesis satisfies all the requirements as a thesis for the degree of Master of Science.

Prof. Dr. Nafiz ALEMDAROĞLU
Head of the Department

This is to certify that we have read this thesis and that in our opinion it is fully adequate, in scope and quality, as a thesis for the degree of Master of Science.

Assoc. Prof. Dr. Ozan TEKİNALP
Supervisor

Examining Committee Members

Prof. Dr. İ. Sinan AKMANDOR (AEE, METU) _____

Assoc. Prof. Dr. Ozan TEKİNALP (AEE, METU) _____

Prof. Dr. Cahit ÇIRAY (AEE, METU) _____

Prof. Dr. Mehmet Şerif KAVSAOĞLU (UUBF, ITU) _____

Dr. Fatih TEZOK (TAI) _____

I hereby declare that all information in this document has been obtained and presented in accordance with academic rules and ethical conduct. I also declare that, as required by these rules and conduct, I have fully cited and referenced all material and results that are not original to this work.

Name, Last name: Segah Özdemir

Signature :

ABSTRACT

MULTI OBJECTIVE CONCEPTUAL DESIGN OPTIMIZATION OF AN AGRICULTURAL AERIAL ROBOT

Segah Özdemir
M.Sc., Department of Aerospace Engineering
Supervisor: Assoc. Prof. Dr. Ozan Tekinalp

September 2005, 182 pages

Multiple Cooling Multi Objective Simulated Annealing algorithm has been combined with a conceptual design code written by the author to carry out a multi objective design optimization of an Agricultural Aerial Robot. Both the single and the multi objective optimization problems are solved. The performance figures of merits for different aircraft configurations are compared. In this thesis the potential of optimization as a powerful design tool to the aerospace problems is demonstrated.

Keywords: Airplane Design, Aerial Agriculture, Agricultural UAV, Multi Objective Optimization, Simulated Annealing, Hide-and-Seek

ÖZ

TARIMSAL ROBOT UÇAK KAVRAMSAL TASARIMI ENİYİLEMESİ

Segah Özdemir

Yüksek Lisans, Havacılık ve Uzay ,Mühendisliği Bölümü
Tez Yöneticisi: Doç. Dr. Ozan Tekinalp

Eylül 2005, 182 sayfa

Çoklu Soğutma-Çok Amaçlı Tavlama Benzetimi Yöntemi yazar tarafından yazılan bir tasarım aracı kullanılarak Tarımsal Robot Uçak çok amaçlı eniyilemesini yapmak üzere birleştirilmiştir. Hem tek hem de çok amaçlı eniyileme problemleri çözülmüştür. Farklı uçak yapılandırmalarının performans değer katsayıları karşılaştırılmıştır. Bu tezde eniyilemenin havacılık ve uzay problemleri için güçlü bir tasarım aracı olabilme potansiyeli gösterilmiştir.

Anahtar kelimeler: Uçak Tasarımı, Havai Tarım, İnsansız Zirai ilaçlama Hava Aracı, Çok amaçlı Eniyileme, Tavlama Benzetimi Yöntemi, Sakla ve Ara.

*To my parents Hacer&Ramazan Özdemir
and my brother Emrah for their love, encouragement, prayers and
support.*

ACKNOWLEDGMENTS

A great amount of gratitude and appreciation is extended to my supervisor Assoc. Prof. Dr. Ozan Tekinalp for his great amount of knowledge, vision, understanding and friendship. I would like to express my sincere thanks to my supervisor for allowing me to work with him and for believing me. I wouldn't have achieved this if he hadn't seen me through this thesis.

The same gratitude is extended to the Department of Aerospace Engineering for training me as a good engineer.

No substantial challenge comes without sacrifice. For this reason, the greatest thanks go to my parents and my brother, Emrah, for providing me their utmost support and also for their endless love and thrust. Their role in this study is inestimable.

My special thanks go to my dear friends, İsmail Karataş, Müjde Sarı, İbrahim Sarı, Kutluk Bilge Arıkan, Dr. Serkan Güröğlü and Ali Emre Turgut for sharing their talents and experience with me.

Also, I would like to thank Mustafa Kaya and Monier El-fara for their moral support and help.

Finally thanks to Dr. Fatih Tezok and my colleagues in TAI for creating me a good environment for me to love my job.

TABLE OF CONTENTS

PLAGIARISM.....	iii
ABSTRACT.....	iv
OZ.....	v
ACKNOWLEDGMENT.....	vii
TABLE OF CONTENTS.....	viii
LIST OF TABLES.....	xii
LIST OF FIGURES.....	xv
NOMENCLATURE.....	xviii
CHAPTER	
1. INTRODUCTION.....	1
1.1. Motivation, Justification, and Purpose.....	1
1.2. Literature Survey	6
1.2.1. History of the Agricultural Aircraft	6
1.2.2. Agricultural UAV's	10
1.2.3. Aircraft Design Optimization	12
1.2.4. Optimization Methods Used in Aircraft Design.....	14
1.2.5. Multi Objective Design Optimization.....	16
1.3. Original Contributions.....	17
1.4. The Scope of the Thesis.....	18
2. AGRICULTURAL MISSION DEFINITION.....	20
2.1. Agricultural Mission, Operational Flying and Techniques.....	20

2.1.1. Take-off Surface.....	21
2.1.2. Loading	21
2.1.3. Taxing	22
2.1.4. Turns	22
2.1.5. Acceleration	24
2.1.6. Wind Direction and Force.....	25
2.1.7. Obstructions	26
2.1.8. Agricultural Patterns.....	27
2.2. Competitor Study and Characteristics of ZIU.....	29
2.3. Requirements.....	30
2.4. The Mission Profile of An Agricultural Aerial Robot.....	31
2.5. Agricultural Spraying Pattern and Flight Characteristics.....	32
2.6. Path Planning For Agricultural Aerial Robot.....	33
3. MATHEMATICAL MODELS USED IN DESIGN	
OPTIMIZATION.....	35
3.1. Overall configuration.....	35
3.1.1. Structural Concept.....	36
3.1.2. Fuselage.....	37
3.1.3. Wing Assembly.....	37
3.1.4. Booms and Tails.....	37
3.1.5. Engine Specification.....	38
3.1.6. Propeller	38
3.1.7. Fuel Storage	39
3.1.8. Hopper Tank	39
3.1.9. Landing Gear System General Description	40

3.2. The Weight Model of the Airplane – First Estimate.....	40
3.2.1. Take off Weight Buildup	40
3.2.2. Empty Weight Fraction Estimation.....	41
3.2.3. Fuel Fraction Estimation.....	42
3.3. Estimation of Critical Performance Parameters	47
3.3.1. Maximum Lift Coefficient.....	47
3.3.2. Wing Loading.....	53
3.3.3. Power to Weight Ratio.....	54
3.4. Configuration Layout -Geometrical Models	56
3.4.1. Wing Configuration Model	56
3.4.2. Fuel Tank Configuration Model.....	58
3.4.3. Horizontal Tail and Vertical Tail Configuration Model.....	60
3.4.4. Control Surfaces Model.....	63
3.4.5. Fuselage Configuration Model.....	65
3.4.4. Propeller Model.....	67
3.4.5. Landing Gear Model and The Wing Location Estimation.....	69
3.5. Agricultural Sizing Model.....	72
3.6. Better Weight Estimate Model.....	74
3.7. Center of Gravity Location Model.....	76
3.8. Aerodynamics Model	79
3.8.1. Lift Curve Slope Calculations	79
3.8.2. Estimation of C_{D0} by Component Buildup Method.....	80
3.8.3. Drag Polar.....	86
3.8.4. Ground Effect.....	87
3.9. Performance Model	88
3.9.1. Figure of Merits for Performance.....	90

4. MULTI OBJECTIVE OPTIMIZATION OF THE AGRICULTURAL AERIAL ROBOT (AAR).....	95
4.1. Problem Formulation	95
4.2. Analysis and Optimization Software.....	98
4.3. AAR Design Parameterization.....	102
4.4. The Single Objective Optimization Problems.....	106
4.5. Multi-Objective Optimization Problems	123
5. CONCLUSION.....	137
REFERENCES.....	140
APPENDICES	
A. AGRICULTURAL AIRCRAFT ZIU.....	146
A.1 Characteristics of ZIU	146
B. ADP INPUTS AND OUTPUTS.....	151
B.1 Multi objective optimization program input file	151
B.2 Pre-assigned Airfoil Variables.....	152
B.3 An example output file of ADP.....	153
C. AGRICULTURAL AIRCRAFT ZIU.....	157
C.1 Agricultural Definitions	157
D. COMPETITOR STUDY.....	158
D.1 Competitor Study	158

LIST OF TABLES

Table 3.1. The technical parameters of the power plant [37].....	39
Table 3.2. Competitor’s airfoil profiles.....	48
Table 3.3. Airfoil candidates’ properties [39].....	50
Table 4.1. Configurations considered in the design optimization studies	96
Table 4.2. Design variables upper and lower bounds together with prescribed initial values.....	103
Table 4.3. Pre-assigned design parameters and their values.....	104
Table 4.4. Pre-assigned variables of airfoils and their values.....	105
Table 4.5. Constraints.....	106
Table 4.6. Single objective optimization results for design variables using NACA 23015 with a fixed engine power of 500 Hp.....	111
Table 4.7. Single objective optimization results for objectives using NACA 23015 with a fixed engine power of 500 Hp. Various figure of merit values are also given.....	112
Table 4.8. Single objective optimization results for design variables using NACA 632615 with a fixed engine power of 500 Hp.....	113
Table 4.9. Single objective optimization results for objectives using NACA 632615 with a fixed engine power of 500 Hp. Various figure of merit values are also given.....	114
Table 4.10. Single objective optimization results for design variables using NACA 23015.....	119
Table 4.11. Single objective optimization results for objectives using NACA 23015. Various figure of merit values are also given.....	120
Table 4.12. Single objective optimization results for design variables using NACA 632615.....	121

Table 4.13. Single objective optimization results for objectives using NACA 23015. Various figure of merit values are also given.....	122
Table 4.14. Penalty coefficients.....	124
Table 4.15. Eleven different weight sets used in MC-MOSA.....	124
Table A.1. Fuselage dimensions of ZIU [37].....	146
Table A.2. Wing dimensions of ZIU [37].....	147
Table A.3. Vertical tail dimensions of ZIU [37].....	147
Table A.4. Horizontal tail dimensions of ZIU [37].....	148
Table A.5. Performance Specifications of ZIU [37].....	148
Table A.6. Engine Specifications of ZIU [37].....	149
Table A.7. Structural Weight Breakdown of ZIU [37].....	149
Table A.8. Basic Empty Weight Breakdown of ZIU [37].....	150
Table A.9. Design Weights of ZIU [37].....	150
Table B.1. initin.txt file.....	152
Table C.1. Agricultural definitions [6].....	157
Table D.1. Competitor database.....	159
Table D.2. Competitor database (continued).....	160
Table D.3. Competitor database (continued).....	161
Table D.4. Competitor database (continued).....	162
Table D.5. Competitor database (continued).....	163
Table D.6. Competitor database (continued).....	164
Table D.7. Competitor database (continued).....	165
Table D.8. Competitor database (continued).....	166
Table D.9. Competitor database (continued).....	167
Table D.10. Competitor database (continued).....	168
Table D.11. Competitor database (continued).....	169
Table D.12. Competitor database (continued).....	170
Table D.13. Competitor database (continued).....	171

Table D.14. Competitor database (continued)..... 172
Table D.15. Competitor database (continued)..... 173
Table D.16. Competitor database (continued)..... 174
Table D.17. Competitor database (continued)..... 175
Table D.18. Competitor database (continued)..... 176
Table D.19. Tabulation of agricultural aircraft, [6]..... 179
Table D.20. Tabulation of agricultural aircraft, [6]..... 180
Table D.21. Tabulation of agricultural aircraft, [6]..... 181
Table D.22. Tabulation of agricultural aircraft, [6]..... 182

LIST OF FIGURES

Figure 1.1. Aircraft design process [3].....	3
Figure 1.2. The seven intellectual pivot points for conceptual design [4].....	4
Figure 1.3. 1950s DH82 Tiger Moth [7].....	8
Figure 1.4. Cessna Ag Husky [7].....	8
Figure 1.5. Hiller 12 Helicopter fitted with spray boom [7].....	10
Figure 1.6. Registered number of Yamaha Aero Robots and application record[8]	11
Figure 1.7. Yamaha industrial – use unmanned helicopter at work [8].....	11
Figure 1.8. TAG UAV performing the role of ‘Crop Duster’ [9].....	12
Figure 2.1. The correctly coordinated turn (I.C.A.O 1968) [6].....	22
Figure 2.2. Stalling speed as a function of angle of bank (I.C.A.O 1968) [6].....	23
Figure 2.3. Faults in turns [6].....	24
Figure 2.4. Variation of wind with height [6].....	25
Figure 2.5. Level flight in a wind with a gradient [6].....	26
Figure 2.6. Descending over an obstacle [6].....	26
Figure 2.7. Climbing over an obstacle [6].....	27
Figure 2.8. Procedures for reversing the aircraft track: A, the classic procedure turn; B, the round robin procedure turn (F.A.O. 1972) [6].....	28
Figure 2.9. The classic procedure turn – correct and incorrect procedures [6].....	28
Figure 2.10. Effect of wind on procedure turn [6].....	29
Figure 2.11. ZIU at flight test [37].....	30
Figure 2.12. Mission profile of AAR	31
Figure 2.13. Schematic representation of the procedure turn	33
Figure 3.1. Conceptual Sketch of AAR	36
Figure 3.2. Maximum lift to drag ratio trends [40].....	46

Figure 3.3. Lift, moment coefficient and airfoil shape for NACA 632-615 [43]....	51
Figure 3.4. Lift, moment coefficient and airfoil shape for NACA 0012 [43].....	52
Figure 3.5. Force diagram for obtaining the load distribution among the tires [4]..	72
Figure 3.6. Sketch of AAR center of gravity locations.....	78
Figure 4.1. Flow chart of the conceptual design code and the optimization algorithm.....	101
Figure 4.2. Fronts obtained while minimizing take off gross weight and maximizing hopper volume together.....	126
Figure 4.3. Fronts obtained while minimizing take off gross weight and minimizing equivalent flat plate area together.....	127
Figure 4.4. Fronts obtained while minimizing take off gross weight and maximizing endurance together.....	128
Figure 4.5. Fronts obtained while minimizing take off gross weight and maximizing lift to drag ratio together.....	129
Figure 4.6. Fronts obtained while minimizing take off gross weight and minimizing take off distance together.....	130
Figure 4.7. Fronts obtained while minimizing take off gross weight and minimizing power required together.....	133
Figure 4.8. Fronts obtained while minimizing take off gross weight and minimizing equivalent flat plate area together.....	134
Figure 4.9. Fronts obtained while minimizing take off gross weight and maximizing endurance together.....	135
Figure 4.10. Fronts obtained while minimizing take off gross weight and maximizing lift to drag ratio together.....	136
Figure 4.11. Fronts obtained while minimizing take off gross weight and maximizing take off distance together.....	137
Figure D.1. Tabulation of agricultural aircraft, [6].....	177
Figure D.2. Tabulation of agricultural aircraft (continued), [6].....	177

Figure D.3. Tabulation of agricultural aircraft (continued), [6]..... 178
Figure D.4. Tabulation of agricultural aircraft (continued), [6]..... 178

NOMENCLATURE

a	Speed of sound, wing lift curve slope
a_t	Tail lift curve slope
AR	Aspect ratio
b	Span
c	Specific fuel consumption, Chord
c_d	Airfoil drag coefficient
$c_{d,0}$	Airfoil drag coefficient at zero angle of attack
c_l	Airfoil lift coefficient
$c_{l,0}$	Airfoil lift coefficient at zero angle of attack
c_{l_α}	Airfoil lift curve slope
c_{m_α}	Airfoil pitching moment curve slope
c_r	Root chord length
c_t	Tip chord length
\bar{c}	Mean aerodynamic chord length
C_D	Drag Coefficient
C_{D_α}	Airplane drag curve slope
$C_{D,0}$	Drag coefficient at zero angle of attack
$C_{DL\&P}$	Drag coefficient with leakages and protuberances
C_f	Flat-plate skin-friction drag coefficient
C_L	Lift coefficient
C_{L_α}	Airplane lift curve slope
d	Diameter

D	Drag, Diameter
D_{fbase}	Fuselage base diameter
e	Oswald's efficiency
E	Endurance
F	Fuselage lift factor
F_M	Total force on the two main wheels
F_N	Force on the nose wheel
g	Gravity
h	Height, Ceiling
h_f	Obstacle height
K_{vs}	Variable sweep constant
L	Lift, Length
L_t	Tail arm
\dot{m}	Mass flow rate
M	Moment, Mach number
n	Load factor
P	Pressure, power
P_{av}	Power available
q	Dynamic pressure
Q	Interference effects on the component drag
r, R_t	Radius turn
R	Range
Re	Reynolds number
R_L	Radius of landing roll
s_L	Landing distance
s_{g-L}	Landing ground roll
s_{f-L}	Landing flare distance

S	Surface area
t	Time
T	Trust
V	Velocity
V_f	Fuel volume
Vol	Volume
V_{SO}	Staling speed at which the airplane is controllable
w	Width
W	Weight
W_0	Take off gross weight
W_{dg}	Design gross weight
W_e	Empty weight
W_f	Fuel weight
x_{acmb}	Aerodynamic center of wing body
x_n	Natural point
\bar{x}	Mean aerodynamic chord x location
\dot{X}	Turning rate
\bar{y}	Mean aerodynamic chord y location
\bar{z}	Mean aerodynamic chord z location

GREEK SYMBOLS

θ	Pitch angle
ρ	Density
η	Efficiency
α	Angle of attack
α_0	Airfoil lift coefficient at zero angle of attack

Δ	Change
μ_γ	Friction coefficient
λ	Taper ratio
Λ	Chord sweep angle
τ	Ratio of tip and root thickness ratios
Γ	Dihedral angle
$\eta_{\substack{\text{fuel tank} \\ \text{end point}}}$	Percentage location of fuel tank
β	Prandtl Glauert
Λ_m	Sweep angle at maximum thickness location
σ	Density ratio
η_p	Propeller efficiency
γ	Steep climb
$\dot{\psi}$	Rate of turn

SUBSCRIPTS

0	Sea level
<i>a c</i>	Aerodynamic center
<i>A</i>	Aft
<i>c</i>	Chord
<i>c.g.</i>	Center of gravity
<i>eng</i>	Engine
<i>exp</i>	Exposed
<i>f, fw, FUS</i>	Fuselage
<i>HT, ht</i>	Horizontal tail
<i>L</i>	Landing
<i>LE</i>	Leading edge

<i>LG</i>	Landing gear
max	Maximum
min	Minimum
<i>misc</i>	Miscellaneous
<i>M</i>	Mid - body
<i>net</i>	Net
<i>N</i>	Nose
<i>plf</i>	Planform
Pr	Propeller
<i>r</i>	Root
<i>ref</i>	Reference
<i>side</i>	Side projected
<i>t</i>	Thickness
<i>TO</i>	Take off
<i>VT, vt</i>	Vertical tail
<i>w</i>	Wing
<i>wb</i>	Wing body
<i>wet</i>	Wetted
∞	Free stream

ACRONYMS

AAR	Agricultural Aerial Robot
FF	Form Factor
FOM	Figure of Merit
FR	Flow Rate
HV	High Volume
MV	Medium Volume
ROC	Rate of Climb

SFC	Specific Fuel Consumption
TOG	Take off ground roll
UAV	Unmanned Air Vehicle
ULV	Ultra Low Volume

CHAPTER I

INTRODUCTION

1.0. Motivation, justification and purpose:

Turkey's agricultural industry hasn't added new aircrafts into its fleet and hasn't received any support from the government for years. The private investors also have not shown any interest to agricultural aviation as well. Old agricultural aircrafts and rather archaic maintenance approaches that do not comply with the standards, cause many accidents every year. Turkey's application area is about 52 million hectare but it is expected to become twice this value when GAP (South East Anatolian Irrigation Project) becomes active. Meanwhile, Turkey's aerial agricultural problems should also be addressed. Otherwise insufficient and aging agricultural fleet may lead to very big losses. In industrialized countries 80% of spraying is performed from air. There are approximately 30000 agricultural aircrafts in the world. Considering these numbers, it is obvious that the Turkish agricultural aviation should be developed [1]. Currently, there are 117 agricultural aircrafts operated by 38 companies in Turkey [2].

Conventionally, the agricultural aviation is based on piloted aircraft. However, agricultural missions are quite dangerous, and require substantial piloting activities. In addition, ground markers are also exposed to great danger, since the aircrafts fly very close to ground with speeds close to stall speed. This essentially may cause aircraft stalling especially during turns. Accidents due to collisions with obstructions such as

electric wires, trees, and sometimes fences occur. For example, from 1994 to 1999 there have been 815 accidents in the United States alone [2]. In these accidents, 77 people have lost their lives.

With the help of today's very accurate navigational aids (Global Positioning System (GPS); Differential Global Positioning System (DGPS), GPS aided Integrated Navigation System (INS), etc.) and automatic flight control systems, it is possible to autonomously carry out agricultural activities. The vehicle flight director may be programmed in advance, and the vehicle will, for example, carry out spraying activities autonomously. The programming may be carried out similar to robotic manipulators. For this purpose, a GPS equipped markers may be manually moved around the field to identify waypoints. The field identification may also be carried out by remotely flying the UAV around the field as well.

Thus, there is not only a need to carry out agricultural aviation tasks without jeopardizing the lives of the human pilots, the current technology is mature enough to realize and operate an autonomously flying agricultural aerial vehicle. In addition, autonomous agricultural vehicles shall also be cheaper to operate. Thus, Turkish agriculture may benefit from autonomous, and/or remotely piloted agricultural aerial vehicles.

The aircraft design process is often divided into several stages, as shown in the Figure 1.1, [3]. It starts from market research, followed by concept development and conceptual design, preliminary design, detailed design, and product support. The conceptual design phase is one of the most important parts of the design process. Many questions regarding what parameters will be used come to mind when describing the design. Will it have a conventional tail or a tail boom? Will it be a twin engine or a single engine airplane? Aircraft conceptual design is the process of determining an aircraft configuration that satisfies a set of mission requirements in which not only the

overall shape, size, weight, and performance of the new design but also the fundamental aspects as the shape of the wings, the location of the wings relative to fuselage, the shape and location of the horizontal and vertical tail, engine size and placements are determined. The major drivers during the conceptual design process are aerodynamics, propulsion, and flight performance [4].

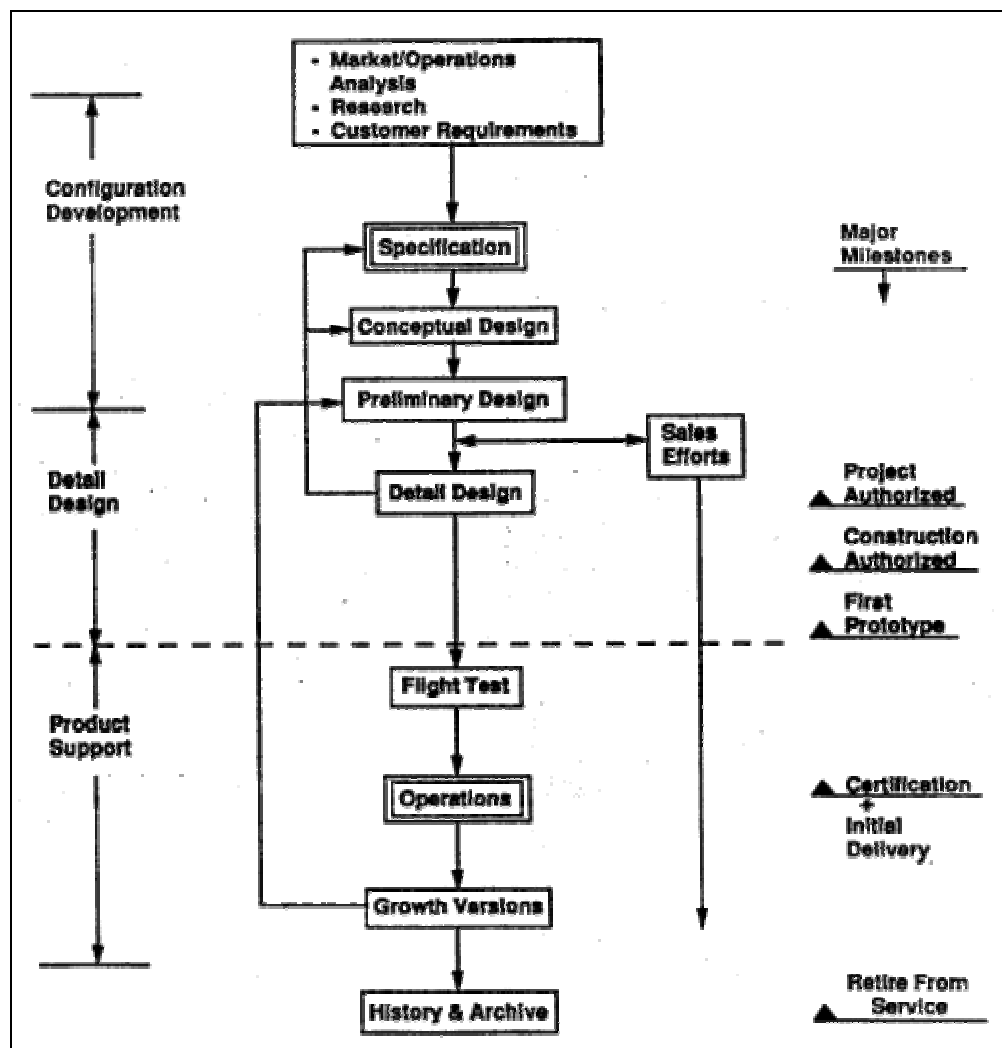


Figure 1.1. Aircraft design process [3]

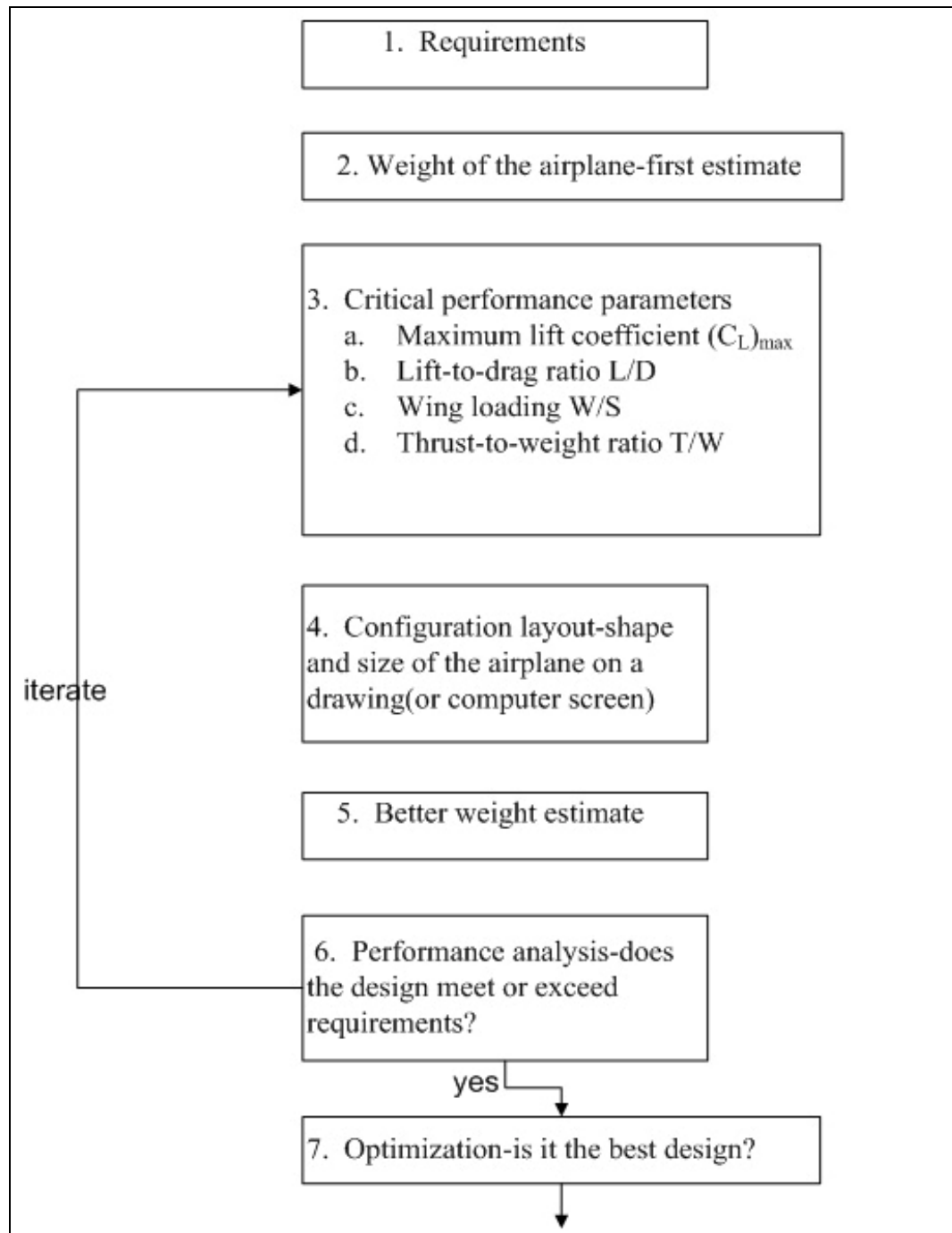


Figure 1.2. The seven intellectual pivot points for conceptual design [4]

The overall conceptual design process is shown in Figure 1.2, [4]. This flow chart describes the usual approach in the manual, conventional design of aircrafts. The approach may be automated using optimization algorithms. Such algorithms require models from various disciplines such as, aerodynamics, propulsion, structures, flight mechanics, etc. In this case, the approach is called multidisciplinary design optimization. A performance function, usually called the cost function is minimized, while various constraints on optimization variables are satisfied. However, as it may be observed from the figure, most design involves trading multiple performance metrics or objectives. Thus, any design automation shall not only be multidisciplinary, it shall also be a multi objective one. For this reason, the study presented here addresses the multidisciplinary and multi objective design of an AAR. In this way it is expected that the resulting design would be optimal to perform agricultural aviation activities in a much more efficient and effective fashion. It is envisaged that aerial robots will carry out many aviation tasks much better than their piloted counterparts in the future, and will be used for different tasks, which are difficult as well as dangerous to carry out, by human pilots (i.e. fire fighting, operating in contaminated zones, delivering emergency supplies to remote areas, etc.).

In this thesis optimization of the design of an Agricultural Aerial Robot (AAR) is presented. The study employs various models to conduct multidisciplinary design optimization. Since any design requires trading multiple objectives, this design optimization study addresses multi objective optimization approach. For this purpose a recently developed algorithm Multiple Cooling Multi Objective Simulated Annealing Algorithm is used [5]. However, technologies behind autonomous flight are not addressed.

2.0. Literature Survey

1.0.0. History of the Agricultural Aircraft

Agricultural aviation is a branch of commercial aviation, which performs the essential task in production, and protection of the world's food and fiber crops. Aerial application is also used in areas such as insect control, fighting forest fires, and protection of biological resources [6].

There have been some significant changes in Agricultural Aviation Industry in the last 20 years. Aircrafts are getting bigger, while turbine power is becoming available for fixed wing aircraft. Many more helicopters are being used. The techniques of aerial applications are becoming refined [7].

Before mid-1920s, a number of individuals began to experiment with uses of flight technology that would later become important parts of general aviation. For example, the first uses of airplanes for crop treatment, aerial surveying, and corporate flying all dated before the mid-1920s. Alfred Zimmermann, a German forester in Detershagen, was the first to identify the 'Agricultural aviation' as a means of combating crop pests. He described the use of aircraft in the application of pesticide (in this case lime-water) in the control of the nun moth (black arc moth) in the European forests in his patent letter, dated 29 March 1911. Although his approach was visionary, suitable aircraft and trained pilots who were able to perform this task were only available after the World War I. In many countries, experiments were conducted in the 1920s, and practical results were recorded by Neillie and Houser (August 1921) in the U.S.A., and Professor V. F. Boldyrev (July 1922) in the U.S.S.R [6].

Ag-1 was the first specially designed aircraft to distribute agricultural chemicals developed in 1949-50 at the Texas A.&M. Aircraft Research Centre. The project was initiated by the National Flying Farmers Association, and was carried out under the sponsorship of the Civil Aeronautics Administration, the U.S. Department of Agriculture and the Texas A.&M. College System. Ag-2 and Ag-3 are other experimental aircrafts followed Ag-1. These aircrafts incorporated pilot safety characteristics with regard to field of view and structural arrangements for protection of the pilot in crashes. Thanks to these experimental aircraft, the foundations of design philosophy for nearly all subsequent specialist aircraft were laid. The Piper Aircraft Corporation assisted in the experimental Ag-3 aircraft. This corporation was the first major aircraft manufacturer to produce a specialist aircraft – The Piper PA-25 Pawnee [6].

There are four main groups of aircraft used throughout the world at the present time [6]:

Group 1: Ex-military aircraft e.g. Boeing Stearman, Grumman Avenger (TBM).

Group 2: Ex-civil aircraft, e.g. Douglas DC-6, Antonov AN-2M, DHC Beaver, Pilatus Turbo Porter, Piper Aztec.

Group 3: Specialist agricultural aircraft, i.e. piper Pawnee, Ayres Thrush, Schweizer Ag-Cat, Cessna Ag-Truck, Embraer Ipanema, Cmelak Z-37, Transavia Skyfarmer T-300, etc. (see Appendix D)

Group 4: Helicopters

Over a period of 50 years, the agricultural aircraft have shown dramatic improvement in performance and safety. DH 82 Tiger Moths was one of the first aircrafts used for dusting, spraying and spreading. It was designed as two-seater trainers. Modifications to them were many but basically involved removing the front cockpit and

replacing it with a hopper. The Tiger Moth was powered by a 130hp engine and had a payload of 33 gallons of spray or 330 lb. of super-phosphate [7].



Figure 1.3. 1950s DH82 Tiger Moth [7]



Figure 1.4. Cessna Ag Husky [7]

In 1960s, the DH82 Tiger Moths were replaced by such aircraft as CA28 Ceres and Transavia PL12 Airtruck, Cessna 188, Piper PA 25 Pawnee, DHC-2 Beaver, G-164 Ag Cat, and the Snow Commander S-2D, to name the most numerous [7].

By the mid 1970s, the Cessna 188 Ag Wagon (230hp), Ag Truck (300hp) or Ag Husky (310hp), became the leading models followed by the Piper PA 25 Pawnee

(235hp) and PA 36 Pawnee Brave (285 & 300hp). The DHC-2 Beaver (450hp) and PAC Fletcher FU 24 dominated the fertiliser spreading business [7].

The hopper size varied from 750L on the Ag Wagon to 1000L on the Ag Husky and from 550L on the PA-25 to 850L on the PA36. In the design of these aircrafts greater attention is paid to pilot safety. The FU24 has a dry solids capacity of just over 1000 kg [7].

The US manufactured Air Tractor and Ayres Thrush models were introduced next. The Air Tractor AT301/2, 401/2, 501/s and 802 model numbering system followed the hopper size in US gallons. The first turbine-engined model was the 400, powered by a Pratt and Whitney Canada PT6A-15 Ag engine with a reversible pitch propeller. A P&WC PT 6A-35 Ag turboprop engine of 750hp powers the AT-502 introduced in the late 1980s. The Ayres Thrush models are descended from the Rockwell Thrush Commander and consist of the Thrush S2R-600 (1340) powered by a P & WR-1340 radial engine; the Bull Thrush S2R-1820 and the Turbo Thrush S2R with options of a P&WC PT 6A-15, -34 and-65 turboprop engines or Garrett TPE 331-10 [7].

The Dromader (Melex M-18) is another aircraft, which is manufactured in Poland by PZL-Miele. Another agricultural aircraft is the GA-200 "Fatman" produced by Gippsland Aeronautics at Morwell, Victoria[7].

There are also several models of helicopters, used for spraying, spreading and stock mustering including the Bell 47 and 206, Hiller 12 E, Hughes 269 and Robinson R-22 [7].



Figure 1.5. Hiller 12 Helicopter fitted with spray boom [7]

2.0.0. Agricultural UAV's

The phrase “Unmanned Aerospace Vehicle (UAV)” is a universally recognized term that includes a wide spectrum of aircraft that are autonomous, semiautonomous, or remotely operated.

In Japan, due to the departure of younger generation from the farming communities, around 10 years ago, Yamaha company started to develop the unmanned helicopters to compensate for the shortage of land workers. These helicopters are intended to be more flexible and precise during spraying. Today, Yamaha helicopters shown in Figure 1.7 have extended its applications area to include the insect pest control of rice paddies, soybeans, and wheat. Yamaha unmanned industrial helicopters is anticipated as a solution for various problems facing the farming communities in Japan and as a contributor to raising the level of food self-sufficiency. The area of applications and the increase in the demand for Yamaha unmanned helicopters are shown in Figure 1.6 [8].

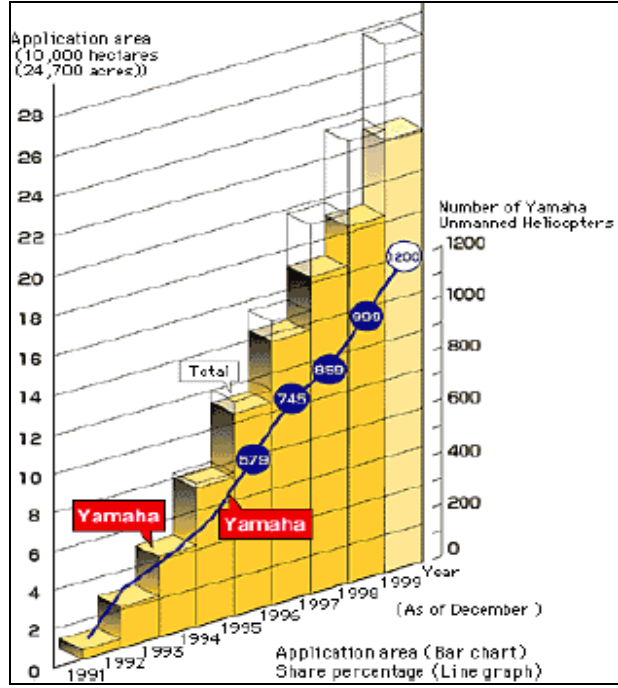


Figure 1.6. Registered number of Yamaha Aero Robots and application record [8]



Figure 1.7. Yamaha industrial – use unmanned helicopter at work [8]

Another UAV designer is a company in USA called Tactical Aerospace Group (TAG). TAG designs and manufactures VTOL Unmanned Aerial Vehicles offering four

UAV aircraft product lines, each designated for a specific market segment or application. TAG UAVs can take on the role of ‘Crop Duster’ when fitted with tanks of liquid pesticide and programmed to dispense the chemicals in a precise pattern over cropland. The payload capacity is in excess of 40 lbs and it has also a GPS-based flight navigation system, [9].



Figure 1.8. TAG UAV performing the role of ‘Crop Duster’ [9]

3.0.0. Aircraft Design Optimization

Many studies have been carried out on aircraft design optimization. For example Sobieski and Chopra studied the application of optimization methodology to aeronautical systems. They concluded that optimization as a tool in aircraft design is rapidly getting ready, in a synergistic symbiosis with the computer technology in order to support the next grand challenges of aircraft industry [10].

MacMillin et. al. optimized the design of a high speed civil transport for minimum take off gross weight, including both aerodynamics and structures to find the wing planform and thickness distribution, fuselage shape, engine placement and thrust, using 29 design variables and 70 constraints to insure realistic results. The constraints include the engine-out and crosswind landing requirements, as well as engine nacelle ground strike, rotation to lift-off attitude; balanced field length and approach trim constraints. They presented results of the MDO design procedure illustrating the effects of numerous trim, control, and performance requirements [11].

A methodology which would enable aircraft multidisciplinary design optimization using analysis methods of varying computational expense, in a manner which leverages the power of parallel computing was developed by Giunta [12]. The variable-complexity response surface modeling (VCRSM) method was used for this purpose. The variable-complexity portion of the method incorporates increasingly sophisticated computational models in successive stages of the design process. The basic format of the VCRSM method was refined through a series of High Speed Civil Transport (HSCT) optimization problems of increasingly complexity. The five and ten variable MDO problems retaining sufficient complexity to preserve the multidisciplinary aspects of aircraft design were handled. This study also puts forward the idea that the VCRSM method functions in a manner similar to the aircraft design methodology used in the aerospace industry where the design process is comprised of stages in which more accurate, and more computationally expensive, analysis techniques employed as an aircraft design is refined [12].

A technique that converts a constrained optimization problem to unconstrained one where conflicting figures of merit were simultaneously considered was combined with a complex mission analysis system by Dovi and Wrenn. They investigated the use of multi objective optimization methods for conceptual aircraft design where conflicting figures of merit considered simultaneously. Three multi objective methods namely the envelope

function formulation, KSOPT, the global criterion formulation and the utility function formulation using a penalty function method, were combined with a complex mission analysis system. The results were compared existing single objective optimization methods. A wide-body transport aircraft is used for this study [13].

Cabral and Paglione developed an optimization tool for the conceptual design of families of aircraft. The resulting tool was based on multi objective design optimization theory and genetic algorithms techniques where a total of 23 parameters were optimized [14].

Giunta et. al. found out that the multi disciplinary optimization of aircraft systems is computationally challenging and that it was impractical to link high fidelity codes representing each discipline directly to an optimizer to perform optimization. They established high speed civil transport design model problem as a testbed for multi disciplinary optimization. They showed that variable-complexity modeling could be effective in reducing the computational time of this type of optimization problems [15].

4.0.0. Optimization Methods Used in Aircraft Design

The optimization algorithm selected is also very important in the success of the design. There are many optimization algorithms available. Those algorithms that use gradient information require function derivatives usually converge to local optimum [16]. The stochastic algorithms such as Genetic Algorithms and Simulated Annealing have been most successful [16]. They do not require function derivatives, and they may converge to global optimum. In this thesis simulated annealing method is employed.

The Simulated Annealing (SA) exploits an analogy between the way in which a metal cools and freezes into a minimum energy crystalline structure (the annealing process) and the search for a minimum in a more general system. [17]. The algorithm uses Metropolis criteria [18], which was originally proposed as a means of finding the

equilibrium configuration of a collection of atoms at a given temperature. Pincus was first to identify the connection between this algorithm and mathematical minimization [19]. However, it was Kirkpatrick et al. [20] who proposed that it form the basis of an optimization technique for combinatorial optimization problems.

In the early 1980's Kirkpatrick introduced the method of simulated annealing (1983), based on ideas formulated in the early 1950's (Metropolis et al., 1953). Bélisle et al. has developed a simulated annealing (SA) algorithm for continuous optimization, called Hide and Seek [21]. The Hide and Seek algorithm has been used by many researchers. For instance, Lu and Khan employed the algorithm to solve the non-smooth trajectory optimization for a high performance, rigid-body aircraft [22]. Utalay and Tekinalp used further Hide and Seek to find the maximum range, as well as specified range minimum flight time trajectories of an air to surface missile. The specified range minimum weight missile configurations were found by optimizing both the control parameters as well as engine design parameters such as thrust and burnout time [23, 24]. Bingöl and Tekinalp, proposed improvements to the basic Hide and Seek algorithm. They have shown that using a better estimator, and treating the equality constraints properly speeds up the convergence of the algorithm. They also used the algorithm to optimize both the design and control variables for multidisciplinary design optimization of a missile [16, 25], and proposed various improvements to the formulation of the problem.

5.0.0. Multi Objective Design Optimization

Most realistic optimization problems, particularly those in design, require the simultaneous optimization of more than one objective function. Aircraft design is a multi-criteria and multi-objective optimization problem involving multiple disciplines. It requires simultaneous optimization of fuel efficiency, payload, and weight. The output of the multi objective design optimization is not a single optimum but it is a hyper-

surface containing optimum points usually occurring at the boundaries of the feasible regions.

There are several optimization algorithms for the multi-objective optimization; the most widely used ones are Heuristic optimization algorithms, especially “Evolutionary Algorithms” (EA) and “Simulated Annealing” (SA). The “Evolutionary Algorithm” based multi-objective methods have been extensively developed; whereas, multi objective methods based on (SA) have very few applications in the literature.

Although Hide and Seek Simulated Annealing is a continuous, robust and fast converging optimization technique with adaptive cooling schedule, it has enjoyed only few applications. Furthermore, there are only few Simulated Annealing based multi-objective algorithms, in the literature. Consequently, there is a need to develop SA based continuous multi-objective optimization algorithms.

Simulated Annealing has recently been adapted for the multi-objective framework by Ulungu and Teghem [26, 27], Tuytens et al. [28] and Serafini [29]. This method is called as UMOSA (Ulungu Multi-Objective Simulated Annealing). The idea used in UMOSA algorithm is to project the multidimensional objective space into a mono-dimensional space using the weighted-sum-scalarizing technique. Different scalarizing functions lead to different projection paradigms [30]. UMOSA has been further improved and tested by Ulungu et al. [31] on the knapsack problem.

Recently, Czyzak et al. [32, 33] (PSA, Pareto Simulated Annealing), and Suppapitnarm et al. [34] (SMOSA, Suppapitnarm multi objective simulated annealing) proposed different simulated annealing based approaches to tackle multi-objective optimization problems. PSA uses a population of interacting solutions, at each iteration. The solutions are called generating solutions. Another idea used in PSA is to control the objective weights used in the multi-objective rules for acceptance probability in order to

assure dispersion of the generating solutions over the whole set of efficient solutions [32]. Other algorithms are Pareto Domination based Multi-Objective Simulated Annealing [35] and Weight based Multi-Objective Simulated Annealing [35]. Kubotani and Yoshimura worked on the acceptance probability functions for multi-objective simulated annealing methods [36].

A new algorithm called Multiple Cooling Multi Objective Simulated Annealing algorithm has recently been developed by O. Tekinalp and G. Karşlı [531]. The algorithm is based on an unconstrained simulated annealing algorithm, Hide-and-Seek. The success of the algorithm in finding the Pareto front for constrained, highly nonlinear problems have been demonstrated. [5].

3.0. Original Contributions

The general specifications of the original Agricultural Aerial Robot concept presented in this thesis are listed below:

1. AAR is to fly autonomously, and carry out the preplanned tasks. For example the way points to be flown over during the spraying of the field will be loaded to the aircraft in advance.
2. If needed AAR shall be flown by remote piloting from a transportable ground control station.
3. The aircraft may takeoff from an unprepared field and also shall be capable of landing to such a field just like an agricultural aircraft. The takeoff and landing may also be carried out autonomously. However, it is not a fundamental requirement.

4. The aircraft shall be small enough for easy transportation by a truck. For this purpose, the wings for example shall be easily assembled and disassembled.

For design optimization the recently developed multi objective simulated annealing algorithm, MC-MOSA, is used. Specifically:

1. A FORTRAN code is written which includes mathematical models for performance, aerodynamics, structural, and propulsion suitable for multidisciplinary design optimization.
2. A study is conducted to find the best configurations for a various performance requirements.
3. Multi objective optimization is carried and Pareto fronts are obtained. The results obtained are evaluated and discussed. It is shown that multi objective optimization results convey much more information to the designer to make proper choices in arriving a suitable design.

4.0. The Scope of the Thesis

An introduction, including the literature survey, agricultural aerial applications, and aircraft design optimization methods, has been presented in this chapter. The remainder of this thesis is organized as follows:

- In Chapter 2, mission requirements and mission profile for an AAR are described.
- In Chapter 3, mathematical models used in the conceptual design of AAR are given.

- In Chapter 4, single and multi objective AAR design problems are solved. Objectives such as minimum takeoff gross weight W_0 , maximum endurance E , minimum equivalent flat plate area $S \cdot C_{D0}$, minimum takeoff gross weight W_0 , - maximum hopper Vol_{hopper} , optimization, minimum takeoff gross weight W_0 –minimum power required P_{req} are employed. The results obtained are presented and discussed.
- In Chapter 5, conclusions are given and suggestions for further research are described.
- In Appendix A, characteristics of ZIU are given. Example inputs and outputs of Aircraft Design Program (ADP) are shown in Appendix B. Agricultural Definitions are given in Appendix C. And finally, competitor study is given in Appendix D.

CHAPTER II

AGRICULTURAL MISSION DEFINITION

2.1. Agricultural Mission, Operational Flying and Techniques

Agricultural flying differs in many aspects from other commercial flights. First of all it is generally executed at a very low altitude for the greater part of the flight, allowing very little room for error. In case of a manned aircraft the pilot has to fly with constant and intense attention during operational flight. Another influence of this low altitude flight is the effect of wind and turbulence. The change of wind speed with height is much more noticeable near to the ground. This gradient of wind has an effect on airplane performance directly. For example, the amount of aileron required in a turn is more critical than it has in a commercial flight. The second aspect of agricultural aviation is the highly variable loading conditions. The weight and the center of gravity can vary considerably in a very short time. This brings a need for frequent re-trimming in order to keep control forces constant [6].

The technique for take-off and landing on a short field is also different than it is in commercial flights. Both the ambient temperature and the elevation of the field have effects on performance.

As to be described below, properly programming the guidance computer and designing autopilot algorithms with proper flight functions may easily alleviate the operational problems identified above.

2.1.1. Take-off Surface

Agricultural aircraft is usually based at a temporary airstrip. And it is not as good as a well-equipped air base. Usually a field length equal to the three times the length of the take-off run will be adequate. The nature of the surface is important because if it is a peat surface the rolling resistance of the wheels cause the take-off run to increase. Another important factor is the gradient of the take-off surface. A windsock should be placed in a suitable position. Depending on the information obtained by the help of a windsock, like the wind direction and the force the adverse combinations, such as tailwind and uphill gradient can be avoided [6].

The AAR takeoff may be conducted by remote piloting or automatically. In any case, similar difficulties exist as piloted agricultural aircrafts.

2.1.2. Loading

For agricultural aviation the amount of the load and its position are important in loading. A heavily loaded aircraft requires a larger take-off run. The rolling resistance of the wheels is increased and the flying speed is higher in this case. When heavily loaded, the aircraft has little performance margin. So it is better to spray small fields after a great part of the load has been applied [6].

In AAR design hopper is located just behind the engine. Since the fuselage furnishes only the engine and the hopper and a small room for avionic equipments, the center of gravity is not expected to vary gradually as spraying progresses. This is good from stability point of view.

2.1.3. Taxiing

Taxiing over loose stony surfaces must be avoided. Flying stones may cause damage to the propeller. Turns on the ground should be made slowly. Turn radius should be large and the r.p.m. should be the lowest possible. Taxiing should be done over a route which is well known and at a speed adapted to terrain roughness [6].

These warnings are also applicable to AAR.

2.1.4. Turns

Turns will be executed after the aircraft has pulled away from the ground. This way there will be more room for maneuvering. The airspeed should not drop too much during pull-up maneuver. Because the lift demanded from the wings and also the stalling speed will be increased in the following turn, in order to counteract the centrifugal force. The coordinated turn will always enable the airplane to have its maximum performance. In a coordinated turn, the lift force is inclined from the vertical towards the center of the turn (Figure 2.1).

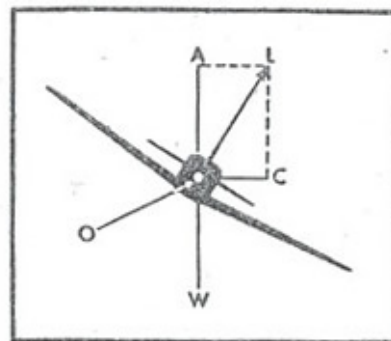


Figure 2.1. The correctly coordinated turn (I.C.A.O 1968) [6]

As the bank is increased, the total lift produced by the wings should be increased to balance the weight of the aircraft. The important characteristic of turning flight is that the stalling speed increases in a turn as the square root of the load factor, This is illustrated in Figure 2.2.

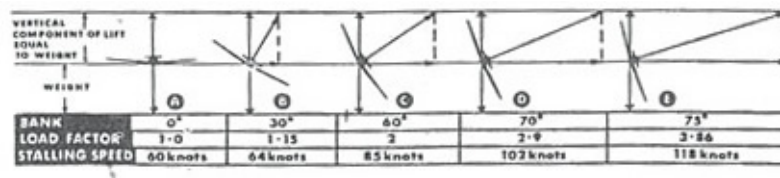


Figure 2.2. Stalling speed as a function of angle of bank (I.C.A.O 1968) [6]

The important point is that an aircraft in a turning flight at low speed can tolerate very small bank angle before stall occurs.

There are three ways of to perform a turn. The coordinated turn is the best. In this flight condition the rudder and aileron are so coordinated as to keep slip indicator in its central position. The skidding turn results from too much rudder into the turn and/ or too much counter aileron during the steady turn. The slip indicator is deflected outside turn (toward the high wing). In this case the low wing will stall first because of the position of the aileron. And the airplane will spin under. A slipping turn results from too much aileron and/or too much top rudder. The slip indicator is deflected inside turn (towards the low wing). The high wing will stall first causing spin over the top (Figure 2.3).

The AAR will be automatically and autonomously piloted. Thus, in the programming phase of the guidance computer the above warnings shall be taken into account. It is quite straightforward to include a coordinated turn function to the autopilot computer. Thus, AAR will always fly with turn coordination, and proper precautions shall be taken in the algorithm to avoid stall during a coordinated turn. Note that to

achieve full autonomy; the AAR autopilot will also include an auto throttle function as well.

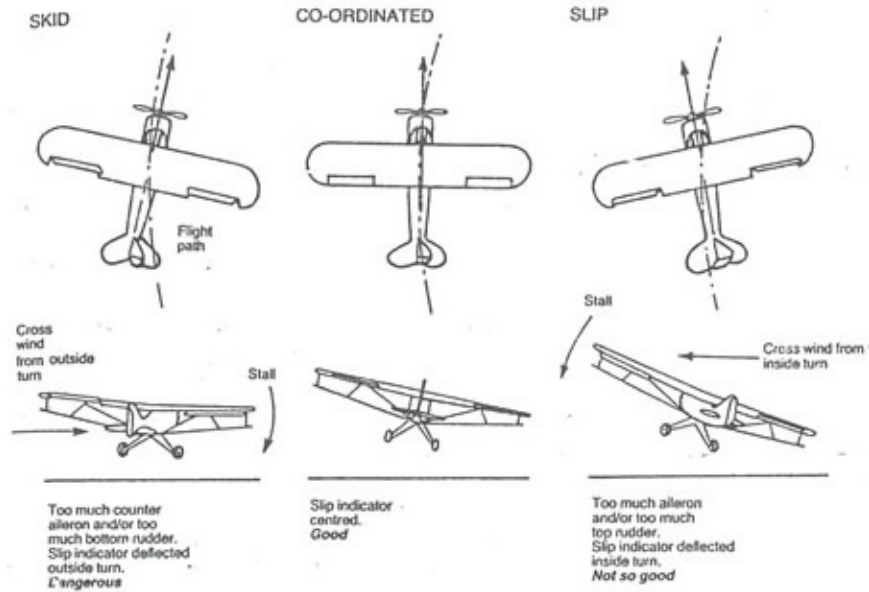


Figure 2.3. Faults in turns [6]

2.1.5. Acceleration

It is undesirable to pull more g-force than necessary in the end-of-swath turn. A higher rate will help the aircraft to come to the next run a few seconds earlier. But its penalty is increased fatigue. The effect of fatigue produced by the g-forces is recognized in military aviation especially in low-level operations. So the wider turns with lower turn rates should be applied in agricultural applications [6].

The flight of AAR will normally be optimized to reduce excessive loads, to reduce fuel consumption, and to realize a more uniform spraying.

2.1.6. Wind Direction and Force

The wind causes aircraft to drift in rectilinear level flight. It is more difficult to take-off and land with a cross-wind. It is better to fly at right angles to the wind direction while spraying. Also it is preferable to work upwind for every spray pass. This way the aircraft will not be flying through the spray. But the main factor that specifies the spraying method is the shape of the field [6].

The wind speed changes with altitude as shown in Figure 2.4. The effect of wind gradient is perceivable at altitudes below 50ft. In the case of a turn at very low height from the ground, the wind gradient will affect this flight.

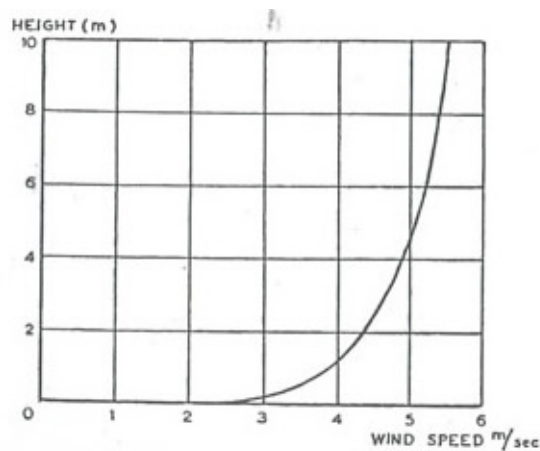


Figure 2.4. Variation of wind with height [6]

As it is shown in Figure 2.5 when flying into the wind the aircraft will deviate from altitude in other words it will be unstable with regard to flying altitude whereas when flying horizontally with the wind aircraft will maintain altitude.

The above difficulties may be eliminated for an AAR with a properly planned flight course. The autopilot will normally alleviate instability problems during such a flight as well.

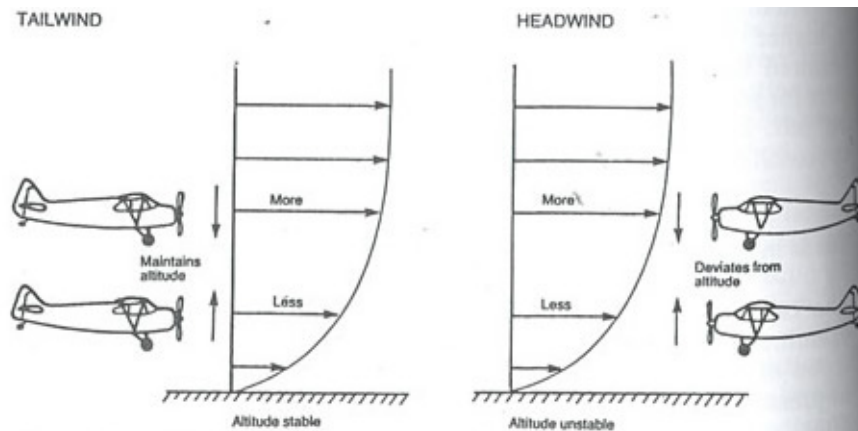


Figure 2.5. Level flight in a wind with a gradient [6]

2.1.7. Obstructions

Obstructions can generally be seen easily except wires, dead trees and dead branches of an otherwise green tree. A tree stump and a pole exactly line up along the flight path are possible obstructions [6].

Due to the characteristics of agricultural flying most of the time is passed at a height of less than 15 ft. This means that tress, wires and all other possible obstacles are encountered regularly. These should be negotiated safely. The correct operating altitude must be reached quickly and held as long as possible. The airspeed should be kept constant in order to avoid uneven distribution of the spray [6].

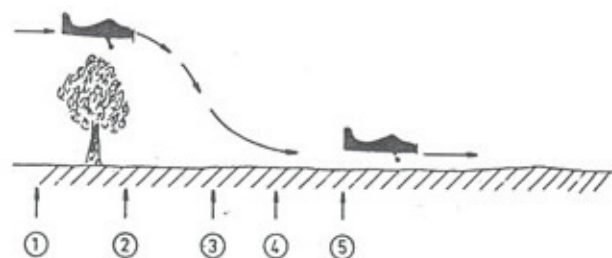


Figure 2.6. Descending over an obstacle [6]

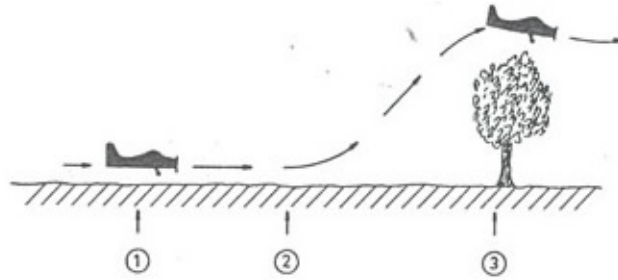


Figure 2.7. Climbing over an obstacle [6]

The field will be surveyed in advance to properly plan the flight trajectory of the AAR.

2.1.8. Agricultural Patterns

The agricultural flight is a low level one and the most critical part of this flight is the procedure turn-around at the end of the swath-run. There are two types of turn. The first one is the classical turn shown in Figure 2.8. The second one is the round robin procedure turn also sketched in the same figure. For the second method more than two human markers or electronic tracking guidance are needed in case of a manned flight.

Figure 2.9 shows how to perform a classical turn. From point a to point b the initial pull-up is made wing level. This way the possibility of striking an obstacle and/or the ground is avoided. The climb is maintained from b to c while the aircraft turns through approximately 45°. At point c coordinated turn is performed in the opposite direction. The aircraft rolls out of the turn at point d. From this point on a straight descent is made to start the next run [6].

AAR will normally use the procedural turns, the first method. It is possible to program the guidance computer of AAR to follow the both flight patterns given in Figure 2.8.

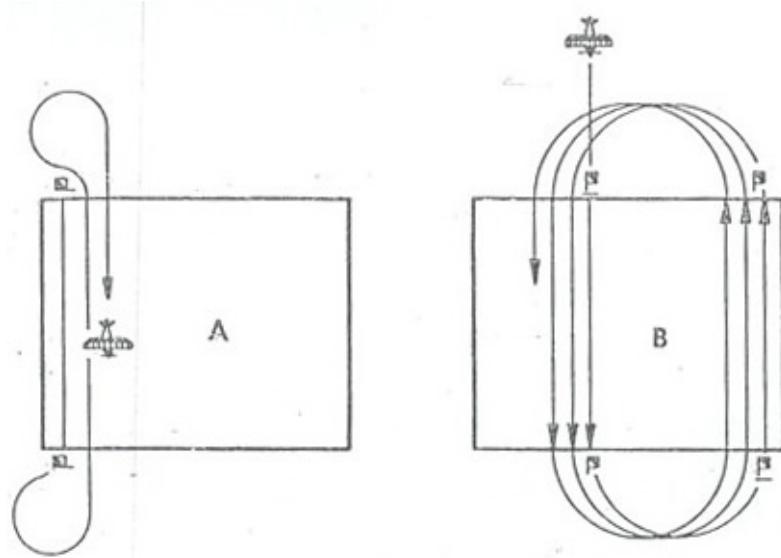


Figure 2.8. Procedures for reversing the aircraft track: A, the classic procedure turn; B, the round robin procedure turn (F.A.O. 1972) [6]

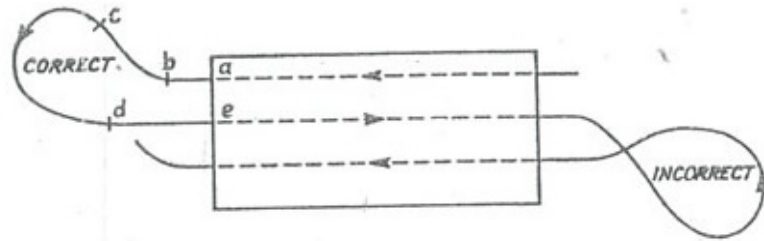


Figure 2.9. The classic procedure turn – correct and incorrect procedures [6]

The importance of the wind direction is shown in Figure 2.10. In order to avoid the drift of the spray the initial turn should be made down the wind direction.

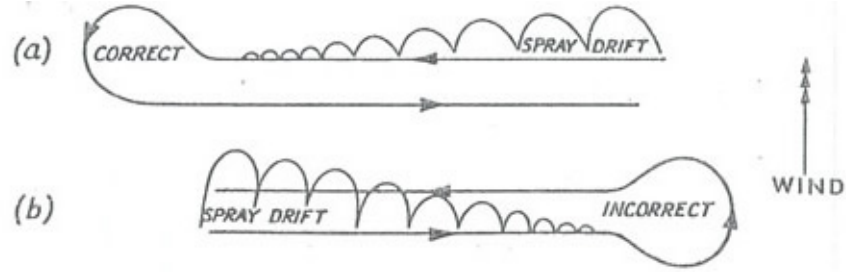


Figure 2.10. Effect of wind on procedure turn [6]

2.2. Competitors Study and Characteristics of ZIU

For design optimization of AAR Turkey's first agricultural aircraft complying with the FAR-23 aviation norms, ZIU is taken as baseline geometry which is TUSAS Aerospace Industry's first indigenous product for a manned aerial vehicle, shown in Figure 2.11 [37]. The specifications of ZIU which are taken from reference [37] are given in Table A.1 to Table A.9 in Appendix A.

Competitor study is carried out with the help of Ref. [38, 6]. Tables are tabulated in Table D.1 to Table D.22 in Appendix D. This study is used for deciding the upper, lower and the initial values of the design variables. Also it is important in evaluating the results of the conceptual design optimization problems. The pictures of the agricultural aircrafts obtained from the literature are also given in Figure D.1 to Figure D.4 in Appendix D.



Figure 2.11. ZIU at flight test [37]

2.3. Requirements

For any new airplane design, there must be some established requirements which serve as the jumping-off point for the design process, and which serve as the focused goal for the completed design. The basic requirements for AAR are as follows:

W_{payload} = 1500 liters (chemical density: 1 kg/liters)

Range = 120 km (64.8 nm)

h_{cruise} = 915 m (@ 3000 ft)

2.4. The Mission Profile of the Agricultural Aerial Robot

The idealized mission profile is divided into ten segments (Figure 2.12).

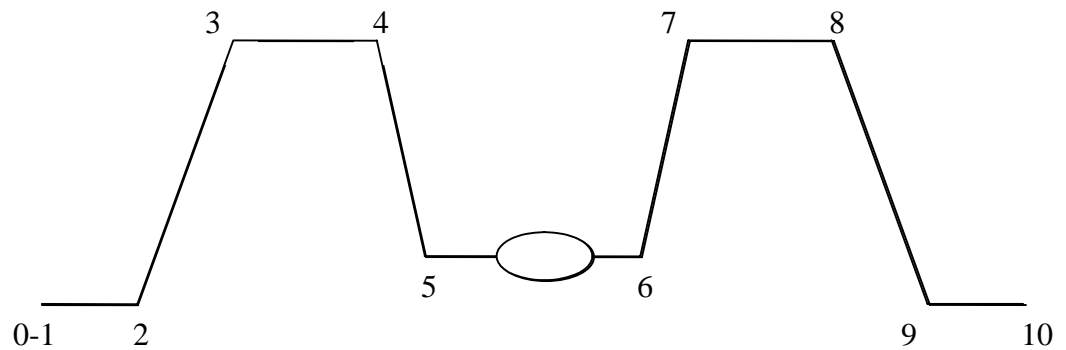


Figure 2.12. Mission profile of AAR

- 0→1** : Warm-up-Taxi-
- 1→2** : Take off
- 2→3** : Climb
- 3→4** : Cruise
- 4→5** : Descent
- 5→6** : Loiter (Agricultural Spraying)
- 6→7** : Climb
- 7→8** : Cruise
- 8→9** : Descent
- 9→10** : Landing

2.5. Agricultural Spraying Pattern and Flight Characteristics

In agricultural work the chemicals used take the form of liquid sprays, granules and dusts. The current version of AAR will use chemicals in liquid form. Thus, the aircraft is fitted with equipment for distributing these chemicals.

While performing agricultural task AAR has a spraying velocity which is assumed as 1.2 times the stall speed, $1.2 \cdot V_{stall}$. In the very beginning of the design stall speed is not known so CS 23 regulations [39] are taken as a baseline. The item CS 23-49 of this regulation states that V_{SO} is the stalling speed at which the aircraft is controllable with. And it is stated in this item that stall speed in landing configuration, V_{SO} , at maximum weight must not exceed 113 km/h (61 knots). Hopper volume may be taken as the design variable and may also be treated as an objective at the same time.

Volume rate (*liters/ha*) is the volume of the liquid sprayed over a unit area of 1 *ha* .The chemical application has three types depending on the volume rate. These are ultra low volume ULV, very low volume VLV, medium volume MV and high volume pesticide applications. ULV is used for the aerial spraying at maximum 5 *liters/ha* , VLV in the range 5 – 50 *liters/ha* , LV in the range 50 – 200 *liters/ha* . Generally HV (high volume) is a term indicating that the crop is wetted over most of its surface, greater than 700 *liters/ha* . MV (medium volume) is a term indicating that a proportion of the crop surface is totally wetted, in the range 200 – 700 *liters/ha* [6]. Typical volumetric rates [6] are given in Table C.1. of Appendix C.

The flow rate (*liters/sec*) of the spraying equipment is volume of the chemical applied in unit time. It is adjusted by the UAV operator. And this value is related to the volume rate, the airplane spraying speed and the effective swath width.

2.6. Path Planning For Agricultural Aerial Robot

The typical field employed in optimization where the aerial robot performs its mission is shown in Figure 2.13. In the flight path shown below the field width, a , and the spray swath, b , values are chosen such that the spraying is to be finished in n complete tours. The field length is taken three times of its width.

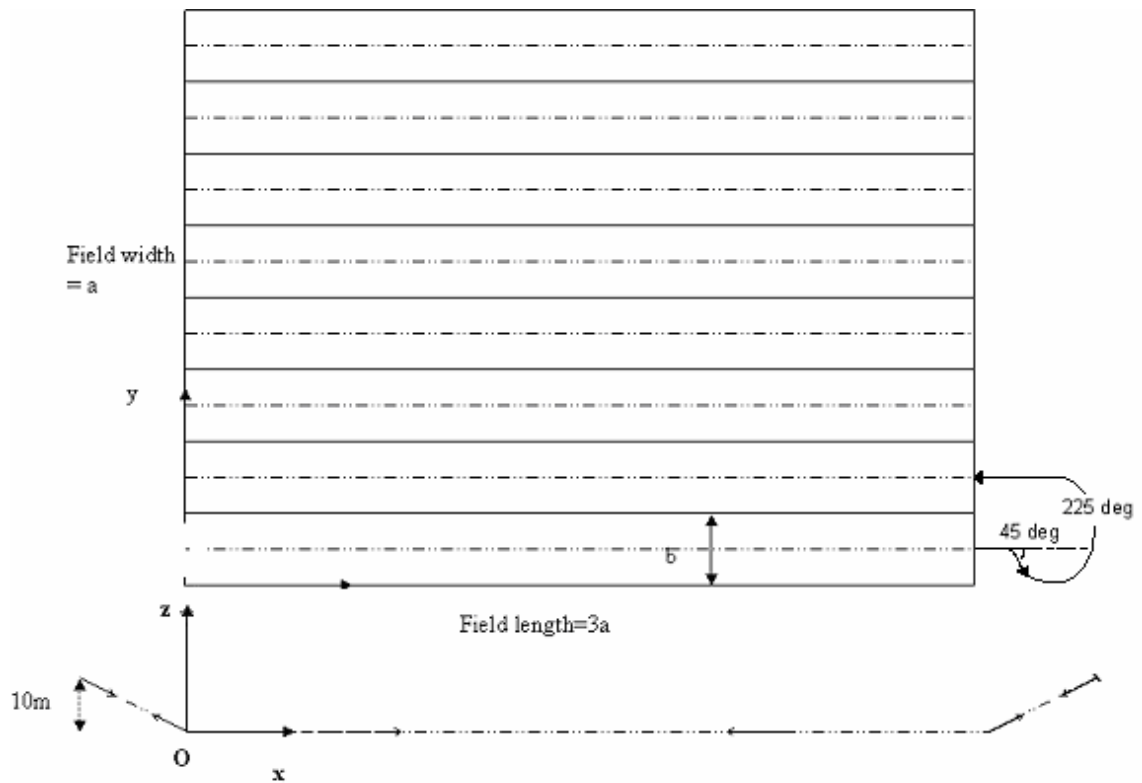


Figure 2.13. Schematic representation of the procedure turn

Under the assumption that, at the beginning of the flight aerial robot will perform the missions like taxi-take off cruise to an altitude and descent to $1m$ outside of the passage entrance. Then the analysis will be for the below flight segments.

1. Cruise at 1 meter height above the crop, level, un-accelerated flight
2. Steady, level, coordinated right turn (45°) “turn radius to be decided”

3. Climb to 10 m height “to be checked if this altitude is possible”
4. Conduct a steady level coordinated right turn (225°)
5. Descent to 1m height above the crop
6. Cruise at the 1 m height above the crop
7. Repeat steps 1 to 6 until the whole field is sprayed.

CHAPTER III

MATHEMATICAL MODELS USED IN DESIGN OPTIMIZATION

3.1. Overall configuration

As shown in Figure 3.1, the AAR airframe has twin booms with conventional tail configuration. A tractor engine is attached in front of the fuselage. Tricycle landing gear is used. However, to achieve sufficient distance between main landing gear struts, a twin boom configuration is used, where the main landing gear retracts into the booms (Figure 3.1), while the front landing gear retracts into the fuselage. Otherwise, a wider and a longer body would have been needed. A longer fuselage forces the center of gravity limits, requiring a larger tail surface area to attain static stability. It is possible to use a tail dragger type landing gear configuration as well. In this case, the main landing gear shall retract into the fuselage with longer struts, since it will be a single boom configuration. In addition, there will be a need of using a rather thick single boom to retract the aft landing gear in. The airframe structure is made of composite materials. The fuselage features a large internal space to accommodate large hopper tank. The upper surface of the fuselage is made of removable covers/panels that can be opened easily and quickly. The fuel is carried in the central "wet" wing. Fuel tanks are of the integral type. The twin wing booms are attached to the central wing and serve as bays for the two retractable main landing gears, and as a carrying structure for the vertical and the horizontal tails. There are seven control surfaces (2 flaps, 2 ailerons, 1 elevator and 2 rudders).

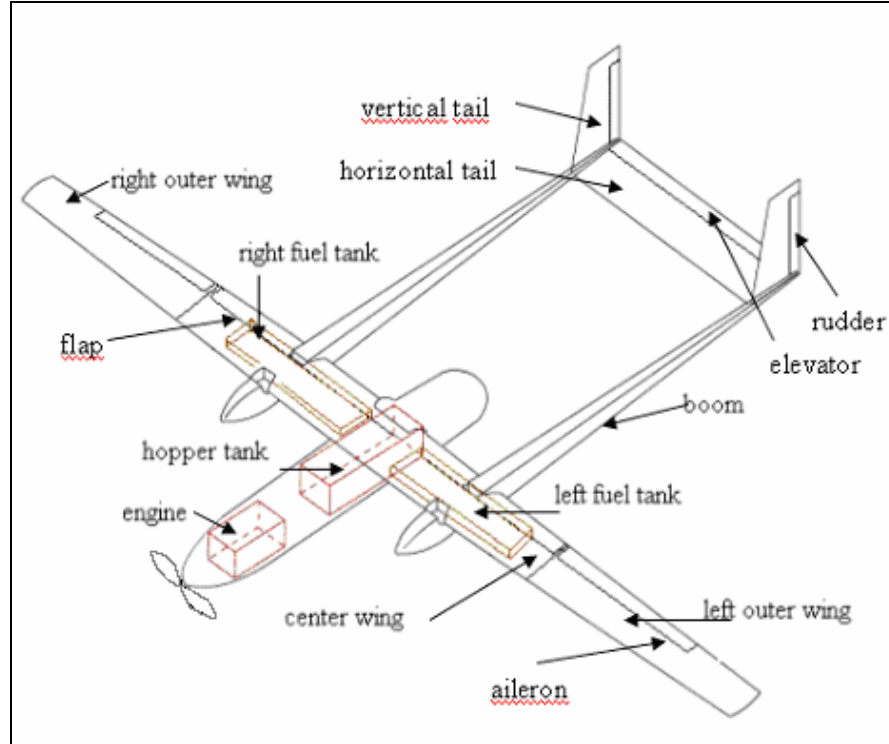


Figure 3.1. Conceptual Sketch of AAR

3.1.1. Structural Concept

The UAV structure is made of composite materials. The main and nose landing gears, are made of metal alloy. The UAV is built for easy assembly and disassembly of its main parts, so that it can be inserted or removed from its shipping container for transportation. The main airframe structure can be dismantled into the following major assemblies:

- a) Fuselage assembly
- b) Wing assembly (central wing + left hand and right hand outboard wings)
- c) Boom assembly
- d) Horizontal stabilizer
- e) Vertical stabilizers

3.1.2. Fuselage

The lower structural part of the fuselage is a "hull/boat" shape with a large base having a trapezoidal cross-section. The frames and bulkheads divide the fuselage into functional compartments. The compartments contain payload (hopper tank and pump), avionics and non-avionics. The fuselage includes covers enabling quick and easy access to components in the fuselage. The fuselage upper part includes a large cover. The tractor engine is mounted in front of the fuselage, and covered by a cowling.

3.1.3. Wing Assembly

It has a low wing similar to its competitors. In this configuration it's much easier to check the fuel and much simpler to put fuel in it without a ladder. This is really a very important consideration for an airplane like AAR because it will often receive fuel near the fields. Visibility is another factor that makes low wing a better choice because while the airplane is in a turn, it's much easier for the pilot to clear the area around him. Since AAR is unmanned this advantage is not applicable. Although the low wing has more interference drag because of the wing-to-fuselage angle it may be compensated for with fairings.

The wing assembly consists of three sections: the center wing section, a left outboard wing section and a right outboard wing section. The center wing is attached to the fuselage and the boom is attached to the wing. There is one flap on each side of the central wing inboard of the booms. The outboard wings are furnished with ailerons one on each side. Fuel will be carried in the wing inside tanks.

3.1.4. Booms and Tails

The twin booms are the carrying structure for the vertical and horizontal tails. It provides the mechanical interface between the centre wing and the tail, and incorporates

the bays required for the two retractable main landing gears. The vertical stabilizers with rudders are attached to the boom with the help of a fitting. They have a rudder on each. The horizontal stabilizer with an elevator is located in between two vertical tails. There is an elevator on the horizontal tail.

3.1.5. Engine Specification

The propulsion system of AAR consists of one Orenda OE600-A piston-prop reciprocating engine. OE600A V8 aero engine provides AAR with instantaneous throttle response, which will enhance maneuverability and performance on takeoff, climb, and in flight. AAR has a tractor configuration which has a number of advantages: the propeller is working in an undisturbed flow, the center of gravity moves front so a smaller tail is sufficient for static stability; the cooling of the engine is better. However, it has the disadvantage of disturbing the flow over the wing and fuselage by propeller slipstream causing increase in the skin friction over the fuselage due to the disturbed flow [4]. The mathematical models used are for piston-propeller driven aircraft.

3.1.6. Propeller

The propeller is a 3 bladed, constant velocity pitch propeller. The propeller is an off-the shelf item, produced by Hoffmann Propeller in Germany. Propeller diameter is 8.83ft.

The power plant technical parameters are specified in Table 3.1.

Table 3.1. The technical parameters of the power plant [37]

<u>ENGINE</u>	
Single Piston Engine	Orenda OE600-A
Height of Engine	2.02 ft
Width of Engine	2.13 ft
Length of Engine	3.74 ft
Take-off Power	600 hp @ 4400 rpm
Max. Continuous Power	500 hp @ 4200 rpm
Weight	691 lb
SFC	0.44 lb/hp/hr
<u>PROPELLER</u>	
Propeller Type	Constant Velocity
Propeller Diameter	106 inch
Number of Blades	3

3.1.7. Fuel Storage

The fuel is contained in two fuel tanks made from composite materials inside wing. Inspections and maintenance are made possible with the help of the access covers located on each tank. The centre wing compartment is divided into two independent left hand and right hand tanks providing independent fuel supply. Fuel contained in the left and right wing tanks is consumed together.

3.1.8. Hopper Tank

The chemicals used in agricultural application are contained in the hopper tank. This tank is fitted internally in the fuselage, aft of the engine. A large door is fitted at the top for loading. At the bottom a gate is fitted for controlling the flow of the hopper.

3.1.9. Landing Gear System General Description

The UAV is equipped with a tricycle landing gear system. The system has two main and one nose landing gear struts, which are equipped with hydro-pneumatic shock absorbers. Each main landing gear retracts into its bay in the boom. The nose landing gear retracts into its bay in the fuselage. A hydraulic actuator accomplishes the retraction/extension of each gear. Each main landing gear is equipped with a hydraulic brake. The landing gears are designed for take off, landing and taxiing on soft field.

3.2. The Weight Model of the Airplane – First Estimate:

In the conceptual design of an airplane, first step is to estimate the takeoff gross weight.

3.2.1. Take off Weight Buildup

Design takeoff gross weight W_0 is the weight of the airplane at the beginning of its mission, including the payload weight, the fuel weight and the empty weight.

$$W_0 = W_{payload} + W_f + W_e \quad (3.1)$$

Payload weight is known from requirements, fuel and empty weights are both dependent on total takeoff weight:

$$W_0 = \frac{W_{payload}}{1 - \frac{W_f}{W_0} - \frac{W_e}{W_0}} \quad (3.2)$$

After getting weight fractions W_e/W_0 and W_f/W_0 subsequent iterations will refine the assumptions and W_0 is converges to a refined value.

3.2.2. Empty Weight Fraction Estimation

Historical, statistical data on previous airplanes provide a starting point for the conceptual design of Agricultural Aerial Robot.

Figure 8.1 which is available in Ref. [4] is a plot of W_e/W_0 versus W_0 for a number of reciprocating engine, propeller driven airplanes. The data for airplanes from 1930's to the present time are given in this plot. The values of W_e/W_0 tend to cluster around 0.62. These airplanes are mostly the ones which have a gross weight less than 10000 lb like AAR. Also the empty weight fraction W_e/W_0 can be estimated from the statistical curve-fit equations for the historical trends given in Table 3.1 given in Ref. [4]. Considering fixed sweep wing, agricultural aircraft:

$$\frac{W_e}{W_0} = 0.74 \cdot W_0^{-0.03} \cdot K_{ws} \quad (3.3)$$

where K_{ws} is a variable sweep constant and it is taken as 1.0 for fixed sweep aircraft.

This equation yields around a value of 0.56. So as a first assumption the weight fraction W_e/W_0 is taken as 0.56 for AAR.

3.2.3. Fuel Fraction Estimation

W_f is the weight of the fuel required for the mission plus reserve fuel. The fuel fraction W_f/W_0 can be estimated based on the mission profile given in Section 2.4 using approximations of the fuel consumption and aerodynamics.

The design mission given in Section 2.4 has eleven mission segments; warm-up, taxi, takeoff, climb, cruise, descent, loiter, climb, cruise, descent and landing. Each segment of the mission profile is associated with a weight fraction which can be expressed as the aircraft weight at the end of segment W_i divided by its weight at the beginning of that segment. First these fractions are estimated for each segment then they are multiplied together to find the total mission weight fraction. For AAR 6% allowance for reserve and trapped fuel is considered, and the total fuel fraction is estimated as:

$$W_f/W_0 = 1.06 \cdot \left(1 - \frac{W_{11}}{W_0}\right) \quad (3.4)$$

where

$$\frac{W_{11}}{W_0} = \frac{W_1}{W_0} \cdot \frac{W_2}{W_1} \cdot \frac{W_3}{W_2} \cdot \frac{W_4}{W_3} \cdot \frac{W_5}{W_4} \cdot \frac{W_6}{W_5} \cdot \frac{W_7}{W_6} \cdot \frac{W_8}{W_7} \cdot \frac{W_9}{W_8} \cdot \frac{W_{10}}{W_9} \cdot \frac{W_{11}}{W_{10}} \quad (3.5)$$

Warm-up, Taxi and Take-off Segment Weight Fractions:

For the initial estimate warm-up (segment 0-1), taxi (segment 1-2) and take-off (segment 2-3) weight fractions are based on historical data.

$$W_1/W_0 = 0.97$$

$$W_2/W_1 = 0.995$$

$$W_3/W_2 = 0.996$$

Climb Segment Weight Fraction:

Again based on the historical data for climb (segment 3-4 and segment 7-8) the weight fractions are;

$$W_4/W_3 = 0.985$$

$$W_8/W_7 = 0.985$$

Cruise Segment Weight Fraction:

For cruise, (segment 4-5 and segment 8-9), W_5/W_4 and W_9/W_8 can be found by using Brequet range equation given in Ref.[40].

$$R = \frac{\eta_{pr}}{c} \cdot \frac{L}{D} \cdot \ln \frac{W_{i-1}}{W_i} \quad (3.6)$$

$$W_5/W_4 = e^{\frac{c \cdot R_{4-5}}{\eta_{pr} \cdot L/D}} \quad (3.7)$$

$$W_9/W_8 = e^{\frac{c \cdot R_{8-9}}{\eta_{pr} \cdot L/D}} \quad (3.8)$$

where range, R , and cruise velocity, V_{cruise} , are known from requirements. The specific fuel consumption, c , value of ZIU is 0.44lb/hp/hr. The same value is taken as the specific fuel consumption value of AAR as well.

$$c = 0.44 \cdot \frac{lb}{hp \cdot hr} \cdot \frac{1hp}{550ft \cdot lb/s} \cdot \frac{1hr}{3600s}$$

$$c = 2.22 \cdot 10^{-7} \frac{lb}{ft \cdot lb/s}$$

Propeller efficiency η_{pr} for cruise is taken from the typical values for propeller engines given in Table 3.4 available in Ref.[40].

$$\eta_{pr} = 0.8$$

This requires an estimation of the lift-to-drag ratio L/D . In conceptual design phase a detailed aerodynamic analysis is not necessary since, the shape is not laid out at this stage. However an approximate value was based on data for Agricultural Airplanes is taken as given in Ref. [41];

$$L/D_{max} \cong 10$$

Since lift-to-drag ratio primarily depends on the wing span and the wetted area, wetted aspect ratio AR_{wet} has to be considered instead of the geometric aspect ratio AR .

Comparing the conceptual sketch of AAR given in Figure 3.1 with Figure 3.2 which shows a spectrum of design approaches and the resulting wetted area ratios, wetted area ratio of AAR is estimated to be;

$$S_{wet}/S_{ref} \approx 4$$

In Figure 3.2 which is given in Ref.[40], the retractable prop aircraft trend line gives the maximum lift-to-drag ratio with respect to the wetted aspect ratio. As an initial estimate taking aspect ratio as $AR = 6$, like most of competitors have, the lift-to-drag ratio will come out to be;

$$AR_{wet} = \frac{AR}{\left(\frac{S_{wet}}{S_{ref}}\right)} = \frac{6}{4} = 1.5$$

$$L/D_{max} \cong 10$$

Note that Ref.[41] also gives the same value for the cruise segment of a propeller aircraft. Consequently this value is used for the conceptual design.

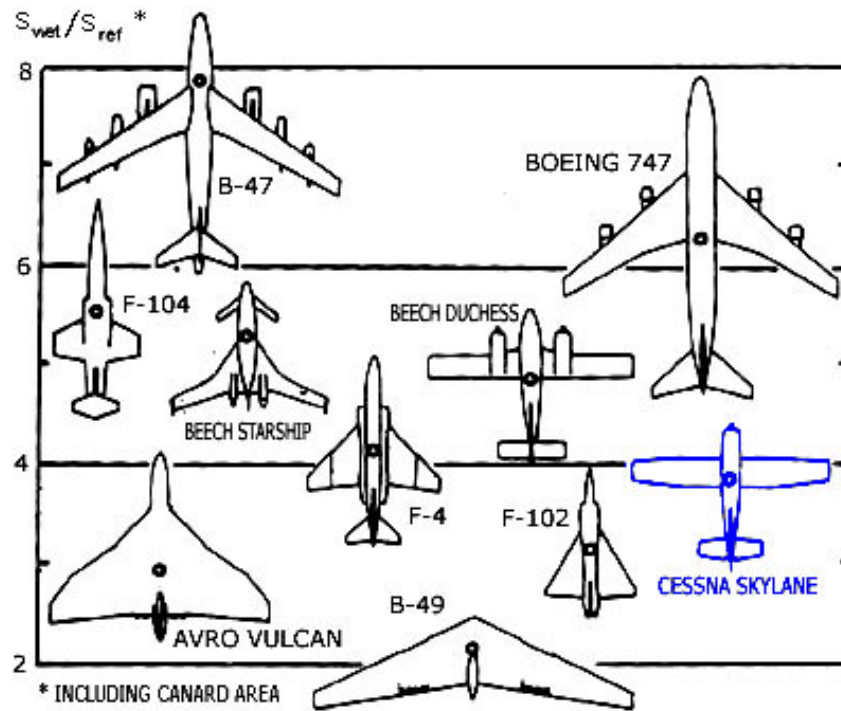


Figure 3.2. Maximum lift to drag ratio trends [40]

Loiter Segment Weight Fraction:

The cruise weight fraction W_4/W_3 can be found from the Brequet endurance equation given in Ref.[40]:

$$E = \frac{\eta_{pr}}{c \cdot V_{loiter}} \cdot \frac{L}{D} \cdot \ln \frac{W_{i-1}}{W_i} \quad (3.9)$$

where the endurance, E , is known from requirements. Using the specific fuel consumption c and lift-to-drag ratio L/D estimated above the cruise weight fraction may be found from Eqn. (3.10).

$$W_4/W_3 = e^{\frac{c \cdot V_{\text{loiter}} \cdot E_{A-5}}{\eta_{PR} \cdot L/D}} \quad (3.10)$$

Descent and Landing Segment Weight Fractions:

Historical data is used for descent and landing (segment 9-10 and segment 11-10) for initial sizing.

$$W_{10}/W_9 = 1.00$$

$$W_{11}/W_{10} = 0.998$$

3.3. Estimation of Critical Performance Parameters

The requirements such as maximum speed, range, ceiling, rate of climb, stalling speed, landing distance, and takeoff distance specify the required performance of AAR. Airplane performance is critically dependent on several parameters, especially (1) maximum lift coefficient $C_{L_{\max}}$; (2) lift-to-drag ratio L/D ; (3) wing loading W/S ; and (4) thrust-to-weight ratio T/W .

3.3.1. Maximum Lift Coefficient

A number of parameters must be chosen before the design layout can be started. These include the airfoils, the wing and tail geometry etc. The airfoil in many aspects is the heart of the airplane. Since it is the main component that provides lift it affects the cruise speed, takeoff distance, landing distance; stall speed, handling qualities and overall

aerodynamic efficiency. There are several parameters in selecting a suitable airfoil for an aircraft.

Competitor agricultural aircrafts (see Appendix D) have employed the NACA four-digit and five-digit, airfoil sections. NACA 23015 is the profile used in ZIU. The NACA five-digit airfoils have a maximum camber which is placed closer to the leading edge than maximum camber of NACA four-digit airfoils. Also these profiles have a maximum lift coefficient $c_{l,max}$ higher than the four-digit series. Their disadvantage is the sharp stalling behavior. Examples of competitor aircrafts and their profiles are tabulated in Table 3.2.

Table 3.2. Competitor's airfoil profiles

Airplane	Root Airfoil Profile	Tip Airfoil Profile
AT-401	NACA 4415	NACA 4415
Ipanema EMB 201A	NACA 23015	NACA 23015
NAC 6 Fieldmaster	NACA 23012	NACA 23012
AG Truck	NACA 2412	NACA 2412

Airfoil

The lift of the airfoil must be as high as possible where as the drag must be minimum. Thus an airfoil with a higher L/D value is proffered. The first consideration in initial airfoil selection is the design lift coefficient. It is the lift coefficient at which the airfoil has the best L/D and it must be high. At this c_l the airfoil is feeling lowest drag.

Stall characteristics of the airfoil also play an important role in the selection as well. Some airfoils exhibit gradual reduction of lift in stall while others show abrupt change, which means sudden loss of lift and controls. Fat airfoils stall from the trailing edge, with a gradual loss of lift while the pitching moment changes only a small amount. Thinner airfoils stall from the leading edge [40].

Airfoil thickness ratio is another important parameter that influences drag, maximum lift and stall characteristics. The drag increases with increasing thickness. The airfoil thickness also affects the structural weight of the wing. Statistical data shows that the wing structural weight varies approximately inversely with the square root of the thickness ratio [40]. Various equipments and more fuel can be installed in the wing if a fat airfoil for the root is chosen.

The design lift coefficient should be high. Maximum lift coefficient $c_{l,max}$ should also be as high as possible. In addition $c_{l\alpha}$ must be high, indicating that large lift is obtained for a small angle of attack change. The airfoils with behavior “A” in Table 3.3 have large $c_{l\alpha}$ have small α_0 . This means they will stall at a lower angle of attack than those with smaller $c_{l\alpha}$ but higher α_0 values. Airfoils with behavior “D” (Table 3.3) display gradual change of lift after stall and the ones with behavior of “A” display abrupt changes in lift. $c_{d,min}$ is also important for performance. As a result the airfoil with minimum $c_{d,min}$ should be selected.

Under the above considerations the selected airfoil profiles for AAR are given below.

Wing root airfoil: 'NACA 63₂615' being fat, has a very good $c_{l,design}$ value and a high $c_{l,max}$ value with a “D” type $c_{l,max}$ behavior. Its $c_{l\alpha}$ is also high and it has a reasonable drag.

Thickness to chord ratio $t/c = 15.05\%$ (approximately)

Camber = 2.04% (approximately)

Wing tip airfoil: Same as root airfoil.

Tail airfoil: 'NACA 0012' being symmetric, has good aerodynamic parameters, and chosen by most competitors.

Table 3.3 shows candidates for airfoil selection with several properties at a specific Reynolds number of 9 million [42].

Table 3.3. Airfoil candidates' properties [42]

Airfoil NACA	Re $\times 10^{-4}$	Behav ior of $c_{l,max}$	$c_{l,max}$ $\times 10^2$	α_0 $\times 10$	$c_{l\alpha}$ $\times 10^3$	$c_{l,design}$ $\times 10^2$	$c_{d\ min}$ $\times 10^4$	$c_{m,ac}$ $\times 10^3$
63 ₃ -415	900	D	167	-30	115	35	0049	-071
63 ₂ -215	900	D	161	-12	120	20	0046	-031
63 ₁ -412	900	D	178	-30	100	32	0045	-075
23012	837	A	174	-12	100	08	0060	-008
23015	890	D	172	-10	104	20	0063	-007
43012	839	A	184	-23	100	26	0068	-019
43009	808	A	172	-24	100	18	0068	-021
63₂-615	900	D	167	-38	120	42	0048	-110
0012	900	B	159	-	106	-	0057	0

The lift, moment coefficient and airfoil shape for NACA 63₂-615 and NACA 0012 airfoils are taken from Ref.[43] and given in Figure 3.3 and Figure 3.4 respectively.

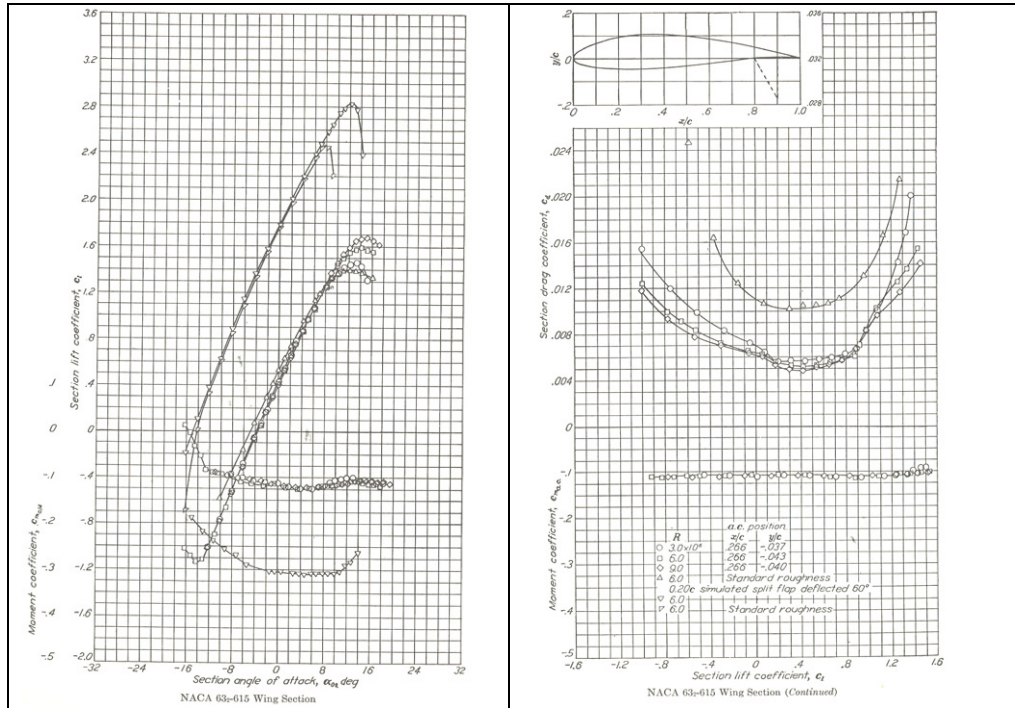


Figure 3.3. Lift, moment coefficient and airfoil shape for NACA 632-615 [43]

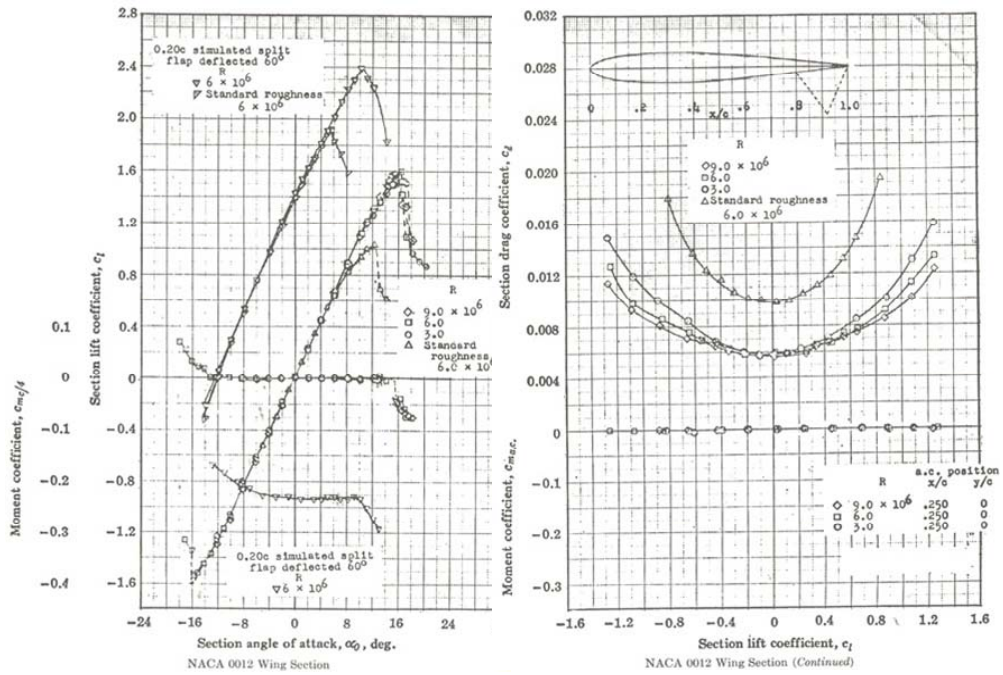


Figure 3.4. Lift, moment coefficient and airfoil shape for NACA 0012 [43]

Eqn (3.11) gives the maximum lift coefficient for finite wings with aspect ratio greater than 5, including three-dimensional effects of the finite aspect ratio. AAR has an aspect ratio greater than 5. So the maximum lift coefficient can be found by using Eqn.(3.11) [40].

For clean configuration;

$$C_{L_{\max}} = 0.9 \cdot cl_{\max} \quad (3.11)$$

Wing will be designed with simple plain trailing-edge flaps. The increase in cl_{\max} value corresponding to a flap deflected of 45° is equal to 0.9 [4].

In landing configuration with full flaps;

$$C_{L\max})_{landing} = 0.9 \cdot (c_{l\max} + \Delta c_{l\max})_{landing} \quad (3.12)$$

At take-off configuration it is assumed that aircraft flies with 25° flaps. Assuming a linear variation of $\Delta c_{l\max}$;

$$\Delta c_{l\max})_{take-off} = 0.9 \cdot \left(\frac{25^\circ}{45^\circ} \right)$$

$$\Delta c_{l\max})_{take-off} = 0.5$$

For take-off configuration with 25° flaps;

$$C_{L\max})_{take-off} = 0.9 \cdot (c_{l\max} + \Delta c_{l\max})_{take-off} \quad (3.13)$$

In conceptual design phase it is a reasonable approximation to use these coefficients as the complete airplane maximum lift coefficients [4].

3.3.2. Wing Loading

Wing loading W/S , is determined by considerations of V_{stall} and landing distance. However, W/S also plays a role in the maximum velocity of the airplane. V_{\max} increases as the W/S increases. For AAR design, which is a low-speed aircraft, the stall speed V_{stall} , and landing distance are the main parameters that determine the wing loading.

$$V_{stall} = \sqrt{\frac{2}{\rho_{\infty}} \cdot \frac{W_0}{S} \cdot \frac{1}{C_{Lmax} }_{take-off}} \quad (3.14)$$

$$\frac{W_0}{S} = \frac{1}{2} \cdot \rho_{\infty} \cdot V_{stall}^2 \cdot C_{Lmax})_{take-off}$$

Landing distance is given by;

$$s_L = s_{g_L} + s_{a_L} + s_{f_L} \quad (3.15)$$

$$s_{a_L} = \frac{50 - h_f}{\tan(\theta_a)} \quad (3.16)$$

where $\theta_a = 3^\circ$

$$h_f = R_L \cdot (1 - \cos \theta_a) \quad (3.17)$$

$$R_L = \frac{V_f}{0.2 \cdot g} \quad (3.18)$$

$$s_{f_L} = R_L \cdot \sin(\theta_a) \quad (3.19)$$

$$s_{g_L} = j \cdot N \cdot \sqrt{\frac{2}{\rho_{\infty}} \cdot \frac{W_0}{S} \cdot \frac{1}{C_{Lmax} }_{landing}} + \frac{j^2 \cdot \left(\frac{W_0}{S} \right)}{g \cdot \rho_{\infty} \cdot C_{Lmax})_{landing} \cdot \mu_r} \quad (3.20)$$

3.3.3. Power to Weight Ratio

The power to weight ratio is the function of take-off distance, rate of climb and maximum velocity constraints [4].

The take of distance is given by

$$s_{TO} = s_{g_TO} + s_{a_TO} \quad (3.21)$$

$$s_{g_TO} = \frac{1.21 \cdot \left(\frac{W_0}{S} \right)}{g \cdot \rho_\infty \cdot C_{L\text{take-off}} \cdot \left(\frac{T}{W_0} \right)_{0.7V_{LO}}} \quad (3.22)$$

Here, take off lift coefficient is the actual lift coefficient at take off. It is not the maximum lift coefficient at take off used for stall calculations. The aircraft usually takes off at about 1.1 times the stall speed. Consequently the take off lift coefficient becomes the maximum take off lift coefficient divided by 1.21 (square of 1.1), [4]

$$C_{L\text{take-off}} = C_{L\text{max,take-off}} / 1.1^2$$

$$R_{TO} = \frac{6.96 \cdot (V_{stall})^2}{g} \quad (3.23)$$

$$\theta_{OB} = \text{Cos}^{-1} \left(1 - \frac{h_{OB}}{R_{TO}} \right) \quad (3.24)$$

$$s_{a_TO} = R_{TO} \cdot \sin \theta_{OB} \quad (3.25)$$

$$V_\infty = 0.7 \cdot V_{LO}$$

$$P_R = T \cdot V_\infty \quad (3.26)$$

$$P_R = \frac{T}{W_0} \cdot W_0 \cdot V_\infty \quad (3.27)$$

$$P_R = P_A \cdot \eta_{pr} \quad (3.28)$$

$$P_A = \frac{P_R}{\eta_{pr}}$$

Rate of climb constraint is given by the following mathematical model for propeller-driven airplanes [4].

$$\left(\frac{R}{C}\right)_{\max} = \frac{\eta_{pr} \cdot P_A}{W_0} - \left(\frac{2}{\rho_\infty} \cdot \sqrt{\frac{K}{3 \cdot C_{D,0}}} \cdot \frac{W_0}{S} \right)^{1/2} \cdot \frac{1.555}{(L/D)_{\max}} \quad (3.29)$$

Maximum velocity constraint

$$P_A = P_R$$

$$P_R = T \cdot V_{\max} = D \cdot V_{\max}$$

$$P_A = D \cdot V_{\max} = \left(\frac{1}{2} \cdot \rho_\infty \cdot V_{\max}^2 \cdot S \cdot C_{D,0} + \frac{2 \cdot K \cdot S}{\rho_\infty \cdot V_{\max}^2} \left(\frac{W_0}{S} \right)^2 \right) \cdot V_{\max} \quad (3.30)$$

This equation is solved iteratively to find the maximum airspeed of AAR.

3.4. Configuration Layout -Geometrical Models

The configuration layout is the shape and size (dimensions) of the airplane as it has evolved to this stage. The critical performance parameters in combination with the initial weight estimate give enough information to approximately size the airplane and configuration.

3.4.1. Wing Configuration Model

A tapered conventional wing will be designed. The wing span b , aspect ratio AR , taper ratio λ , quarter chord sweep angle Λ_{LE} , and wing incidence angle i are

design parameters. Using these inputs the planform shape is constructed. The mathematical model for the wing geometry is presented below [4, 40, 41].

$$AR = \frac{b^2}{S} \quad (3.31)$$

$$S = \frac{b^2}{AR}$$

$$c_r = \frac{2 \cdot S}{(\lambda + 1) \cdot b} \quad (3.32)$$

$$c_t = \lambda \cdot c_r \quad (3.33)$$

$$\bar{c} = \frac{2}{3} c_r \cdot \left(\frac{1 + \lambda + \lambda^2}{1 + \lambda} \right) \quad (3.34)$$

$$\bar{y} = \frac{b}{6} \cdot \left(\frac{1 + 2 \cdot \lambda}{1 + \lambda} \right) \quad (3.35)$$

$$\tan(\Lambda_{LE}) = \tan(\Lambda_{c/4}) + \left(\frac{1 - \lambda}{AR \cdot (1 + \lambda)} \right) \quad (3.36)$$

$$\bar{x} = \bar{y} \cdot \tan(\Lambda_{LE}) \quad (3.37)$$

The wing root at wing-fuselage intersection

$$c_r)_{fw} = c_r \cdot \left(1 - \left(\frac{w_{f-\max}}{b} \cdot (1 - \lambda) \right) \right) \quad (3.38)$$

The exposed wing taper ratio

$$\lambda)_{fw} = \frac{c_t}{c_r)_{fw}} \quad (3.39)$$

The exposed wing root thickness ratio

$$\left(\frac{t}{c}\right)_{fw} = \frac{\left(\frac{t}{c} - \left(\frac{w_{f_max}}{b}\right)\right) \cdot \left(\frac{t}{c} - (\lambda)_{fw} \cdot \frac{t}{c}\right)}{\left(1 - \left(\frac{w_{f_max}}{b}\right)\right) \cdot (1 - \lambda)_{fw}} \quad (3.40)$$

The ratio of the tip and root thickness ratios of the exposed wing

$$\tau)_{fw} = \frac{\frac{t}{c}}{\left(\frac{t}{c}\right)_{fw}} \quad (3.41)$$

Net wing area is the wing reference area less the part of the wing covered by the fuselage. It is also referred as exposed wing area.

$$S_{net_w} = \left(\frac{c_r)_{fw} + c_t}{2}\right) \cdot \left(\frac{b - w_{f_max}}{\cos(\Gamma)}\right) \quad (3.42)$$

$$S_{wet_w} = 2 \cdot S_{net_w} \cdot \left(1 + 0.25 \cdot \frac{t}{c}\right)_{fw} \cdot \frac{(1 + \tau)_{fw} \cdot \lambda)_{fw}}{(1 + \lambda)_{fw}} \quad (3.43)$$

3.4.2. Fuel Tank Configuration Model

Since the fuel weight is estimated in Initial Sizing Module the fuel tank volume of AAR becomes,

$$Vol_{fuel} = \frac{W_{fuel}}{\rho_{fuel}} \quad (3.44)$$

An assumption is made for the internal wing structure for conceptual design purposes. Accordingly, the front spar is located at 12% of the chord from the leading edge, and the rear spar located at 60% from the leading edge. The height of the fuel tank is two third of the chord thickness. Two trapezoidal tanks will be placed, one in the left wing and one in the right wing with a total capacity of the fuel volume needed. Using the formulas to calculate the volume of a trapezoid the length of the fuel tank is found subjected to the constraints such that it can not be equal to 0 or greater than half span. Then, the end of fuel tank station in terms of half span is,

$$\eta_{\substack{\text{fuel tank} \\ \text{end point}}} = \frac{L}{b/2} \quad (3.45)$$

The wing chord length at a given spanwise station is determined from:

$$c_{\substack{\text{given} \\ \text{spanwise location}}} = \left(1 - \frac{2 \cdot L}{b}\right) \cdot c_r + \frac{2 \cdot L \cdot \lambda \cdot c_r}{b} \quad (3.46)$$

where $c_i = \lambda \cdot c_r$

width of fuel tank at any location = $0.48 \cdot c$

height of fuel tank at any location = $\frac{t}{c} \cdot c \cdot \frac{2}{3}$

So integrating the area of a rectangle, the volume of the fuel tank is obtained. Since the volume of the fuel is known from the mission analysis the only unknown in this equation is the corresponding length of the fuel tank.

$$\int_0^{L_{\text{fuel tank}}} w_{\text{fuel tank}} \cdot h_{\text{fuel tank}} \cdot dL \quad (3.47)$$

$$\int_0^{L_{fuel_tan\ k}} 0.48 \cdot \left(\left(1 - \frac{2 \cdot L}{b} \right) \cdot c_r + \frac{2 \cdot L \cdot \lambda \cdot c_r}{b} \right)^2 \cdot \frac{2}{3} \cdot t/c \cdot dL \quad (3.48)$$

Solving these equations the length of fuel tank $L_{fuel_tan\ k}$ is found.

3.4.3. Horizontal Tail and Vertical Tail Configuration Model

A conventional tail will be designed. The horizontal tail volume coefficient is taken as 0.5 [35] and dihedral angle Γ_{HT} is zero. The aspect ratio AR_{HT} , taper ratio λ_{HT} , quarter chord sweep angle Λ_{LE_HT} are design parameters. The mathematical model for the horizontal tail geometry is as follows [4, 40, 41].

$$V_{HT} = \frac{l_{HT} \cdot S_{HT}}{\bar{c} \cdot S} \quad (3.49)$$

$$b_{HT} = \sqrt{S_{HT} \cdot AR_{HT}} \quad (3.50)$$

$$c_{r_HT} = \frac{2 \cdot S_{HT}}{(\lambda_{HT} + 1) \cdot b_{HT}} \quad (3.51)$$

$$c_{t_HT} = \lambda_{HT} \cdot c_{r_HT} \quad (3.52)$$

$$\bar{c}_{HT} = \frac{2}{3} c_{r_HT} \cdot \left(\frac{1 + \lambda_{HT} + \lambda_{HT}^2}{1 + \lambda_{HT}} \right) \quad (3.53)$$

$$\bar{y}_{HT} = \frac{b_{HT}}{6} \cdot \left(\frac{1 + 2 \cdot \lambda_{HT}}{1 + \lambda_{HT}} \right) \quad (3.54)$$

The horizontal tail at tail-fuselage intersection

$$c_{r_HT} \Big|_{fw} = c_{r_HT} \cdot \left(1 - \left(\frac{w_{f_max}}{b_{HT}} \cdot (1 - \lambda_{HT}) \right) \right) \quad (3.55)$$

The exposed horizontal tail taper ratio

$$\lambda_{HT})_{fw} = \frac{c_{t-HT}}{c_{r-HT})_{fw}} \quad (3.56)$$

The exposed horizontal tail root thickness ratio

$$\left(\frac{t}{c_{HT}}\right)_{fw} = \frac{\left(\frac{t}{c_{HT}} - \left(\frac{w_{f-max}}{b_{HT}}\right)\right) \cdot \left(\frac{t}{c_{HT}} - (\lambda)_{fw} \cdot \frac{t}{c_{HT}}\right)}{\left(1 - \left(\frac{w_{f-max}}{b_{HT}}\right)\right) \cdot (1 - \lambda_{HT})_{fw}} \quad (3.57)$$

The tip and root thickness ratios of the exposed horizontal tail are;

$$\tau_{HT})_{fw} = \frac{\frac{t}{c_{HT}}}{\left(\frac{t}{c_{HT}}\right)_{fw}} \quad (3.58)$$

$$S_{net-HT} = \left(\frac{c_{r-HT})_{fw} + c_{t-HT}}{2}\right) \cdot \left(\frac{b_{HT} - w_{f-max}}{\cos(\Gamma_{HT})}\right) \quad (3.59)$$

$$S_{wet-HT} = 2 \cdot S_{net-HT} \cdot \left(1 + 0.25 \cdot \frac{t}{c_{HT}}\right)_{fw} \cdot \frac{(1 + \tau_{HT})_{fw} \cdot \lambda_{HT})_{fw}}{(1 + \lambda_{HT})_{fw}} \quad (3.60)$$

Like for horizontal tail the vertical tail volume coefficient is also taken as constant and equal to 0.04 [40]. The dihedral angle Γ_{VT} is also zero. The aspect ratio AR_{VT} , taper ratio λ_{VT} , quarter chord sweep angle Λ_{LE-VT} , are chosen as design parameters. The mathematical model of the vertical tail geometry is given below [4, 40, 41].

$$V_{VT} = \frac{l_{VT} \cdot S_{VT}}{c \cdot S} \quad (3.61)$$

$$h_{HT} = \sqrt{S_{VT} \cdot AR_{VT}} \quad (3.62)$$

$$c_{r_VT} = \frac{2 \cdot S_{VT}}{(\lambda_{VT} + 1) \cdot h_{VT}} \quad (3.63)$$

$$c_{t_VT} = \lambda_{VT} \cdot c_{r_VT} \quad (3.64)$$

$$\bar{c}_{VT} = \frac{2}{3} c_{r_VT} \cdot \left(\frac{1 + \lambda_{VT} + \lambda_{VT}^2}{1 + \lambda_{VT}} \right) \quad (3.65)$$

$$\bar{z}_{HT} = \frac{h_{VT}}{6} \cdot \left(\frac{1 + 2 \cdot \lambda_{VT}}{1 + \lambda_{VT}} \right) \quad (3.66)$$

The vertical tail at tail-fuselage intersection

$$c_{r_VT})_{fw} = c_{r_VT} \cdot \left(1 - \left(\frac{w_{f_max}}{h_{VT}} \cdot (1 - \lambda_{VT}) \right) \right) \quad (3.67)$$

The exposed vertical tail taper ratio

$$\lambda_{VT})_{fw} = \frac{c_{t_VT}}{c_{r_VT})_{fw}} \quad (3.68)$$

The exposed horizontal tail root thickness ratio

$$\left. \frac{t}{c_{VT}} \right)_{fw} = \frac{\left(\frac{t}{c_{VT}} - \left(\frac{w_{f-max}}{h_{VT}} \right) \right) \cdot \left(\frac{t}{c_{VT}} - (\lambda)_{fw} \cdot \frac{t}{c_{VT}} \right)}{\left(1 - \left(\frac{w_{f-max}}{h_{VT}} \right) \right) \cdot (1 - \lambda_{VT})_{fw}} \quad (3.69)$$

The tip and root thickness ratios of the exposed vertical tail are;

$$\tau_{VT})_{fw} = \frac{\frac{t}{c_{VT}}}{\left. \frac{t}{c_{VT}} \right)_{fw}} \quad (3.70)$$

$$S_{net_VT} = \left(\frac{c_{r_VT})_{fw} + c_{t_VT}}{2} \right) \cdot \left(\frac{h_{VT} - w_{f-max}}{\cos(\Gamma_{VT})} \right) \quad (3.71)$$

$$S_{wet_VT} = 2 \cdot S_{net_VT} \cdot \left(1 + 0.25 \cdot \left. \frac{t}{c_{VT}} \right)_{fw} \cdot \frac{(1 + \tau_{VT})_{fw} \cdot \lambda_{VT})_{fw}}{(1 + \lambda_{VT})_{fw}} \right) \quad (3.72)$$

3.4.4. Control Surfaces Model

The main control surfaces are the ailerons, an elevator and a rudder. The detailed sizing of these surfaces is based on the dynamic analysis. In conceptual design phase the sizing of these control surfaces are carried out following the guidelines given in Ref.[40].

According to these guidelines ailerons extend from about 50% to about 90% of the span. Wing flaps occupy the wing span inboard of ailerons. Elevators and rudders, on the other hand, generally begin at the side of the fuselage and extend to the tip of the tail or to about 90% of the tail span.

Control surfaces are usually tapered in chord by the same taper ratio as the wing or tail surface. Ailerons and flaps are typically about 15-25% of the wing chord. Rudders and elevators are about 25-50% of the tail chord.

The control surface geometry of AAR is taken as;

$$c_{r_aileron} = 0.25 \cdot c_r \quad (3.73)$$

$$c_{t_aileron} = \lambda \cdot c_{r_aileron} \quad (3.74)$$

$$b_{aileron} = 0.35 \cdot b \quad (3.75)$$

$$c_{r_flap} = 0.25 \cdot c_r \quad (3.76)$$

$$c_{t_flap} = \lambda \cdot c_{r_flap} \quad (3.77)$$

$$b_{flap} = 0.40 \cdot b \quad (3.78)$$

$$c_{r_elevator} = 0.35 \cdot c_{r_HT} \quad (3.79)$$

$$c_{t_elevator} = \lambda_{HT} \cdot c_{r_elevator} \quad (3.80)$$

$$b_{elevator} = b_{HT} \quad (3.81)$$

$$S_{elevator} = \frac{1}{2} (c_{r_elevator} + c_{t_elevator}) \cdot b_{elevator} \quad (3.82)$$

$$c_{r_rudder} = 0.30 \cdot c_{r_VT} \quad (3.83)$$

$$c_{t_rudder} = \lambda_{VT} \cdot c_{r_rudder} \quad (3.84)$$

$$b_{rudder} = 0.95 \cdot h_{HT} \quad (3.85)$$

3.4.5. Fuselage Configuration Model

The fuselage design must be such that it must be large enough to contain the engine in the nose (Table 3.1) and the hopper tank. The length, width, and the height of the engine are given. Since the fuselage is to have a cylindrical shape, maximum diameter of the fuselage should be large enough to contain the engine in it. The diameter of the hopper tank is taken as the 70% of the maximum diameter of the fuselage. Since the hopper volume is a design parameter the corresponding length is found from;

$$L_{HopperTank} = \frac{Vol_{Hopper} \cdot 4}{\pi \cdot D_{HopperTank}^2} \quad (3.86)$$

$$L_f = L_{eng} + L_{HopperTank} \quad (3.87)$$

The nose and aft of the fuselage are taken as 30% and 20% of the overall length of fuselage respectively;

$$L_{f_N} = 0.30 \cdot L_f \quad (3.88)$$

$$L_{f_A} = 0.20 \cdot L_f \quad (3.89)$$

Fuselage mid-body length is;

$$L_{f_M} = L_f - L_{f_N} - L_{f_A} \quad (3.90)$$

The fuselage fineness ratio is defined as the fuselage length over diameter. The fineness ratio of 3 gives near minimum C_{D0} for subsonic flight [44].

$$Fineness\ Ratio = \frac{L_f}{D_{f\ max}} \quad (3.91)$$

Fuselage fineness ratio of 5.70 is suitable for drag minimization [45]. For circular mid-section fuselages where fineness ratio values equal to greater than 4.5 fuselage volume is [45];

$$Vol_f = \frac{\pi}{4} \cdot D_{f\ max}^2 \cdot L_f \cdot \left(1 - \frac{2}{Fineness\ Ratio}\right) \quad (3.92)$$

Then the wetted area is,

$$S_{wet_f} = \pi \cdot D_{f\ max} \cdot L_f \cdot \left(1 - \frac{2}{Fineness\ Ratio}\right)^{\frac{2}{3}} \cdot \left(1 + \frac{1}{Fineness\ Ratio^2}\right) \quad (3.93)$$

For streamline body fuselages the following formulas are used [45];

$$Vol_f = \frac{\pi}{4} \cdot D_{f\ max}^2 \cdot L_f \cdot \left(0.5 + 0.135 \cdot \frac{L_{fN}}{L_f}\right) \quad (3.94)$$

$$S_{wet_f} = \pi \cdot D_{f\ max} \cdot L_f \cdot \left(0.5 + 0.135 \cdot \frac{L_{fN}}{L_f}\right)^{\frac{2}{3}} \cdot \left(1.015 + \frac{0.3}{Fineness\ Ratio^{1.5}}\right) \quad (3.95)$$

$$S_{f_max\ frontal} = \frac{\pi \cdot D_{f\ max}^2}{4} \quad (3.96)$$

$$S_{wetFOR_f} = 1.2687 \cdot (h_{f\max} + w_{f\max}) \cdot L_{fN} \quad (3.97)$$

$$S_{wetMID_f} = 1.5706 \cdot (D_{f\max} + w_{f\max}) \cdot L_{fM} \quad (3.98)$$

$$S_{wetAFT_f} = \pi \cdot L_{fA} \cdot dg \cdot \left(1 - \frac{1}{3} \cdot \left(1 - \frac{D_{fbase}}{dg} \right) \cdot \left(1 - 0.18 \cdot \left(\frac{dg}{L_{fA}} \right)^{5/3} \right) \right) \quad (3.99)$$

Then total wetted area of the fuselage becomes;

$$S_{wet_f} = S_{wetFOR_f} + S_{wetMID_f} + S_{wetAFT_f} \quad (3.100)$$

The planform area is found using,

$$S_{plf_f} = \frac{\pi \cdot L_{fN} \cdot w_{f\max}}{4} + w_{f\max} \cdot L_{fM} + \frac{\pi \cdot L_{fA} \cdot (w_{f\max} - D_{fbase})}{4} + D_{fbase} \cdot L_{fA} \quad (3.101)$$

Finally, side projected area is calculated from the following equation,

$$S_{side_f} = \frac{\pi \cdot L_{fN} \cdot h_{f\max}}{4} + h_{f\max} \cdot L_{fM} + \frac{\pi \cdot L_{fA} \cdot (h_{f\max} - D_{fbase})}{4} + D_{fbase} \cdot L_{fA} \quad (3.102)$$

3.4.6. Propeller Model

It is necessary to determine the propeller diameter at the conceptual design phase. This diameter will also dictate the length of the landing gear since the propeller tip must clear the ground. It is well known that as the diameter gets larger the efficiency of the propeller is also increases [4].

In AAR design a three-blade, constant-speed propeller is chosen. The main concerns are such that the tip speed of the propeller should be less than the speed of sound. Consequently the tip speed is selected to be equal to the speed of sound at sea level,

$$V_{tip} = 1,117 \text{ ft / sec}$$

The tip speed of the propeller when the airplane is standing still is;

$$(V_{tip})_0 = \pi \cdot n \cdot D \quad (3.103)$$

The actual tip velocity relative to the airflow is;

$$V_{tip} = \sqrt{(V_{tip})_0^2 + V_\infty^2} \quad (3.104)$$

Then the diameter of the propeller can be found by substituting Eqn. (3.103) into Eqn. (3.104);

$$D = \sqrt{\frac{V_{tip}^2 - V_\infty^2}{\pi^2 \cdot n^2}} \quad (3.105)$$

Also propeller diameter is found as a function of horsepower [40];

$$\text{Three blade (agricultural)} : d = 20 \cdot \sqrt[4]{Hp}$$

It is assumed that an off-the-shelf propeller which has a diameter close to the one calculated is actually available.

3.4.7. Landing Gear Model and The Wing Location Estimation

The landing gear type of AAR is decided as tricycle arrangement in Section 3.1.9. This arrangement requires that the main wheels be aft of the c.g. of the airplane and an auxiliary wheel be forward of the c.g. In this way the aircraft stability during the ground roll becomes possible. So it allows the airplane to land at a very large “crab” (i.e. nose not aligned with the runway) angle. Main landing gear of AAR will retract into the boom while the boom will extend from the wing. So the location of the wing relative to fuselage has to be determined as a first step.

The c.g. location $\bar{x}_{c.g.}$, is calculated in the Center of Gravity Module. As a first guess the mean aerodynamic center of the wing is placed at the first estimate of the c.g. location without the wing. Then the weight of the wing is added to the calculations to obtain a better estimate.

Static stability considerations give the location of the wing which can be accepted for the conceptual design phase. Longitudinal stability requires that the aerodynamic center of the airplane, so called neutral point, must be behind the airplane’s center of gravity. Desired static margin for AAR is taken as 10%, and neutral point x_n location is found from Eqn. (3.106).

$$Static\ margin \equiv \frac{\bar{x}_n - \bar{x}_{c.g.}}{\bar{c}} \quad (3.106)$$

Under the assumption that the aerodynamic center of the wing-body (wing-fuselage) combination is very close to the aerodynamic center of the wing while the lift slope of tail and airplane are almost equal;

$$x_{a.c.wb} = (x_{a.c.})_{wing} \quad (3.107)$$

$$a_t = a \quad (3.108)$$

Then the location of the aerodynamic center of the wing body $x_{a.c.wb}$ may be found using the following relation:

$$x_{a.c.wb} = x_n - V_{HT} \cdot \frac{a_t}{a} \quad (3.109)$$

Since the wing will be located such that its mean aerodynamic center is x_{acwb} behind the nose of the airplane, the location of the leading edge of the root chord is;

$$x_{L.E.} = x_{acwb} - \bar{x} - \frac{\bar{c}}{4} \quad (3.110)$$

Next step is to place and size the landing gear. The center of the wing is a convenient place for the installation of the boom and the landing gear. The center position of the wing which equals to the distance of the main landing gear from the nose of the aircraft is found as,

$$x_{wingcenter} = x_{mainL.G.} = x_{L.E.} + \frac{c_r}{2} \quad (3.111)$$

The nose wheel is located so that it can be folded rearward and upward into the fuselage. Its location from the nose of the aircraft is estimated as 25% of the distance of the main landing gear location to the nose of the aircraft.

$$x_{noseL.G.} = 0.25 \cdot x_{mainL.G.} \quad (3.112)$$

The loads on the wheels are shown in Figure 3.5. The load carried by each wheel is represented by equal and opposite forces exerted on the wheel by the ground. F_N

denotes the force on the nose wheel; F_M denotes the total force on the two main wheels. Take off gross weight acts through center of gravity. These forces may be found from static equilibrium equations;

$$F_M = \frac{W_0 \cdot x_1}{x_3} \quad (3.113)$$

$$F_N = \frac{W_0 \cdot x_2}{x_3} \quad (3.114)$$

where;

$$x_3 = x_1 + x_2 \quad (3.115)$$

The tire sizes are estimated using the Eqn.(3.116) to Eqn.(3.119) below given in Ref.[40]

$$\text{Main wheel diameter} = 1.51 \cdot \left(\frac{F_M}{2} \right)^{0.349} \quad (3.116)$$

$$\text{Main wheel width} = 0.715 \cdot \left(\frac{F_M}{2} \right)^{0.312} \quad (3.117)$$

$$\text{Nose wheel diameter} = 1.51 \cdot (F_N)^{0.349} \quad (3.118)$$

$$\text{Nose wheel width} = 0.715 \cdot (F_N)^{0.312} \quad (3.119)$$

where all the dimensions are in *inches*.

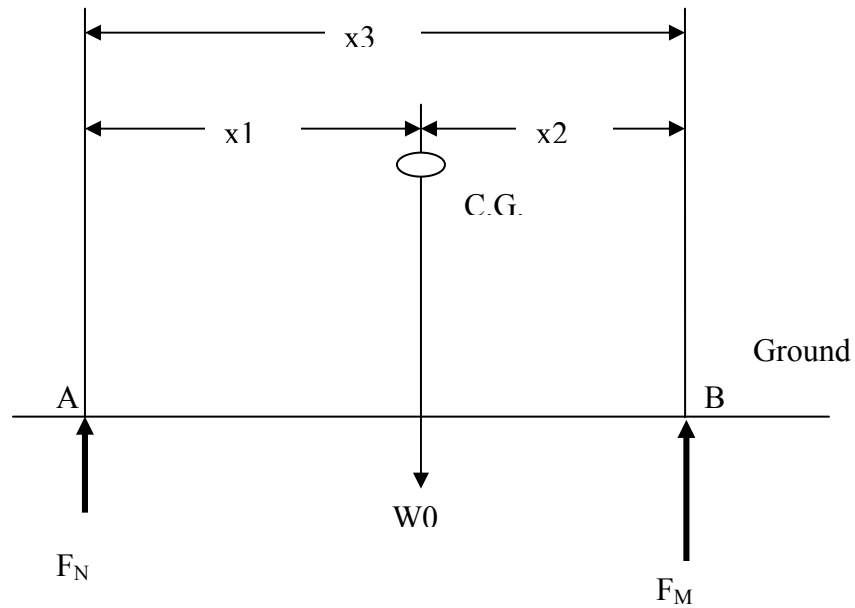


Figure 3.5. Force diagram for obtaining the load distribution among the tires [4]

The off-the-shelf tires from the manufacturers will be used. Consequently the tires that are close to the sizes calculated will be chosen.

In all these calculation it is assumed that the c.g. location is fixed. In detailed analysis the shift in c.g. position due to changes in hopper and fuel may be taken into account.

3.5. Agricultural Sizing Model

Agricultural model uses the spraying pattern given in Chapter II, flying at a spraying velocity which is 1.2 times the stall speed, $1.2 \cdot V_{stall}$. Since stall speed is not known at the beginning of the design, CS 23 regulations [39] are taken as a baseline. The item CS 23-49 of this regulation states that V_{SO} is the staling speed at which the air

vehicle is controllable with. And it is stated in this item that V_{SO} at maximum weight must not exceed 113 km/h (61 knots).

Ultra low volume ULV type is used for the AAR aerial spraying, Volume rate being 5 liters/ha for the AAR design. This value may be changed by the designer. Detailed information about volume rates are given in Table C.1 of Appendix C. The flow rate (liters/sec) of the spraying equipment is related to the volume rate, the airplane spraying speed and the effective swath width and found as;

$$FR = VR \cdot V_{spraying} \cdot w_{swath} \quad (3.120)$$

Then the spraying endurance is found as,

$$E_{spraying} = \frac{Vol_{hopper}}{FR} \quad (3.121)$$

and range over field is,

$$R_{spraying} = V_{spraying} \cdot E_{spraying} \quad (3.122)$$

According to the relative dimensions of the length and the width of the field area,

$$w_{field} = \sqrt{R_{spraying} \cdot b \cdot \frac{3}{10}} \quad (3.123)$$

$$l_{field} = \frac{10}{3} \cdot w_{field} \quad (3.124)$$

The field area is,

$$S_{field} = l_{field} \cdot w_{field} \quad (3.125)$$

Number of turns becomes,

$$Number\ of\ turns = \frac{w_{field}}{b} + 1 \quad (3.126)$$

3.6. Better Weight Estimate Model

The initial weight estimate is given in Section 3.2. A better weight estimate is possible using, the statistical group weights method [40]. The component weights are computed for general aviation aircraft according to Eqn.15.46 to Eqn.15.59 given in Ref.[40]. Also, in order to include the weight savings of each component, the fudge factors for composites in (Table 15.4 in Ref.[40]) are also taken into consideration where it is 0.85 for wing, 0.83 for tails, 0.90 for fuselage, and 0.95 for landing gears.

$$W_{wing} = 0.85 \cdot 0.036 \cdot S_w^{0.758} \cdot W_{fuel}^{0.0035} \cdot \left(\frac{A}{\cos^2 \Lambda} \right)^{0.6} \cdot q^{0.006} \cdot \lambda^{0.04} \cdot \left(\frac{100 \cdot t/c}{\cos \Lambda} \right)^{-0.3} \cdot (N_z \cdot W_0)^{0.49} \quad (3.127)$$

$$W_{horizontal\ tail} = 0.83 \cdot 0.016 \cdot (N_z \cdot W_0)^{0.414} \cdot q^{0.168} \cdot S_{ht}^{0.896} \cdot \left(\frac{100 \cdot t/c}{\cos \Lambda} \right)^{-0.12} \cdot \left(\frac{A}{\cos^2 \Lambda_{ht}} \right)^{0.043} \cdot \lambda^{-0.02} \quad (3.128)$$

$$W_{vertical\ tail} = 0.83 \cdot 0.073 * \left(1 + 0.2 \cdot \frac{H_t}{H_v} \right) \cdot (N_z \cdot W_0)^{0.376} \cdot q^{0.122} \cdot S_{vt}^{0.873} \cdot \left(\frac{100 \cdot t/c}{\cos \Lambda_{vt}} \right)^{-0.49}$$

$$\times \left(\frac{A}{\cos^2 \Lambda_{ht}} \right)^{0.357} \cdot \lambda_{vt}^{0.039} \quad (3.129)$$

$$W_f = 0.90 \cdot 0.052 \cdot S_f^{1.086} \cdot (N_z \cdot W_{dg})^{0.177} \cdot L_t^{-0.051} \cdot (L/D)^{-0.072} \cdot q^{0.241} + W_{press} \quad (3.130)$$

where W_{press} is the weight penalty due to pressurization. It is taken as zero.

Statistical value for the weight of landing gear is taken from Ref.[41]

$$W_{landing\ gear} = 0.043 \cdot W_0 \quad (3.131)$$

and the weight of the power plant can be found from Ref.[40] as;

$$W_{power\ plant} = 5.47 \cdot P_{av}^{0.78} \quad (3.132)$$

$$W_{hopper_tank} = 100\ kg\ \text{same as ZIU}$$

Fixed equipment includes hopper tank, flight controls, battery, electrical system, avionics, electronics and instruments, air conditioning, pressurizing, anti&, de-icing system and miscellaneous items. From Ref.[4] these are estimated to be;

$$W_{fixed\ equipment} = 0.1 \cdot W_0 \quad (3.133)$$

The weight of the agricultural system is taken as the same of ZIU.

$$W_{agricultural\ system} = 118\ kg$$

Then, the total empty weight becomes:

$$\begin{aligned}
 W_e = & W_{wing} + W_{fuselage} + W_{horizontal\ tail} + W_{vertical\ tail} + W_{landing\ gear} + W_{power\ plant} \\
 & + W_{agricultural\ system} + W_{fixed\ equipment}
 \end{aligned}
 \tag{3.134}$$

$$W_{payload} = Vol_{hopper} * \rho_{fertilizer}
 \tag{3.135}$$

where the chemical density is,

$$\rho_{chemical} = 1 \frac{kg}{m^3}$$

The gross weight is obtained as,

$$W_0 = W_e + W_{payload} + W_{fuel} + W_{fixed\ equipment}
 \tag{3.136}$$

This is an iterative process which starts with a first guess of W_0 . This process is repeated until convergence is obtained. A better weight estimate is obtained at the end of this process.

3.7. Center of Gravity Location Model

The locations of major weight components are estimated in fractions of center of gravity locations from 'nose' of components. The sketch of center of gravity locations is shown in Figure 3.6. A very preliminary estimation of center of gravity does not include the contributions of the wing, fuel tank, horizontal and vertical tails. Since their location

are not known at this stage. First, the center of gravities for engine, hopper, hopper tank and fuselage are found;

$$x_{c.g. engine} = 0.5 \cdot L_{eng} \quad (3.137)$$

$$x_{c.g. hopper\ tan\ k} = L_{eng} + \frac{L_{hopper\ tan\ k}}{2} \quad (3.138)$$

$$x_{c.g. payload} = L_{eng} + \frac{L_{hopper\ tan\ k}}{2} \quad (3.139)$$

$$x_{c.g. f} = 0.4 \cdot (L_f - L_{eng}) + L_{eng} \quad (3.140)$$

Then the center of gravity of the aircraft containing these major components is calculated by:

$$M_{c.g.} = x_{c.g. engine} \cdot W_{engine} + x_{c.g. hopper\ tan\ k} \cdot W_{hopper\ tan\ k} + x_{c.g. payload} \cdot W_{payload} + x_{c.g. f} \cdot W_f \quad (3.141)$$

$$W_{c.g.} = W_{engine} + W_{hopper\ tan\ k} + W_{payload} + W_f \quad (3.142)$$

$$\bar{x}_{c.g.} = \frac{M_{c.g.}}{W_{c.g.}} \quad (3.143)$$

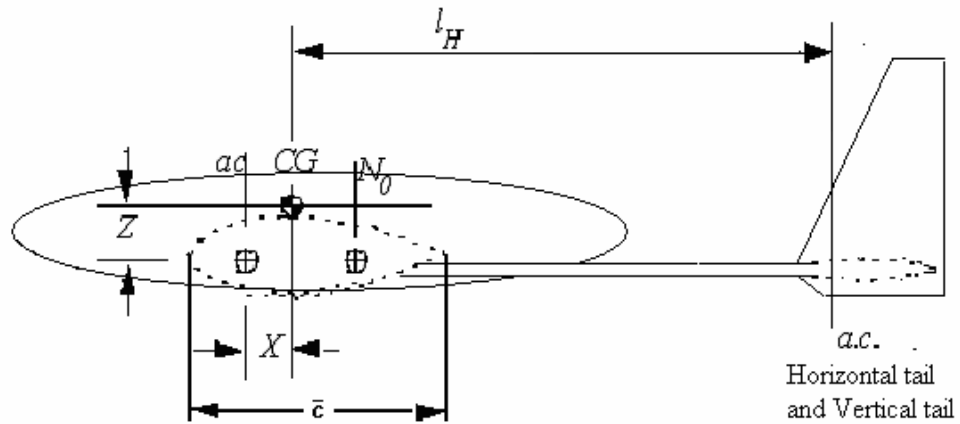


Figure 3.6. Sketch of AAR center of gravity locations

The contributions of wing and fuselage are taken into account in an approximate manner. To include the weight of the wing the mean aerodynamic center of the wing is placed at the c.g. location calculated above. In design process the wing will be relocated to achieve desired static margin. Also it is assumed that the mean aerodynamic center of the wing is 25% of the mean aerodynamic chord from the leading edge while the center of gravity of the wing is usually at the 40% of the mean aerodynamic chord.

$$x_{c.g. wing} = (0.40 - 0.25) \cdot \bar{c} \quad (3.144)$$

$$x_{c.g. fuel\ tank} = x_{c.g. w} \quad (3.145)$$

The contributions of the horizontal and vertical tails are also included in this step.

$$x_{c.g. HT} = l_{HT} \quad (3.146)$$

$$x_{c.g. VT} = l_{VT} \quad (3.147)$$

Finally, the center of gravity location of the aircraft measured from the nose of the aircraft can be found as,

$$M_{c.g.} = M_{c.g.} + x_{c.g.w} \cdot W_w + x_{c.g.fuel\ tan\ k} \cdot W_{fuel\ tan\ k} + x_{c.g.HT} \cdot W_{HT} + x_{c.g.VT} \cdot W_{VT} \quad (3.148)$$

$$W_{c.g.} = W_{c.g.} + W_w + W_{fuel\ tan\ k} + W_{HT} + W_{VT} \quad (3.149)$$

$$\bar{x}_{c.g.} = \frac{M_{c.g.}}{W_{c.g.}} \quad (3.150)$$

3.8. Aerodynamics Model

3.8.1. Lift Curve Slope Calculations

Lift curve slope $C_{L\alpha}$ can be found using the following semi-empirical formula given in Ref. [40]:

$$C_{L\alpha} = \frac{2 \times \pi \times A \times (S_{exp} / S_{ref}) \times F}{2 + \sqrt{(4 + \frac{(A\beta)^2}{\eta^2} (\frac{1 + \tan^2 \Lambda_{max,t}}{\beta^2}))}} \quad (3.151)$$

Wing sweep at maximum thickness station Λ_{max} is taken to be equal to the wing sweep at quarter chord location $\Lambda_{c/4}$. Then, aspect ratio and $\Lambda_{c/4}$ are a design variables while S_{exp} is given in Section 3.4.1.

β is calculated as,

$$\beta = 1 - M_{cruise}^2 \quad (3.152)$$

where cruise Mach number is found as,

$$M_{cruise} = \frac{V_{cruise}}{a_0} \quad (3.153)$$

Airfoil efficiency is found from,

$$\eta = \frac{c_{l\alpha}}{(2\pi / \beta)} \quad (3.154)$$

where the lift curve slope $c_{l\alpha}$ of the airfoil characteristics are given in Section 3.3.1.

Fuselage lift factor F accounts for the fact that fuselage of diameter D_{max} creates some lift due to the spill over of lift from the wing,

$$F = 1.07 \cdot \left(1 + \frac{D_{max}}{b}\right)^2 \quad (3.155)$$

3.8.2. Estimation of C_{D0} by Component Buildup Method.

The component buildup method estimates the subsonic parasite drag of each component of the aircraft using a flat-plate skin-friction drag coefficient (C_f) and a component “form factor” (FF) that estimates the pressure drag due to viscous separation. Then the interference effects on the component drag are estimated as a factor “ Q ” and the total component drag is determined as the product of the wetted area, C_f , FF , Q . Miscellaneous drags (C_{Dmisc}) for special features of aircraft such as flaps, un-

retracted landing gear, an upswept aft fuselage, and base area are then estimated and added to the total, along with estimated contributions for leakages and protuberances ($C_{DL\&P}$) [40].

$$(C_{D0})_{subsonic} = \frac{\sum (C_{f_c} \cdot FF_c \cdot Q_c \cdot S_{wet_c})}{S_{ref}} + C_{Dmisc} + C_{DL\&P} \quad (3.156)$$

Q is chosen in the light of explanations in Ref [40].

Table 9-1 Interference factor Q values [40]

	Wing	H- tail	Fuselage
Q	1.1	1.08	1

When the flow is laminar flow; flat plate skin friction coefficient is a function of Reynolds number:

$$Laminar : C_{f_c} = 1.328 \cdot \sqrt{Re} \quad (3.157)$$

In turbulent flow flat plate skin friction coefficient C_f depends on Mach number, skin roughness, Reynolds number and expressed by:

$$Turbulent : C_{f_c} = \frac{0.455}{(\log_{10} Re)^{2.58} \cdot (1 + 0.144M^2)^{0.65}} \quad (3.158)$$

which in most cases covers the whole aircraft. If the surface is relatively rough, the friction coefficient will be higher than indicated by the above equation. This may be accounted for using the “cut-off Reynolds number” [40].

Component Form Factor Calculations [40]

For wing and tail:

$$FF = \left[1 + \frac{0.6}{\left(\frac{x}{c}\right)_m} \cdot \left(\frac{t}{c}\right) + 100 \cdot \left(\frac{t}{c}\right)^4 \right] \cdot \left[1.34M^{0.18} \cdot (\cos \Lambda_m)^{0.28} \right] \quad (3.159)$$

For fuselage:

$$FF = \left(1 + \frac{60}{f^3} + \frac{f}{400} \right) \quad \text{where} \quad f = \frac{l}{d} = \frac{l}{\sqrt{\left(\frac{4}{\pi}\right) \cdot A_{max}}} \quad (3.160)$$

Fuselage:

$$Re_{FUS} = \frac{\rho \cdot V \cdot l_{FUS}}{\mu} \quad (3.161)$$

$$C_{f_{FUS}} = \frac{0.455}{(\log_{10} Re_{FUS})^{2.58} \cdot (1 + 0.144M^2)^{0.65}} \quad (3.162)$$

$$f_{FUS} = \frac{l_{FUS}}{d_{FUS}} = \frac{l_{FUS}}{\sqrt{\left(\frac{4}{\pi}\right) \cdot A_{max_FUS}}} \quad (3.163)$$

$$FF_{FUS} = \left(1 + \frac{60}{f_{FUS}^3} + \frac{f_{FUS}}{400} \right) \quad (3.164)$$

$$(C_{D0})_{FUS} = \frac{C_{f_{FUS}} \cdot FF_{FUS} \cdot Q_{FUS} \cdot S_{wet_FUS}}{S_{ref}} \quad (3.165)$$

Wing:

$$Re_{WING} = \frac{\rho \cdot V \cdot \bar{c}_{WING}}{\mu} \quad (3.166)$$

$$C_{f_{WING}} = \frac{0.455}{(\log_{10} Re_{WING})^{2.58} \cdot (1 + 0.144M^2)^{0.65}} \quad (3.167)$$

$$FF_{WING} = \left[1 + \frac{0.6}{\left(\frac{x}{c}\right)_{m_WING}} \cdot \left(\frac{t}{c}\right)_{WING} + 100 \cdot \left(\frac{t}{c}\right)_{WING}^4 \right] \cdot \left[1.34M^{0.18} \cdot (\cos \Lambda_{m_WING})^{0.28} \right] \quad (3.168)$$

$$(C_{D0})_{WING} = \frac{C_{f_{WING}} \cdot FF_{WING} \cdot Q_{WING} \cdot S_{wet_WING}}{S_{ref}} \quad (3.169)$$

Horizontal Tail:

$$Re_{HT} = \frac{\rho \cdot V \cdot \bar{c}_{HT}}{\mu} \quad (3.170)$$

$$C_{f_{HT}} = \frac{0.455}{(\log_{10} Re_{HT})^{2.58} \cdot (1 + 0.144M^2)^{0.65}} \quad (3.171)$$

$$FF_{HT} = \left[1 + \frac{0.6}{\left(\frac{x}{c}\right)_{m_HT}} \cdot \left(\frac{t}{c}\right)_{HT} + 100 \cdot \left(\frac{t}{c}\right)_{HT}^4 \right] \cdot \left[1.34M^{0.18} \cdot (\cos \Lambda_{m_HT})^{0.28} \right] \quad (3.172)$$

$$(C_{D0})_{HT} = \frac{C_{f_{HT}} \cdot FF_{HT} \cdot Q_{HT} \cdot S_{wet_HT}}{S_{ref}} \quad (3.173)$$

Vertical Tail:

$$Re_{VT} = \frac{\rho \cdot V \cdot \bar{c}_{VT}}{\mu} \quad (3.174)$$

$$C_{f_{VT}} = \frac{0.455}{(\log_{10} Re_{VT})^{2.58} \cdot (1 + 0.144M^2)^{0.65}} \quad (3.175)$$

$$FF_{VT} = \left[1 + \frac{0.6}{\left(\frac{x}{c}\right)_{m_{VT}}} \cdot \left(\frac{t}{c}\right)_{VT} + 100 \cdot \left(\frac{t}{c}\right)_{VT}^4 \right] \cdot \left[1.34M^{0.18} \cdot (\cos \Lambda_{m_{VT}})^{0.28} \right] \quad (3.176)$$

$$(C_{D0})_{VT} = \frac{C_{f_{VT}} \cdot FF_{VT} \cdot Q_{VT} \cdot S_{wet_{VT}}}{S_{ref}} \quad (3.177)$$

Miscellaneous Drag Effects

Landing Gear:

The landing-gear drag is estimated as the summation of the wheels, struts, and other gear components, refer to Table 12.5 in Ref.[40]:

$$\text{Tire frontal area} = D_{maingear} \cdot w_{maingear} \quad (3.178)$$

$$\left. \frac{D}{q} \right)_{main\ gear} = \frac{D/q}{\text{Frontal area (Ft}^2\text{)}} \Bigg)_{main\ gear} \cdot \text{main gear frontal area} \quad (3.179)$$

$$\text{Strut frontal area} = L_{strut} \cdot w_{strut} \quad (3.180)$$

$$\left(\frac{D}{q}\right)_{strut} = \frac{D/q}{\text{Frontal area (ft}^2)} \Bigg)_{strut} \cdot \text{strut frontal area} \quad (3.181)$$

$$(C_{D0})_{main\ gear} = \frac{\left(\frac{D}{q}\right)_{main\ gear}}{S_{ref}} \quad (3.182)$$

$$(C_{D0})_{strut} = \frac{\left(\frac{D}{q}\right)_{strut}}{S_{ref}} \quad (3.183)$$

$$(C_{D0})_{landing\ gear} = (C_{D0})_{main\ gear} + (C_{D0})_{strut} \quad (3.184)$$

Drag coefficient for nose landing gear is found in the same way.

To account for overall interference effects 20% additional drag is added.

Base area:

Base area produces a drag according to;

$$\left(\frac{D}{q}\right)_{base} = [0.139 + 0.419 \cdot (M - 0.161)^2] \cdot A_{base} \quad (3.185)$$

$$(C_{D0})_{base} = \frac{\left(\frac{D}{q}\right)_{base}}{S_{ref}} \quad (3.186)$$

Engine drag:

$$\left(\frac{D}{q}\right)_{engine} = (2 \times 10^{-4}) \cdot bhp$$

$$(C_{D0})_{engine} = \frac{\left(\frac{D}{q}\right)_{engine}}{S_{ref}} \quad (3.187)$$

Leakage and Protuberance Drag Effects:

For normal production propeller aircraft; leakage and protuberance effects ($L \& P$) are between 5%-10%. It is taken as 0.05 for AAR.

$$C_{DL\&P} = (L \& P) \times \left(\frac{\sum (C_{fc} \cdot FF_c * Q_c * S_{wet_c})}{S_{ref}} + C_{Dmisc} \right) \quad (3.188)$$

3.8.3. Drag Polar

The total drag is ;

$$(Total\ drag) = (parasite\ drag) + (induced\ drag) \quad (3.189)$$

Parasite drag coefficient composed of its value at zero lift C_{D0} and the increment in parasite drag due to lift $k1 \cdot C_L^2$ where $k1$ is proportionality constant. $k1$ is the coefficient which shows how sectional drag coefficient c_d is changed with c_l^2 , [4].

Induced drag coefficient is given by;

$$K = \frac{1}{\pi \cdot e \cdot AR} \quad (3.190)$$

Then the drag polar becomes;

$$C_D = C_{D0} + (k_1 + K) \cdot C_L^2 \quad (3.191)$$

3.8.4. Ground Effect

Ground effect is also considered in this study. It is a phenomenon of aerodynamics where the flow of air around the wing of an aircraft is interrupted by the ground. And it has an effect on the performance of AAR since it flies close to ground to perform its mission. In this case the induced drag is reduced due to the close proximity of the wings to the ground. This effect is simulated by multiplying the K by the factor given in Ref.[4];

$$\frac{C_{D_i} \text{ (in - ground effect)}}{C_{D_i} \text{ (out - of - ground effect)}} \equiv G = \frac{(16 \cdot h/b)^2}{1 + (16 \cdot h/b)^2} \quad (3.192)$$

It can be embedded into drag polar as;

$$C_D = C_{D0} + (k_1 + G \cdot K) \cdot C_L^2 \quad (3.193)$$

Whereas climbing out of ground effect will have the opposite effect.

3.9. Performance Model

The formulations given in Section 3.3.2 and Section 3.3.3 are used for the calculation of the stall speed, take off distance, landing distance, maximum airspeed and rate of climb values.

Range and endurance are calculated using the formulas for propeller-driven airplanes given in Ref.[4]. Range is given by,

$$R = \frac{\eta_{pr}}{c} \cdot \left(L/D \right)_{\max} \cdot \ln \frac{W_0}{W_{final}} \quad (3.194)$$

For range calculation 20% of fuel is taken as reserved.

$$W_{final} = W_0 - 0.8 \cdot W_{fuel}$$

Lift to drag ratio can be found as;

$$C_{L,\min} = \sqrt{\frac{C_{D0}}{K}} \quad (3.195)$$

$$C_{D0,\min} = 2 \cdot C_{D0} \quad (3.196)$$

$$\left(L/D \right)_{\max} = \frac{C_{L,\min}}{C_{D0,\min}} \quad (3.197)$$

$$\left(L/D \right)_{\max} = \frac{1}{2 \cdot \sqrt{C_{D0} \cdot K}} \quad (3.198)$$

The best endurance velocity is given by,

$$V_{best_range} = \sqrt{\frac{2 \cdot W_0}{\rho \cdot S}} \cdot \sqrt{\frac{K}{C_{D0}}} \quad (3.199)$$

$$E = \frac{\eta_{pr}}{c} \cdot \sqrt{2 \cdot \rho_\infty \cdot S} \cdot \frac{C_L^{3/2}}{C_D} \cdot \left(W_{final}^{-1/2} - W_0^{-1/2} \right) \quad (3.200)$$

The value of $\frac{C_L^{3/2}}{C_D}$ which is referred as $\frac{L/D}{loiter}$ is given by,

$$\frac{C_L^{3/2}}{C_D} = \frac{1}{4} \cdot \left(\frac{3}{K \cdot C_{D0}^{1/3}} \right) \quad (3.201)$$

The best endurance velocity is given by,

$$V_{best_endurance} = \sqrt{\frac{2 \cdot W_0}{\rho \cdot S}} \cdot \sqrt{\frac{K}{3 \cdot C_{D0}}} \quad (3.202)$$

Maximum load factor n , is calculated using below equation given in Ref.[6],

$$n_{max} = 2.1 + \frac{24000}{W_0 + 10000} \quad (3.203)$$

Turn performance characteristics such as turn radius, turn rate and bank angle are found using Ref.[4] as,

$$R_t = \frac{V_{turn}^2}{g \cdot \sqrt{n_{max}^2 - 1}} \quad (3.204)$$

In a sustained turn thrust must equal to the drag and lift must equal to the load factor n times the weight. Thus the maximum load factor for sustained turn can be expressed as the product of the thrust to weight ratio and lift to weight ratios. At “sustained” turn rate, the thrust of the aircraft is just sufficient to maintain velocity and altitude in the turn.

Sustained bank angle is calculated as,

$$\phi = \sqrt{n^2 - 1} \quad (3.205)$$

Then, the sustained turn rate equation is as follows [4]:

$$\dot{\psi} = \frac{g \sqrt{n^2 - 1}}{V} \quad (3.206)$$

3.9.1. Figure of Merits for Performance

The key relationships that define the best performance are known as figure of merit (FOM) expressions. These are used to compare the performance of two or more aircraft or to determine the effects of change in one or more of the physical characteristics of an aircraft upon its performance during the design process. These FOM expressions use basic external geometry dimensions and physical characteristics of AAR in an explicit manner rather than as the lift-to-drag ratio and the best-range speed, Ref.[46].

Some FOM expressions are given below,

1. Level flight

a. Range

i. Best mileage (ft/lb).

$$\text{Best mileage} = \frac{330 \cdot \eta_p}{\hat{c} \cdot \left(\frac{W_0}{b} \right)} \cdot \left(\frac{e}{S \cdot C_{D0}} \right)^{1/2} \quad (3.207)$$

ii. Maximum range (ft)

$$\text{Maximum range} = \frac{330 \cdot \eta_p \cdot W_f}{\hat{c} \cdot \left(\frac{W_0}{b} \right)} \cdot \left(\frac{e}{S \cdot C_{D0}} \right)^{1/2} \quad (3.208)$$

iii. Maximum-payload range (lb-ft)

$$\text{Maximum payload - range} = \text{Best mileage} \cdot W_{\text{payload}} \times W_f \quad (3.209)$$

iv. Best-range airspeed (ft/sec)

$$V_{\text{best range}} = 15 \cdot \left(\frac{W_0/b}{\sigma} \right)^{1/2} \cdot \left[\frac{1}{e \cdot (S \cdot C_{D0})} \right]^{1/4} \quad (3.210)$$

b. Endurance

i. Minimum fuel-flow rate (lb/h)

$$\text{Minimum fuel-flow rate} = \frac{0.04 \cdot \hat{c}}{\eta_p} \cdot \left(\frac{\left(\frac{W_0}{b} \right)}{\sigma} \right)^{1/2} \cdot \left(\frac{S \cdot C_{D0}}{e^3} \right) \quad (3.211)$$

ii. Maximum endurance (h)

$$\text{Maximum endurance} = \frac{W_f}{\text{Minimum fuel-flow rate}} \quad (3.212)$$

c. Fastest airspeed (ft/sec)

$$V_{\max} = 50 \cdot \left(\frac{\eta_p \cdot P_{av}}{\sigma \cdot (S \cdot C_{D0})} \right)^{1/3} \quad (3.213)$$

2. Vertical flight

a. Minimum take-off run (ft)

$$TOG_{\min} = \frac{1.2 \cdot W_0^{2.5}}{\eta_p \cdot \sigma^{1.5} \cdot P_{av} \cdot (S \cdot C_{L_{\max,TO}})^{1.5}} \quad (3.214)$$

b. Maximum ceiling (ft)

$$h_{\max} = 20000 \cdot \ln \left[\frac{32 \cdot \eta_p \cdot P_{av}}{\sigma_{cr} \cdot \left(\frac{W_0}{b} \right)^{1.5}} \cdot \left(\frac{e^3}{S \cdot C_{D0}} \right)^{1/4} \right] \quad (3.215)$$

c. Climbing flight

i. Steepest climb angle (deg)

$$\gamma_{\max} = 1600 \cdot \left\{ \frac{e \cdot [\eta_p \cdot P_{av}]^2}{W_0 \cdot \left(\frac{W_0}{b} \right)^2} \right\} \quad (3.216)$$

ii. Maximum rate of climb (fpm)

$$ROC_{\max} = \frac{33000}{W_0} \cdot \left[\eta_p \cdot P_{av} - 0.04 \cdot \left(\frac{W_0}{b} \right)^{1.5} \cdot \left(\frac{S \cdot C_{D0}}{e^3} \right)^{1/4} \right] \quad (3.217)$$

iii. Minimum time to altitude (min)

$$t_{\min} = \frac{61000}{ROC_{\max}} \cdot \left[\exp\left(\frac{h}{H}\right) - 1 \right] \quad (3.218)$$

3. Turning flight

a. Maximum load factor (g's)

$$n_{\max} = \frac{8.5}{W_0/b} \cdot \left[(\eta_p \cdot P_{av})^2 \cdot \left(\frac{e^3}{S \cdot C_{D0}} \right)^{1/2} \right]^{1/3} \quad (3.219)$$

b. Fastest turning rate (deg/s)

$$\dot{\chi}_{\max} = \frac{1900 \cdot \eta_p \cdot e \cdot P_{av}}{\left(\frac{W_0}{b} \right)^2} \quad (3.220)$$

c. Tightest turn (minimum radius turn) (ft)

$$r_{\min} = 0.023 \cdot \left[\frac{\left(W_0/b \right)^2}{\eta_p \cdot e \cdot P_{av}} \right]^2 \quad (3.221)$$

Another figure of merit is the gross figure of merit (GFOM), which is a good measure showing the effect of a number of parameters at the same time. It is the product of the wing span loading $\left(W_0/b \right)$, the equivalent flat-plate area $(S \cdot C_{D0})$, and the operational empty weight fraction $\left(W_e/W_0 \right)$ [46].

$$GFOM = \left(W_0/b \right) \cdot (S \cdot C_{D0}) \cdot \left(\frac{W_e}{W_0} \right) \quad (3.222)$$

CHAPTER IV

MULTI OBJECTIVE OPTIMIZATION OF THE AGRICULTURAL AERIAL ROBOT (AAR)

4.1. Problem Formulation

In this chapter a recently developed multi objective simulated annealing algorithm, called Multiple Cooling Multi Objective Simulated Annealing algorithm [5] is used for the single and bi-objective optimization studies of the AAR. For this purpose MCMOSA algorithm is coupled with the Aircraft Design Program (ADP) written in FORTRAN, developed for the conceptual design of AAR.

The main design problem is to minimize the take off gross weight of the Agricultural Aerial Robot (AAR) with an engine power of 500 horsepower and a payload of 1500lt hopper. The design mission has eleven mission segments; warm-up, taxi, takeoff, climb, cruise, descent, loiter, climb, cruise, descent and landing. Besides this problem a set of other cases are also examined.

Take off gross weight was selected as the main objective function since it represents a composite measure of merit for the aircraft as a system. The take off gross weight includes the empty weight, payload weight and the fuel weight. The empty weight together with the payload weight may be considered proportional to the initial acquisition cost of the aircraft. The fuel weight, on the other hand represents the yearly recurring costs of aircraft operations. Thus, an aircraft that has a lower take off gross weight, may also mean an aircraft with a lower operational cost as well.

Two main types of configuration are considered. In the first type a fixed engine with a constant available power of 500 hp is optimized. In this case depending on the objective function hopper volume is either taken as a design variable or a constant value of 1500 liters is used. In the second type the required power is calculated from performance requirements. A regression formula is used to calculate the mass of the engine that satisfies power requirements. However, the dimensions are taken as constant (i.e., equal to the dimensions of the 500 hp engine considered above). Thus, engine power is the minimum needed and the hopper volume is fixed to 1500 liters.

Two different wing profiles are used for each of the AAR design optimization problems: NACA 23015 and NACA 63₂615. Consequently, a total of six or cases are considered in this study. All these cases are summarized in Table 4.1.

Table 4.1. Configurations considered in the design optimization studies

Engine Power	Hopper Volume	Wing Profile	Case
Fixed	1500 lt	NACA 23015	A
		NACA 63 ₂ 615	B
	Design Variable	NACA 23015	C
		NACA 63 ₂ 615	D
Lowest power needed	1500 lt	NACA 23015	E
		NACA 63 ₂ 615	F

The relationships that define various performance metrics are known as figure of merit expressions which are explained in Section 3.9.1. These figures of merit expressions may be used to compare the performances of two or more aircrafts. It may also be used to determine the effects of changes in one or more of the physical characteristics of an aircraft on its particular performance. The figures of merit expressions use individual and specific characteristics, such as weight, wing area, wingspan, and thrust, which are quite useful for the design process [46].

While comparing different configurations the data needed to obtain the configurations and performances of the aircraft are the zero lift drag coefficient C_{D0} , the Oswald efficiency e , the specific fuel consumption c , the propeller efficiency η_p . C_{D0} and e values are calculated by Aircraft Design Program (ADP). c and η_p values are equal to those of ZIU.

Take off gross weight W_0 is taken as objective. Other data such as, the wing span b and the payload weight W_{hopper} are chosen as the design variables, and in some cases they are also treated as objectives to be optimized depending on the problem. The wing area S , the empty weight W_e and the fuel weight W_{fuel} are calculated in ADP.

The groupings such as the ratio of the aircraft weight to the wing span, W_0/b , with the dimension of lb/ft is used in this thesis. This ratio is also referred as span loading. Reducing the magnitude of the span loading usually improves many, aspects of the performance of an aircraft. The second is the product of the wing area and the zero lift drag coefficient SC_{D0} , with the dimensions of ft^2 . It is also referred as equivalent flat-plate area. For all aspects of performance the lowest possible value for SC_{D0} is desired. It is a measure of the lowest possible drag [46].

For each case the single objective problems are treated while comparing the figure of merit expressions for different cases and configurations. Then, multi objective problems are solved. These figures of merit expressions are also considered and compared for different cases and configurations for multi objective problems.

4.2. Analysis and Optimization Software

Aircraft Design Program (ADP), developed in this thesis may be used for trade studies, and also for preliminary performance predictions. This FORTRAN code offers a tool which combines analysis methods for each discipline (aerodynamics, performance, weight, configuration sizing) for initial layout design, sizing to a mission profile, and prediction of preliminary aerodynamics and performance. Thus, the code has geometry modules for design layout, and analysis modules for aerodynamics, performance and weights. Also included is aircraft initial sizing (mission analysis). The mathematical models used in the code are from the textbooks which are distilled from the classical and time-proven first-order techniques commonly used in aircraft industry [4, 40, 41, and 46]. These models are given in Chapter III. This code when coupled with the MCMOSA algorithm, automates the analysis to obtain a family of optimum solutions. At this stage, no graphical user interface is programmed. Consequently, ADP is run using the inputs entered by the user in a text file.

The *Configuration Module* permits rapidly developing initial aircraft geometry for conceptual design purposes. The design capabilities of this module include wing, horizontal tail, vertical tail, fuselage, power plant and landing gear. Wing and tails are defined by the trapezoidal planform geometry parameters such as area, aspect ratio, and sweep. Also, wing fuel tanks are defined and sized for the needed volume of fuel. This configuration data is then used by the Aerodynamics, Performance and Weight modules.

The *Aerodynamics Module* estimates lift curve slope, parasite drag (subsonic and supersonic), drag due to lift. Analysis methods are based on classical techniques as well as semi-empirical formulas. Subsonic parasite drag of each component of the aircraft is estimated by using the component buildup method. Drag due to lift is calculated by the Oswald span efficiency method [40].

Maximum Lift Module estimates the maximum lift coefficient using the airfoil data. Also the mathematical model used in this module permits the calculation of maximum lift coefficients for take off and landing configurations where flaps are partially, as well fully down.

Statistical group weights method [40] is used in *Weights and Balance Module* to estimate take off gross weight W_0 . Results including structures group weight (fuselage, wing, etc...), propulsion group, equipment group, and useful load group. Factors permit estimation of the weight impact of non-standard materials and other emerging technologies. It is desired to manufacture AAR from composite material. The corresponding factors are also used in mathematical model. Center of gravity is determined from individual component locations.

The horsepower, specific fuel consumption, the dimensions of the engine, the calculation of the diameter of the propeller and clearance of spinner for piston-propeller engine are given in *Propulsion Module*.

Initial Sizing Module deals with 11 missions segments (warm up, taxi, takeoff, climb, cruise, etc...). AAR is sized to the given mission, resulting in the sized design takeoff weight and the fuel weight to perform that mission. It is also possible to analyze the as-drawn aircraft for range and loiter.

Performance Module calculates takeoff, landing, climb and turn performance characteristics. A set of figures of merit is selected for performance. Performance constraints for requirements such as takeoff distance and landing distance are also included. The multi objective optimizer permits rapid simultaneous optimization for W_0/S , aspect ratio, sweep, taper ratio, and thickness ratio, with minimization of a selected weight parameter as well satisfaction of numerous other performance constraints. It is possible to quickly find the effect of parametric variations in parasite drag, drag due to lift, specific fuel consumption, payload weight, and range on aircraft gross and empty weight

The results were verified against a commercial software package: AAA Program [47] during the development phases. But this verification study is not included in this thesis.

Figure 4.1 shows how these analysis and optimization tools are coupled to perform optimization of AAR configuration.

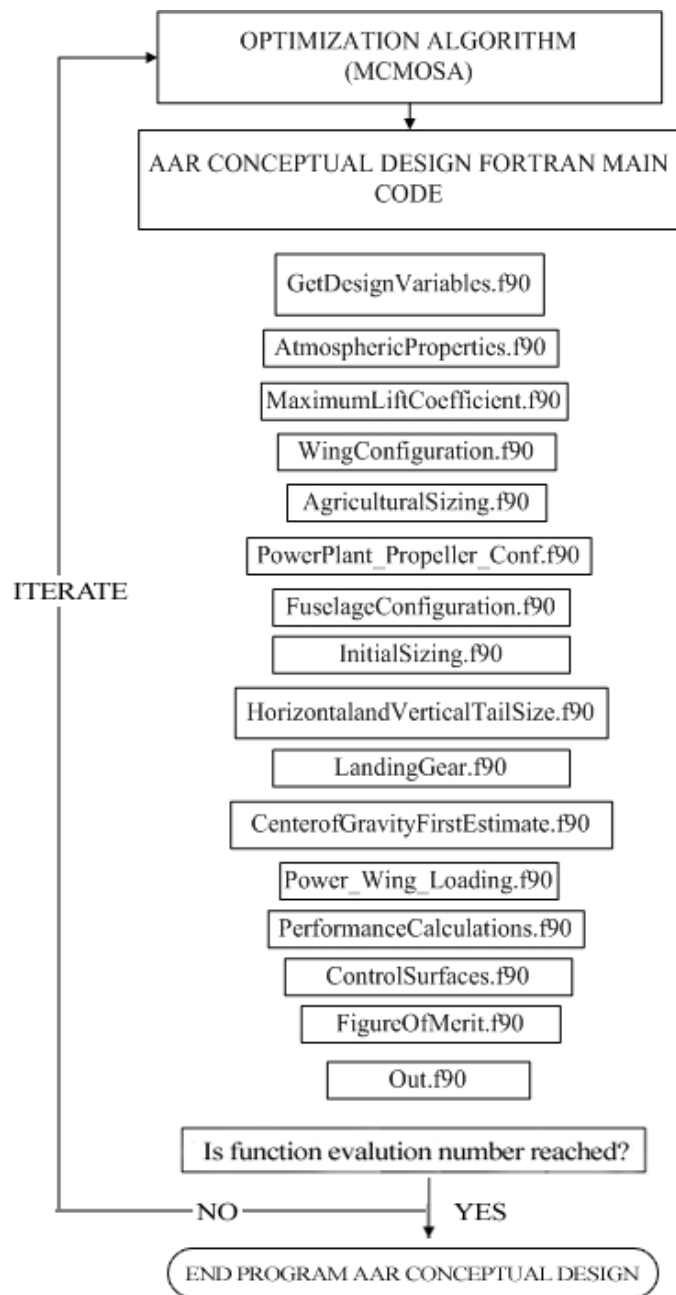


Figure 4.1. Flow chart of the conceptual design code and the optimization algorithm

4.3. AAR Design Parameterization

In the design scheme of AAR there are two sets of parameters. The first set is composed of design variables, varied by the optimization program, MCMOSA. The second set of parameters are pre-assigned, and fixed. Their values are chosen referring to the competitors and ZIU.

There are 15 design variables used in the optimization of AAR configuration (Table 4.2). They are related to the geometrical properties and the hopper amount. Six of these variables describe the geometric layout of the wing, three variables describe the geometric layout of the horizontal tail, and three variables describe the geometric layout of the vertical tail. Only one variable define the fuselage maximum diameter and the last one defines the volume of the hopper. Engine power is also an optimization variable in certain problems. The upper, lower values for these variables are decided with reference to the competitor aircrafts, as well as operational considerations, while the initial values are taken equal to those values of ZIU (Table 4.2). There are other pre-assigned parameters are kept fixed during optimization. These are given in Table 4.3. The airfoil related pre-assigned parameters and their values are listed in Table 4.4. These are also fixed during optimization.

Constraints on geometrical and performance related parameters are listed in Table 4.5. The performance related constraints on the stall speed at landing configuration and the maximum load factors are based on the requirements given in Ref. [33].

Table 4.2. Design variables upper and lower bounds together with prescribed initial values

Design Variable (x) Number	Variable Description	Lower Value	Upper Value	Initial Value
1	Wing span(ft), b	35.	45.	45.486
2	Wing aspect-ratio, AR	5.5	10.	6.45
3	Wing taper ratio, λ_w	0.5	1.0	1.0
4	Wing incidence (deg), i_w	0.0	3.0	2.0
5	Wing sweep (deg), Λ_w	0.0	7.0	0.0
6	Wing dihedral (deg), Γ_w	0.0	9.0	7.0
7	Horizontal tail taper ratio, λ_{HT}	0.5	1.0	1.0
8	Vertical tail taper ratio, λ_{VT}	0.5	1.0	0.478
9	Horizontal tail sweep (deg), Λ_{HT}	0.0	7.0	0.0
10	Vertical tail sweep (deg), Λ_{VT}	0.0	15.0	13.584
11	Horizontal aspect-ratio (deg), AR_{HT}	3.40	8.26	3.91
12	Vertical tail aspect-ratio (deg), AR_{VT}	0.78	2.27	1.492
13	Fuselage maximum diameter (ft), $D_{f\max}$	3.0	4.278	4.278
14	Hopper Volume (liters), Vol_{Hopper}	500.	1500.	1500.0

Table 4.3. Pre-assigned design parameters and their values

Pre-assigned Variable Number	Variable Description	Value
1	Fuel density	43.7
2	Specific fuel consumption (lb/hp/hr)	0.44
3	Horizontal tail volume ratio	0.5
4	Vertical tail volume ratio	0.04
5	Horizontal tail dihedral	0.0
6	Vertical tail dihedral	0.0
7	Height of vertical tail portion hiding inside the fuselage	0.0
8	Cruise velocity (ft/sec)	168.0
9	Maximum cruise velocity (ft/sec)	255.2

Table 4.4. Pre-assigned variables of airfoils and their values

Pre-assigned Variable Number	Variable Description	Wing profile NACA 23015	Wing profile NACA 63,615	Tail profile NACA 0012
1	Sectional maximum lift coefficient ($c_{l_{max}}$)	1.7	1.67	1.5
2	Sectional zero-lift angle-of-attack (α_0)	-1.2	-3.8	0.0
3	Sectional lift curve slope, (rad^{-1}) ($c_{l\alpha}$)	5.9588	6.875	6.2504
4	Thickness to chord ratio, (t/c)	0.15	0.15	0.12
5	Chord-wise location of the airfoil maximum thickness point ($(x/c)_{max}$)	0.25	0.3	0.3
6	Sectional lift coefficient at zero angle of attack, (c_{l0})	0.10	0.40	0.0
7	Sectional drag coefficient at zero angle of attack, (c_{d0})	0.0062	0.0049	0.0058
8	Sectional moment coefficient wrt. aerodynamic center, (rad^{-1}), ($c_{m.a.c.}$)	-0.007	-0.11	0.0

Table 4.5. Constraints

Constraint number	Geometric Constraints
1	Horizontal tail area $\leq 57.05 \text{ ft}^2$
2	Wing area $\leq 320.55 \text{ ft}^2$
3	Vertical Tail Area $\leq 33.05 \text{ ft}^2$
4	Fuselage length $\leq 20 \text{ ft}$
5	Root chord length $\leq 10. \text{ft}$
	Performance Related Constraints
6	Stall speed at landing configuration $\leq 102.95 \text{ knot}$
7	Take off distance $\leq 1000.0 \text{ ft}$
8	Landing distance $\leq 1640.4 \text{ ft}$
9	Maximum load factor $\leq 3.8 \text{ g}$

The performance figures of merit for ZIU are also calculated and tabulated in Table 4.16. All results are compared with these values.

4.4. The Single Objective Optimization Problems

Before addressing a multi objective optimizations, two different single-objective optimization problems are solved.

The first problem is to find the optimum configuration using a fixed engine of 500 hp, and a payload of 1500 liters i.e., Cases A and B in Table 4.1. The objectives of the single-objective are listed below:

1. Minimize takeoff gross weight, W_0
2. Minimize equivalent flat plate area, $S \cdot C_{D0}$
3. Minimize take-off distance
4. Maximize endurance, E

The next one uses hopper volume as an optimization variable as well as an objective, while engine power is still fixed to 500 Hp. They correspond to Cases C and D in Table 4.1.

5. Maximize hopper volume Vol_{hopper}

The design variables and optimization results are given for Cases A and C in Table 4.6 and Table 4.7 which corresponds to NACA 23015, Cases B and D. The results that correspond to NACA 63₂615 are given in Table 4.8 and Table 4.9. In the last columns of these tables design variables and performance figures of merits for ZIU are also given. Program termination is based on the number of function evaluations. In all single objective runs, the number of function evaluations is taken as 10000. This numbers give the instant the optimization program is terminated. The constraints given in Table 4.5 were also satisfied in all cases.

The figures of merit are calculated for each case, using the expressions of Section 3.9.1. Although the primary purpose of these figures of merit is either to compare one or more cases with each other or to evaluate the effects of modifying the characteristics of an individual aircraft, the values themselves are representative of the sea level performance of the aircraft.

When the output of each case for NACA 23015 is compared with the values calculated for the baseline, ZIU, it is apparent that they all have better performance

figures than ZIU. For example if the GFOM with the values of Table 4.7 and Table 4.9 are compared with the values given for ZIU, it may be observed that they all have a much lower GFOM values than that of ZIU. GFOM is definitely a gross figure of merit and that is primarily a measure of the relative performance at level flight, particularly range. Although it provides no details on comparative performance, the GFOM approach is quick and easy to use. Furthermore it emphasizes the importance of the design parameters namely the span loading $\left(\frac{W_0}{b}\right)$, the equivalent flat-plate area $(S \cdot C_{D0})$, the operational empty weight fraction $\left(\frac{W_e}{W_0}\right)$. When using the GFOM, the smaller the value is the better performance. This is contrary to the majority of the FOM's.

When the cases are compared with each other the results obtained by maximizing endurance, i.e. objective 4 (column 4, Table 4.7) appears to be the best at first glance in most areas of performance. It has the best GFOM value. In level and climbing flight, it is better, particularly with respect to the wing span loading, lift to drag ratio, endurance, maximum-payload range, maximum rate of climb and tightest turn radius, by virtue of its lower span loading. Unfortunately it is the heaviest one. It has a take off gross weight 4 percent more than the first column where the objective is to minimize the take off gross weight. In any design there is not a unique design which is best from all aspects. While maximizing a figure of merit (objective) others may deteriorate. For example when the objective is to minimize the take off distance the wing loading is also minimized (Table 4.7). However it is not the lightest aircraft.

The performance of the first and the second column are penalized due to their larger wing loadings $\left(\frac{W_0}{S}\right)$, where the objectives are to minimize the take off gross weight and the equivalent flat plate area respectively. Decreased $\left(\frac{W_0}{b}\right)$ with respect to other cases improves the range performance of column 4 that has an objective of

minimizing endurance. The take off distance of in column 3 of Table 4.7 is decreased by increasing the wing area rather than increasing the lift coefficient or the power available since they are constant. This results in an increase in equivalent flat plate area ($S \cdot C_{D0}$), and the take off gross weight.

When the results using NACA 63₂615 (Table 4.9) are examined, no truly significant differences with Table 4.7 may be observed. Performance figures of merit show the same trend.

These two different airfoils have different sectional force coefficients. For example NACA 63₂615 has a minimum drag coefficient $c_{d,\min}$ less than NACA 23015, besides its maximum lift coefficient $c_{l,\max}$, is close to that of NACA 23015 (see Chapter III, Table 3.3). These are the characteristics that will affect the overall drag polar of the aircraft and the performance as well. However the analysis concept in ADP is focuses on point performance characteristics. It does not deal with stability considerations in which the differences of two airfoils may be more clearly observed. In this thesis the mathematical model for aerodynamics is such that while calculating the parasite drag coefficient of the aircraft the component build up method is used. This method takes into consideration only the geometrical properties of the components of the aircraft. It does not consider the sectional characteristics. The slight difference between maximum lift coefficients is the only thing that shows the difference of these two airfoils. The stall speeds also differ slightly due to maximum lift coefficients. Consequently the results for two airfoils differ only slightly as it is expected.

From Tables 4.6 to 4.9 the effect of design variables on the objectives may be observed. In the first case (minimizing take off gross weight) it is seen that the wing span b , has the lowest value among all solutions. This leads to a smaller wing area S , value. But reduced wing area results in a longer take off distance TOD . When the the

equivalent flat plate area ($S \cdot C_{D0}$) is minimized, it may be observed from the table that the design variable values are rather close to the values obtained in the minimum weight problem. This is due to the nature of the aircraft design problem. When minimizing the equivalent flat plate area the take off gross weight is also minimized. In the third case (minimizing take off distance) optimization code maximizes the wing area, close to the wing area of ZIU, with a wing span slightly larger than that of ZIU. Besides the wing incidence, sweep and the dihedral angles are the greatest. In maximizing the endurance, design variables such as wingspan value and the aspect ratio are the largest of all other cases as expected. This results in largest lift to drag ratio, lowest wingspan loading, GFOM, and fuel flow rate, as well as best mileage together with the endurance. For the fifth objective (maximizing hopper volume), the fuselage diameter is increased so that the hopper volume can be maximized. But it has a weight penalty with a higher parasite drag value. Most of its design variable values are close to the values obtained in minimizing the *TOD*.

Similar trends are obtained when the optimizations are carried out for NACA 63₂615 (Table 4.9 and Table 10).

Table 4.6. Single objective optimization results for design variables using NACA 23015 with a fixed engine power of 500 Hp

	CASE A	CASE A	CASE A	CASE A	CASE C	ZIU
	Minimize W_0	Minimize $S.C_{D0}$	Minimize TOD	Maximize $Endurance$	Maximize $Hopper Volume$	
b	38.63	38.75	47.49	53.95	46.08	45.49
AR	5.54	5.57	7.05	9.99	8.22	6.45
λ_w	0.50	0.56	0.88	0.91	0.82	1.0
i_w	0.34	0.21	2.53	1.66	2.11	2.0
Λ_w	0.80	3.29	4.68	2.09	4.42	0.0
Γ_w	4.81	3.85	6.57	1.25	7.07	7.0
λ_{HT}	0.83	0.57	0.71	0.77	0.62	1.0
λ_{VT}	0.83	0.51	0.80	0.75	0.73	0.465
Λ_{HT}	6.39	4.58	1.28	3.54	1.81	0.0
Λ_{VT}	4.12	4.54	7.76	2.61	8.50	13.584
AR_{HT}	6.81	8.14	5.98	3.85	4.75	3.91
AR_{VT}	0.92	1.29	0.79	1.21	1.07	1.48
$D_{f\max}$	3.01	3.01	3.01	3.00	3.51	4.28

Table 4.7. Single objective optimization results for objectives using NACA 23015 with a fixed engine power of 500 Hp. Various figure of merit values are also given

	CASE A	CASE A	CASE A	CASE A	CASE C	ZIU
	Minimize W_0	Minimize $S.C_{D0}$	Minimize TOD	Maximize $Endurance$	Maximize $Hopper Volume$	
Gross Weight (lb) *	5895.36	5903.90	6060.13	6136.43	6066.18	7718.0
SCD_0 * (ft ²)	4.49	4.51	5.22	4.92	5.06	7.69
Minimum take-off distance * (ft)	999.00	999.96	878.01	980.47	947.33	902.23
Maximum endurance (hr)	2.90	2.91	3.22	3.39	3.23	2.18
Vol_{Hopper}	1500.00	1500.00	1500.00	1500.00	1499.98	1500.0
S (ft ²)	269.37	269.69	319.95	291.43	296.53	320.55
CD_0 *	1.668E-02	1.674E-02	1.631E-02	1.688E-02	1.707E-02	2.411E-02
Minimum take-off run (ft) *	796.11	797.55	658.85	781.98	740.28	990.87
Wing loading * (lb/ft ²)	21.89	21.89	18.94	21.06	20.46	24.08
Horsepower to weight ratio (HP/lb)	8.481E-02	8.469E-02	8.251E-02	8.148E-02	8.242E-02	6.48E-02
Aspect ratio	5.54	5.57	7.05	9.99	8.03	6.46
Max. Lift to Drag ratio	15.18	15.18	16.86	18.75	17.30	13.00
Wing span loading * (lb/ft)	152.60	152.35	127.61	113.75	124.30	169.66
GFOM *	209.08	210.32	215.76	186.28	204.56	644.68
Best mileage (ft/lb)	9205.41	9194.02	9945.81	10924.06	10192.47	6397.60
Maximum_range (ft)	1.852E+06	1.849E+06	1.832E+06	1.895E+06	1.843E+06	3.95E+06
Stall speed @TO(ft/sec)	108.59	108.60	101.02	106.51	104.99	102.00
Best range airspeed (ft/sec)	201.27	200.92	179.66	176.56	180.20	181.94
Minimum fuel flow rate * (lb/hr)	69.27	69.23	57.23	51.20	56.01	90.09
Fastest airspeed (ft/sec)	337.27	336.74	320.84	327.21	324.12	279.30
Maximum ceiling (ft)	30711.73	30721.63	34530.78	36755.37	34960.98	22793.12
Maximum rate of climb (fpm)	1564.68	1562.75	1636.17	1672.17	1646.06	1073.03
Maximum load factor (g_s)	2.21	2.21	2.51	2.71	2.55	1.80
Fastest turning rate (deg/sec)	28.83	28.90	39.10	44.46	39.83	22.44
Tightest turn * (ft)	99.88	99.43	54.32	42.00	52.34	164.86

*The smaller the value, the better the performance

Table 4.8. Single objective optimization results for design variables using NACA 63₂615 with a fixed engine power of 500 Hp

	CASE B	CASE B	CASE B	CASE B	CASE D	ZIU
	Minimize W_0	Minimize $S.C_{D0}$	Minimize TOD	Maximize $Endurance$	Maximize $Hopper Volume$	
b	38.85	39.46	47.89	53.77	42.61	45.49
AR	5.51	5.66	7.16	9.94	6.25	6.45
λ_w	0.56	0.57	0.69	0.53	0.82	1.0
i_w	1.25	1.35	2.13	1.16	2.71	2.0
Λ_w	4.00	1.09	4.28	4.38	2.43	0.0
Γ_w	3.37	2.72	3.24	6.03	7.91	7.0
λ_{HT}	0.81	0.84	0.57	0.83	0.77	1.0
λ_{VT}	0.62	0.59	0.62	0.66	0.86	0.465
Λ_{HT}	2.19	0.68	3.79	6.16	5.55	0.0
Λ_{VT}	5.73	4.08	13.68	13.39	5.27	13.584
AR_{HT}	4.77	3.42	7.95	4.36	4.53	3.91
AR_{VT}	1.60	0.84	2.01	1.28	2.25	1.48
$D_{f\max}$	3.00	3.00	3.00	3.00	3.11	4.28

Table 4.9. Single objective optimization results for objectives using NACA 63₂615 with a fixed engine power of 500 Hp. Various figure of merit values are also given

	CASE B	CASE B	CASE B	CASE B	CASE D	ZIU
	Minimize W_0	Minimize $S.C_{D0}$	Minimize TOD	Maximize $Endurance$	Maximize $Hopper Volume$	
Gross Weight (lb) *	5911.72	5909.97	6077.42	6122.73	5984.65	7718.0
SCD_0 * (ft ²)	4.44	4.38	5.14	4.77	4.85	7.69
Minimum take-off distance * (ft)	1000.00	996.51	892.51	992.85	960.59	902.23
Maximum endurance (hr)	2.96	2.98	3.28	3.44	3.07	2.18
Vol_{Hopper}	1500.00	1500.00	1500.00	1500.00	1499.98	1500.0
S (ft ²)	274.11	274.97	320.53	291.00	290.71	320.55
CD_0 *	1.619E-02	1.592E-02	1.603E-02	1.638E-02	1.668E-02	2.411E-02
Minimum take-off run (ft)*	797.97	793.63	676.22	796.36	753.35	990.87
Wing loading* (lb/ft ²)	21.57	21.49	18.96	21.04	20.59	24.08
Horsepower to weight ratio (HP/lb)	8.458E-02	8.460E-02	8.227E-02	8.166E-02	8.355E-02	0.0648
Aspect ratio	5.51	5.66	7.16	9.94	6.25	6.46
Max. Lift to Drag ratio	15.37	15.67	17.11	19.01	15.92	13.00
Wing span loading* (lb/ft)	152.17	149.76	126.89	113.87	140.45	169.66
GFOM*	206.84	201.06	212.06	179.80	214.44	644.68
Best mileage (ft/lb)	9294.04	9480.63	10062.62	11097.93	9508.41	6397.60
Maximum_range (ft)	1.887E+06	1.897E+06	1.870E+06	1.941E+06	1.853E+06	3.95E+06
Stall speed @TO(ft/sec)	108.57	108.39	101.80	107.24	106.08	102.00
Best range airspeed (ft/sec)	201.54	200.90	180.03	177.99	190.63	181.94
Minimum fuel flow rate* (lb/hr)	68.70	67.13	56.68	50.81	63.52	90.09
Fastest airspeed (ft/sec)	338.66	340.18	322.53	330.72	328.81	279.30
Maximum ceiling (ft)	30876.20	31337.66	34723.03	36909.44	32445.20	22793.12
Maximum rate of climb (fpm)	1565.85	1581.54	1636.69	1679.60	1596.48	1073.03
Maximum load factor (g_s)	2.22	2.26	2.53	2.72	2.34	1.80
Fastest turning rate (deg/sec)	29.03	29.80	39.39	44.45	33.20	22.44
Tightest turn* (ft)	98.52	93.47	53.50	42.03	75.34	164.86

*The smaller the value, the better the performance

The above results show that the existing engine of 500 hp satisfies the requirements. Another optimization problem is solved, where the required power is adjusted within ADP to satisfy the performance constraints given in Table 4.5. Then a rubber engine sizing is made where the engine weight is taken proportional to its power. The objectives of the study are listed below:

6. Minimize equivalent flat plate area, $S \cdot C_{D0}$
7. Minimize take-off distance
8. Maximize endurance, E
9. Minimize power required, P_{req}

The design variables and optimization results are given for Cases E and F in Table 4.10 and Table 4.11 for NACA 23015. The results of NACA 63₂615 are given in Table 4.12 and Table 4.13.

The values of design variables are given in Table 4.10 for NACA 23015, Table 4.12 for NACA 63₂615. In Table 4.11 and Table 4.13 the objectives and the performance figures of merit are for each of the airfoils are tabulated.

When power is minimized (column 4, Table 4.11 and Table 4.13) the take off gross weight being 5854.96 lb and 5875.65 lb for NACA 23015 and NACA 63₂615 respectively were also the smallest. These are smaller than the take off gross weight values (5895.36 lb and 5911.72 lb) obtained in the previous problem. Thus, all requirements are met with an engine power of 347.48 hp (NACA 23015) and 372.28 hp (NACA 63₂615) leading to a lower gross weight. Besides, this case has the minimum the take off gross weight for NACA 23015 and NACA 63₂615.

When the results are compared with the values calculated for ZIU, it may be observed that they are better than ZIU. The GFOM values obtained are very close to CASE A to CASE D of previous problem as well. At the same time they are lower than the GFOM value of ZIU. Among all cases the results obtained by maximizing endurance is the best in most measures of performance. For example, it has the smallest GFOM value as well as the tightest turn radius.

Similar to above solutions (CASES A-D) due to the mathematical formulation the expected difference in minimum equivalent flat plate area ($S \cdot C_{D0}$) and maximum lift to drag ratios between NACA 23015 and NACA 63₂615 can not be observed clearly in these results.

Minimizing the equivalent flat plate area ($S \cdot C_{D0}$) also gives the best rate of climb. The performance of column 1 and 2 (Table 4.11 and Table 4.13) are penalized due to their larger wing loading $\left(\frac{W_0}{S}\right)$ and span loading $\left(\frac{W_0}{b}\right)$.

From the above solutions it may be easily observed that there is no single objective that gives the best figures of merits.

From tables 4.10 and 4.12 the relation between the design variables and objectives may be observed. The wingspan b became the lowest when flat plate area ($S \cdot C_{D0}$) is minimized. Thus the optimization program reduced the wing area S , which results in a longer *TOD*. The take off distance minimization results in the largest wing area as before with a large wing span. The wing incidence, sweep, and the dihedral angles are largest of all cases. Again maximizing the endurance, results in the largest wing span value and aspect ratio as expected. This causes the best lift to drag ratio, wingspan loading, GFOM, minimum fuel flow rate, and mileage together with the endurance. To minimize the power required, value the take off gross weight is decreased, in the last

objective. By this way the configuration has a lower parasite drag value than all other three cases.

Similar trends are observed when the above optimizations are repeated, this time using NACA 63₂615 (Table 4.11 and Table 12) airfoil profile.

Table 4.10. Single objective optimization results for design variables using NACA 23015

	CASE E	CASE E	CASE E	CASE E	ZIU
	Minimize $S.C_{D0}$	Minimize TOD	Maximize $Endurance$	Minimize $Power$ $Required$	
b	37.64	44.71	53.90	47.89	45.49
AR	5.58	6.69	9.96	7.16	6.45
λ_w	0.52	0.64	0.88	0.83	1.0
i_w	2.10	2.73	2.73	2.20	2.0
Λ_w	4.77	5.12	0.27	5.70	0.0
Γ_w	4.17	8.27	2.45	0.60	7.0
λ_{HT}	0.54	0.66	0.93	0.81	1.0
λ_{VT}	0.93	0.74	0.79	0.71	0.465
Λ_{HT}	6.16	2.73	0.10	6.44	0.0
Λ_{VT}	9.96	10.70	9.78	11.12	13.584
AR_{HT}	3.64	4.89	4.33	5.02	3.91
AR_{VT}	0.82	2.05	0.88	1.34	1.48
$D_{f\max}$	3.00	3.07	3.00	3.01	4.28
P_{av}	593.15	574.30	468.21	347.48	500

Table 4.11. Single objective optimization results for objectives using NACA 23015. Various figure of merit values are also given

	CASE E	CASE E	CASE E	CASE E	ZIU
	Minimize $S.C_{D0}$	Minimize TOD	Maximize $Endurance$	Minimize $Power$ $Required$	
Gross Weight (lb) *	5996.30	6084.59	6086.04	5854.96	7718.0
SCD_0^* (ft ²)	4.23	5.03	4.91	5.21	7.69
Minimum take-off distance * (ft)	999.67	900.00	999.89	999.60	902.23
Maximum endurance (hr)	2.84	3.10	3.40	3.29	2.18
Vol_{Hopper}	1500.00	1500.00	1500.00	1500.00	1500.0
S (ft ²)	253.82	298.71	291.73	320.54	320.55
CD_0^*	1.667E-02	1.684E-02	1.682E-02	1.625E-02	2.411E-02
Minimum take-off run (ft) *	765.48	666.05	816.81	867.46	990.87
Wing loading * (lb/ft ²)	23.62	20.37	20.86	18.27	24.08
Horsepower to weight ratio (HP/lb)	9.892E-02	9.102E-02	7.693E-02	5.935E-02	6.48E-02
Aspect ratio	5.58	6.69	9.96	7.16	6.46
Max. Lift to Drag ratio	15.23	16.27	18.77	16.99	13.00
Wing span loading * (lb/ft)	159.32	136.09	112.91	122.25	169.66
GFOM*	211.64	222.56	181.93	194.17	644.68
Best mileage (ft/lb)	9079.90	9557.84	11025.29	10374.00	6397.60
Maximum_range (ft)	1.879E+06	1.831E+06	1.897E+06	1.836E+06	3.95E+06
Stall speed @TO(ft/sec)	112.82	104.76	106.02	99.20	102.00
Best range airspeed (ft/sec)	208.85	186.66	175.99	176.10	181.94
Minimum fuel flow rate * (lb/hr)	72.87	61.87	50.57	53.78	90.09
Fastest airspeed (ft/sec)	364.27	336.04	320.42	284.39	279.30
Maximum ceiling (ft)	33114.87	35016.15	35690.22	28495.34	22793.12
Maximum rate of climb (fpm)	1913.98	1819.40	1554.08	1039.58	1073.03
Maximum load factor (g_s)	2.40	2.55	2.61	2.06	1.80
Fastest turning rate (deg/sec)	31.33	38.56	42.29	29.50	22.44
Tightest turn * (ft)	84.57	55.85	46.42	95.43	164.86

*The smaller the value, the better the performance

Table 4.12. Single objective optimization results for design variables using NACA 63₂615

	CASE F	CASE F	CASE F	CASE F	ZIU
	Minimize <i>S.C_{D0}</i>	Minimize <i>TOD</i>	Maximize <i>Endurance</i>	Minimize <i>Power Required</i>	
<i>b</i>	37.95	45.13	53.72	47.16	45.49
<i>AR</i>	5.59	6.59	9.89	7.05	6.45
λ_w	0.54	0.97	0.87	0.59	1.0
i_w	1.47	2.47	1.21	2.11	2.0
Λ_w	0.27	3.08	5.04	3.31	0.0
Γ_w	3.54	6.61	7.86	4.39	7.0
λ_{HT}	0.80	0.85	0.54	0.98	1.0
λ_{VT}	0.50	0.84	0.65	0.64	0.465
Λ_{HT}	6.68	0.39	4.21	3.64	0.0
Λ_{VT}	4.75	11.82	6.58	13.38	13.584
AR_{HT}	3.43	4.18	4.83	4.21	3.91
AR_{VT}	0.79	1.47	1.96	2.19	1.48
$D_{f\max}$	3.00	3.03	3.01	3.00	4.28
P_{av}	599.70	569.85	494.41	372.28	500

Table 4.13. Single objective optimization results for objectives using NACA 23015. Various figure of merit values are also given

	CASE F	CASE F	CASE F	CASE F	ZIU
	Minimize $S.C_{D0}$	Minimize TOD	Maximize $Endurance$	Minimize $Power Required$	
Gross Weight (lb) *	6012.05	6066.04	6137.99	5875.69	7718.0
SCD_0^* (ft ²)	4.18	5.00	4.86	5.01	7.69
Minimum take-off distance * (ft)	998.48	900.00	999.81	1000.00	902.23
Maximum endurance (hr)	2.89	3.19	3.43	3.30	2.18
Vol_{Hopper}	1500.00	1500.00	1500.00	1500.00	1500.0
S (ft ²)	257.44	309.16	291.70	315.36	320.55
CD_0^*	1.622E-02	1.616E-02	1.665E-02	1.587E-02	2.411E-02
Minimum take-off run (ft) *	762.37	675.06	807.49	855.33	990.87
Wing loading * (lb/ft ²)	23.35	19.62	21.04	18.63	24.08
Horsepower to weight ratio (HP/lb)	9.975E-02	8.675E-02	8.055E-02	6.336E-02	0.0648
Aspect ratio	5.59	6.59	9.89	7.05	6.46
Max. Lift to Drag ratio	15.45	16.51	18.83	17.10	13.00
Wing span loading * (lb/ft)	158.43	134.43	114.26	124.58	169.66
GFOM*	208.61	216.97	184.52	191.11	644.68
Best mileage (ft/lb)	9188.49	9728.05	10964.87	10402.38	6397.60
Maximum_range (ft)	1.913E+06	1.878E+06	1.928E+06	1.878E+06	3.95E+06
Stall speed @TO(ft/sec)	112.98	103.56	107.25	100.92	102.00
Best range airspeed (ft/sec)	208.97	185.66	177.39	179.38	181.94
Minimum fuel flow rate * (lb/hr)	72.05	60.46	51.25	54.63	90.09
Fastest airspeed (ft/sec)	367.19	331.14	327.42	294.88	279.30
Maximum ceiling (ft)	33560.71	34454.04	36510.22	29559.70	22793.12
Maximum rate of climb (fpm)	1945.54	1718.23	1647.21	1139.03	1073.03
Maximum load factor (g_s)	2.43	2.51	2.68	2.13	1.80
Fastest turning rate (deg/sec)	32.02	37.69	43.72	30.54	22.44
Tightest turn* (ft)	80.97	58.46	43.45	89.03	164.86

*The smaller the value, the better the performance

4.5. Multi-Objective Optimization Problems

In this section multi objective conceptual design optimization results are presented. Due to the difficulty of visualizing more than two objectives only bi-objective problems are solved. The penalty coefficients related to the constraints are given in Table 4.14. Eleven linear fitness functions are used with equally spaced weight sets (Table 4.15). The solutions of the previous section are used to normalize the objectives. In every run the optimization is terminated after 20000 function evaluations.

The multi objective optimization problems where the engine power is fixed are listed below,

1. Minimize takeoff gross weight, W_0 - maximize hopper volume, Vol_{Hopper} ,

Vol_{hopper} is a design variable.

2. Minimize takeoff gross weight, W_0 - minimize equivalent flat plate area, $S \cdot C_{D0}$.
3. Minimize takeoff gross weight, W_0 – maximize endurance, E .
4. Minimize takeoff gross weight, W_0 – maximize Lift to Drag ratio, L/D .
5. Minimize takeoff gross weight, W_0 – minimize Take off Distance.

These cases are run for both NACA 23015 and NACA 632615.

Table 4.14. Penalty coefficients

Penalty coeff.	Penalty coeff.
1	0.10
2	0.01
3	0.01
4	0.10
5	0.10
6	0.10
7	0.10
8	0.10
9	1.00

Table 4.15. Eleven different weight sets used in MC-MOSA

Weight of f_1	Weight of f_2
1.00	0.00
0.90	0.10
0.80	0.20
0.70	0.30
0.60	0.40
0.50	0.50
0.40	0.60
0.30	0.70
0.20	0.80
0.10	0.90
0.00	1.00

The multi objective optimization results are given in are given in Figure 4.2 to Figure 4.6. For each case the fronts obtained for NACA 23015 and NACA 632615 are plotted separately. And then they are plotted together in one plot.

Figure 4.2 gives the solutions obtained when minimizing the take off gross weight and maximizing the hopper volume. The non-dominated results obtained for each airfoil are given together. The fronts are almost a straight line. It may also be observed from the figure that there is not any significant difference between the two fronts.

Figure 4.3 gives the results obtained while minimizing take off gross weight and equivalent flat plate area $S \cdot C_{D0}$, together. In each case the solutions are first plotted separately. Then the non-dominated results are given together. From the figures it may be observed that the feasible region is quite narrow and non-dominated points converge to a small corner.

The multi objective solutions of minimizing take off gross weight and maximizing endurance is given in Figure 4.4. The expected front is obtained. The non-dominated points are also plotted together shows that there is no significant difference between the results. As explained above, this is due to the mathematical models used in drag calculations namely the component buildup approach.

In Figure 4.5 the fronts obtained while maximizing lift to drag ratio and minimizing take off gross weight are given. Maximum lift to drag ratio depends on the parasite drag coefficient C_{D0} together with the induced drag coefficient K . And K depends on aspect ratio AR . Again the expected front, referring to a feasible region of a multi objective problem where it is required to minimize one objective while maximizing the other one, is obtained and shown in Figure 4.5.

The last case is the minimization of the take off gross weight W_0 , and the take off distance together, Figure 4.6. The resultant front shows that the maximum value of the take off distance is limited by the performance constraint given in Table 4.5 (i.e. less than 1000ft) and the minimum value that can be obtained is around 875 ft. In this case NACA 23015 results slightly dominates the results of NACA63₂615.

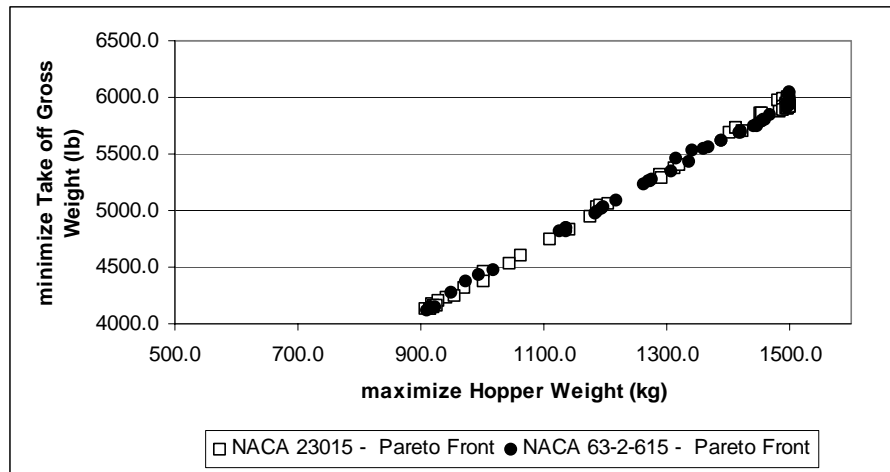


Figure 4.2. Fronts obtained while minimizing take off gross weight and maximizing hopper volume together

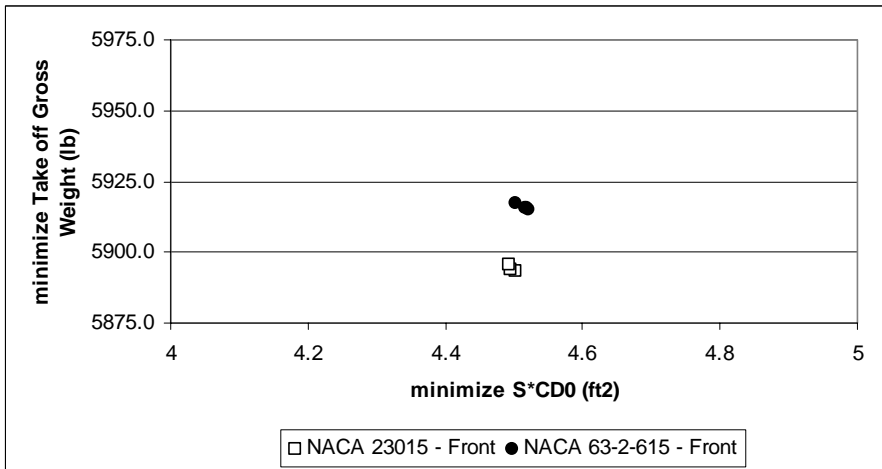
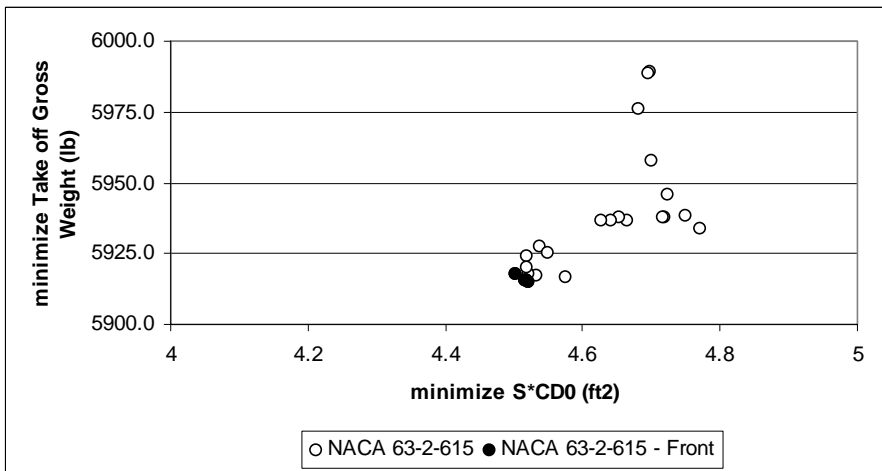
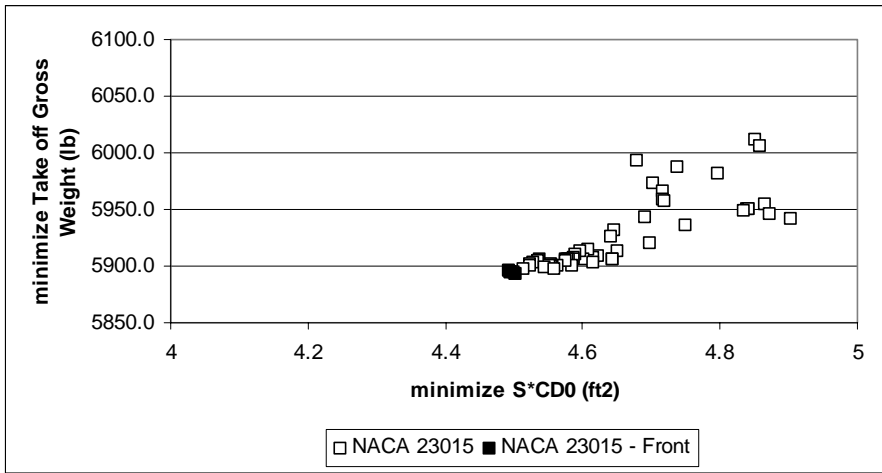


Figure 4.3. Fronts obtained while minimizing take off gross weight and minimizing equivalent flat plate area together

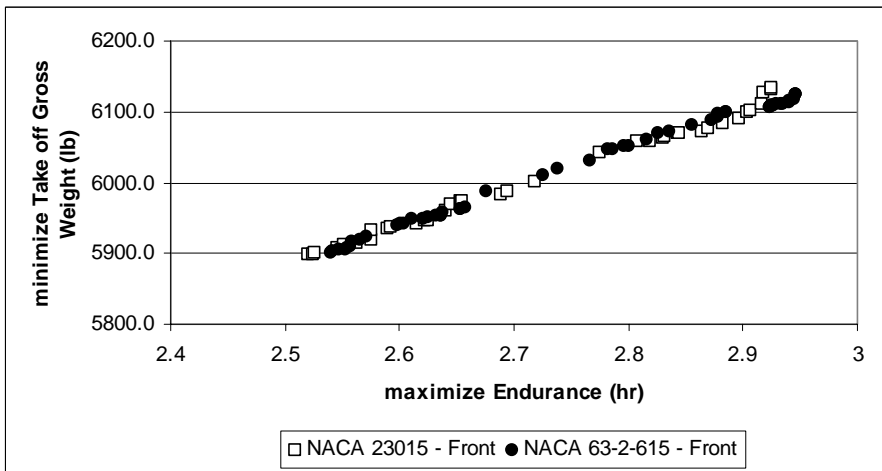
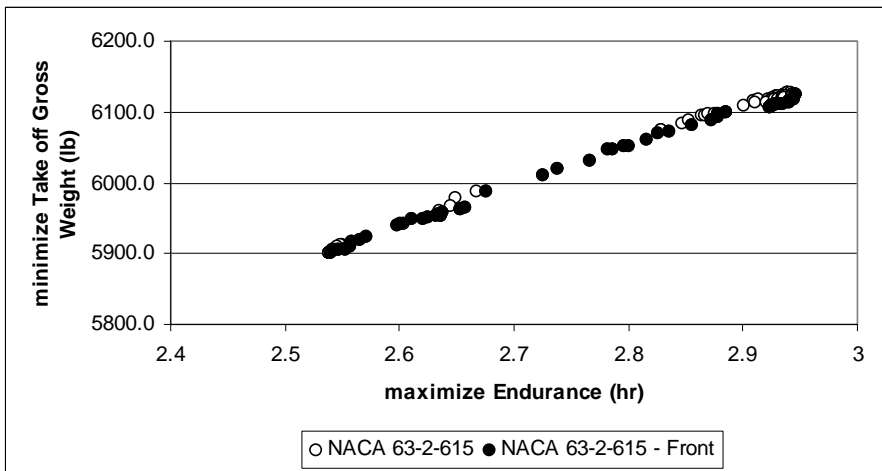
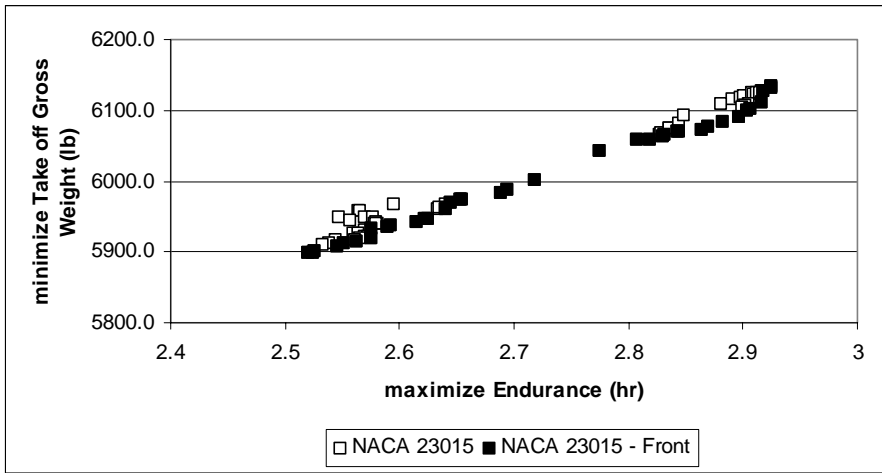


Figure 4.4. Fronts obtained while minimizing take off gross weight and maximizing endurance together

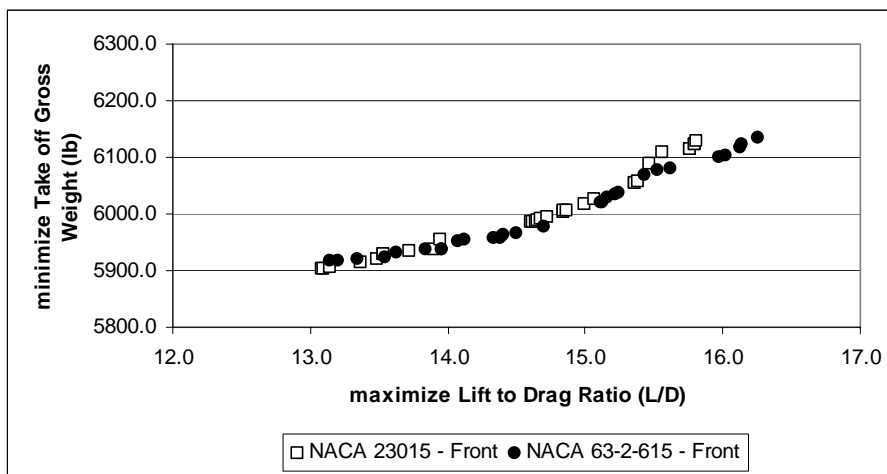
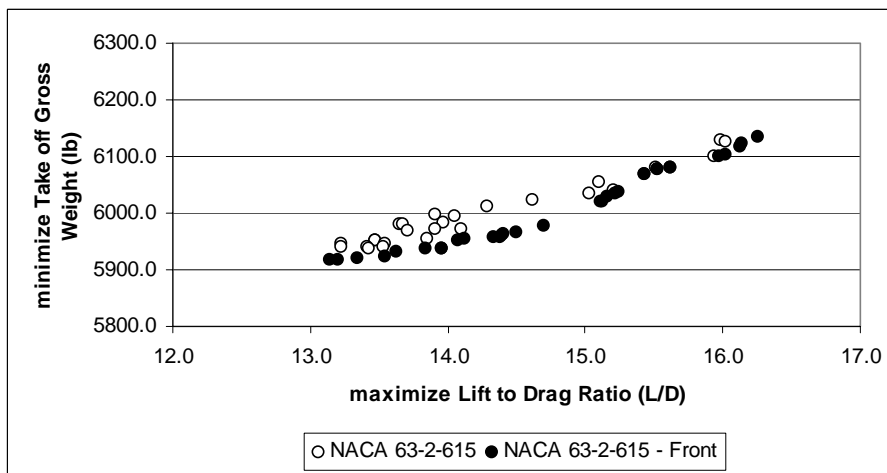
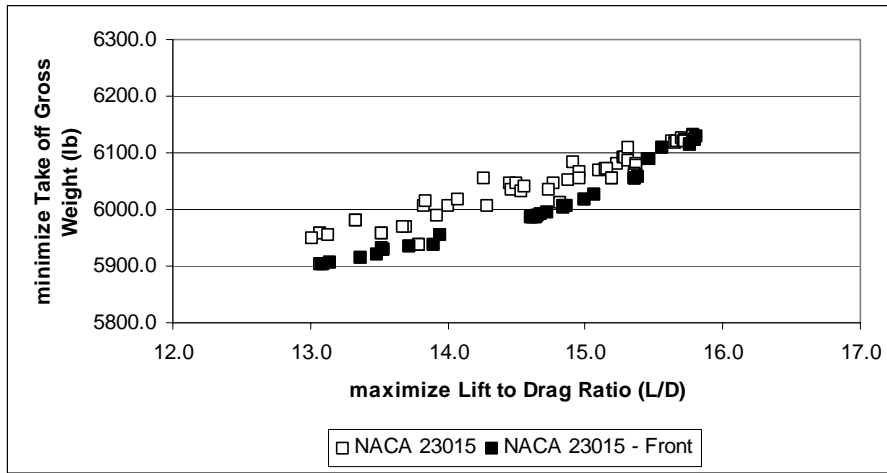


Figure 4.5. Fronts obtained while minimizing take off gross weight and maximizing lift to drag ratio together

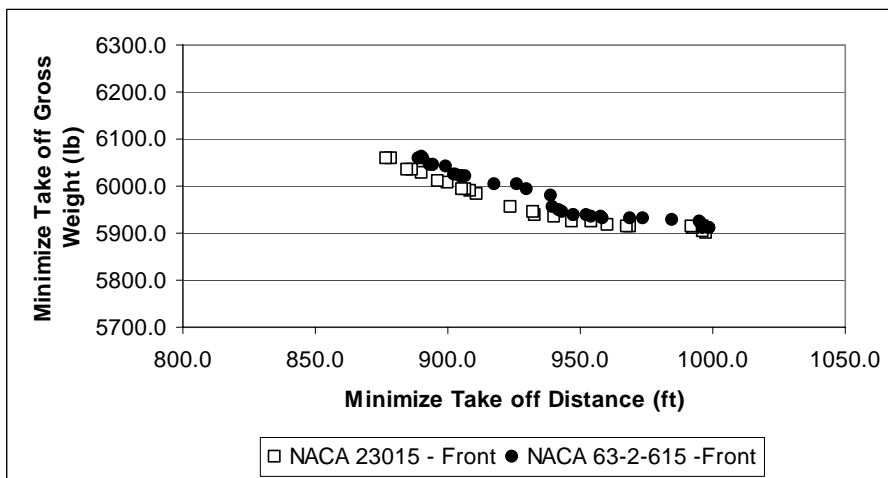
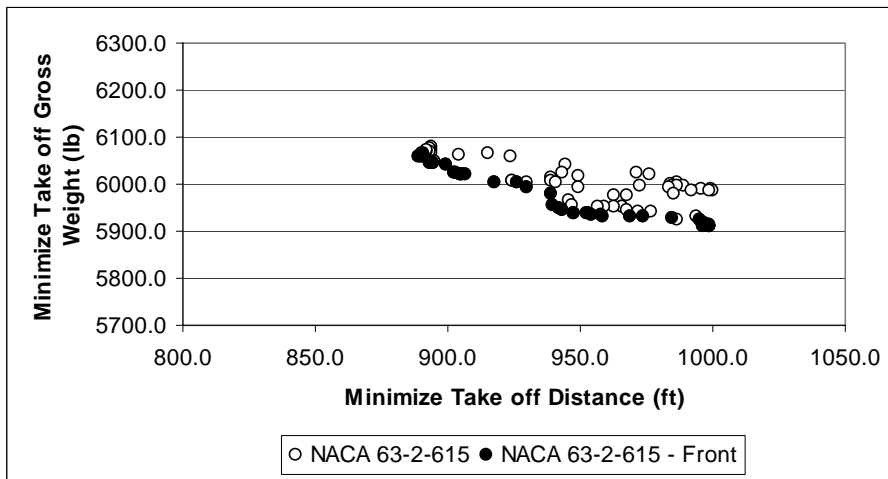
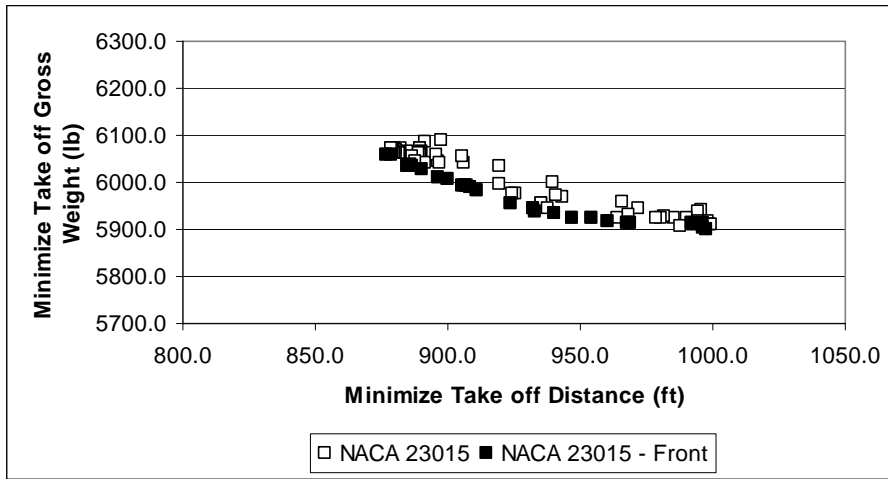


Figure 4.6. Fronts obtained while minimizing take off gross weight and minimizing take off distance together

In the following multi objective optimizations required power P_{req} is calculated within ADP. Thus, it is no longer a fixed value. As before the problems considered are;

6. Minimize takeoff gross weight, W_0 - minimize power available, P_{av} .
7. Minimize takeoff gross weight, W_0 - minimize equivalent flat plate area, $S \cdot C_{D0}$.
8. Minimize takeoff gross weight, W_0 – maximize endurance, E .
9. Minimize takeoff gross weight, W_0 – maximize Lift to Drag ratio, L/D .
10. Minimize power required, P_{req} . – minimize Take off Distance.

Minimum power required for minimum weight is shown in Figure 4.7. In the optimization the lower bound for the required power was specified to be 300 hp. However to meet constraints, the lowest value is around 350 hp. Note that the take off gross weight obtained by NACA 23015 is less than that obtained by NACA 63₂615 at the same power.

The fronts that minimize takeoff gross weight, W_0 together with the equivalent flat plate area $S \cdot C_{D0}$ are shown in Figure 4.8. This front may be compared to the one given previously in Figure 4.3. In former case the power was fixed. Here power is adjusted to meet performance requirements. That's why the feasible region is not narrow and the front does not converge to a rather sharp corner. Instead it spreads quite well.

In Figure 4.9 the front obtained for minimizing take off gross weight and maximizing endurance is plotted. The expected front is obtained.

The resultant front for the problem of maximizing lift to drag ratio while minimizing the take off gross weight is shown in Figure 4.10. The front obtained by NACA 231015 is much smoother than that obtained by NACA 63₂615.

The last problem is to minimize the power required and the take off distance at the same time. The front is plotted in Figure 4.11. It can be seen from the graph that the maximum value of the take off distance is limited by the performance constraint given in Table 4.5 (i.e. 1000 ft). The minimum value of the take of distance however converges to 900 ft for all values of power required. The front obtained from NACA 23015 dominates the front of NACA 63₂615. Thus for the same take off distance NACA 23015 requires slightly less power.

It is clear that bi-objective results presented in this section gives more information about the nature of the problem than single objective optimization results. Thus better judgments can be made in arriving the final optimum design. On the other hand MC-MOSA algorithm does not require excessive function evaluations. In fact with the same number of function evaluations many more solutions are obtained to choose from as illustrated in this section.

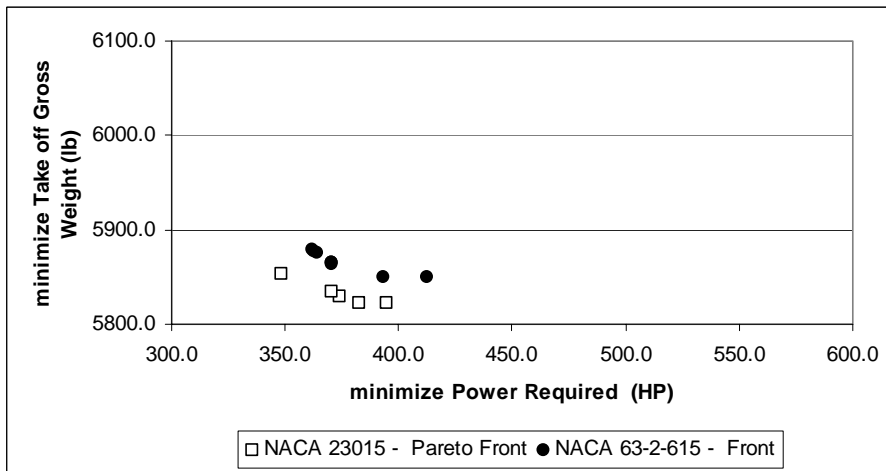
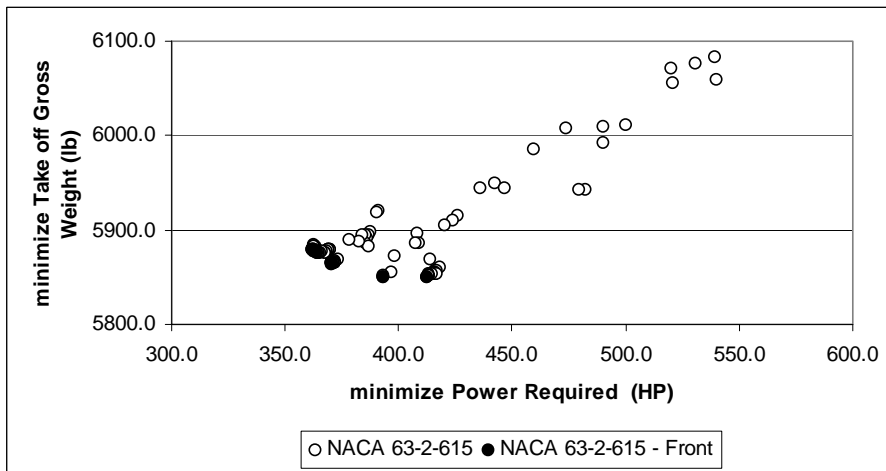
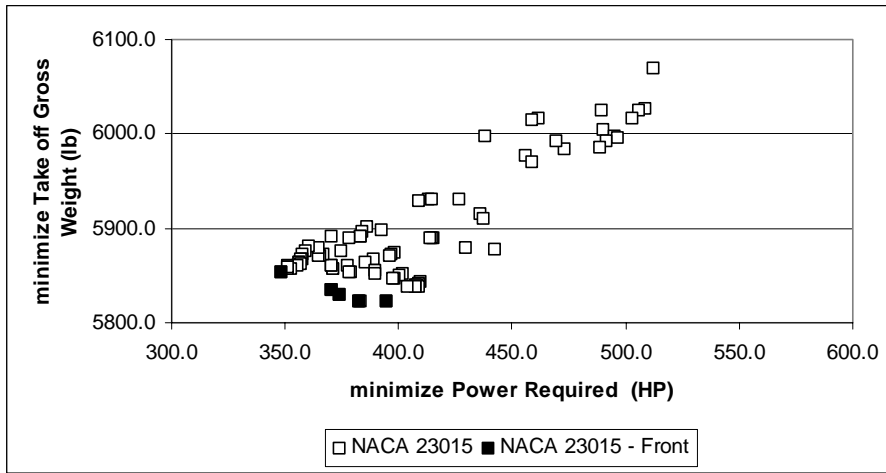


Figure 4.7. Fronts obtained while minimizing take off gross weight and minimizing power required together

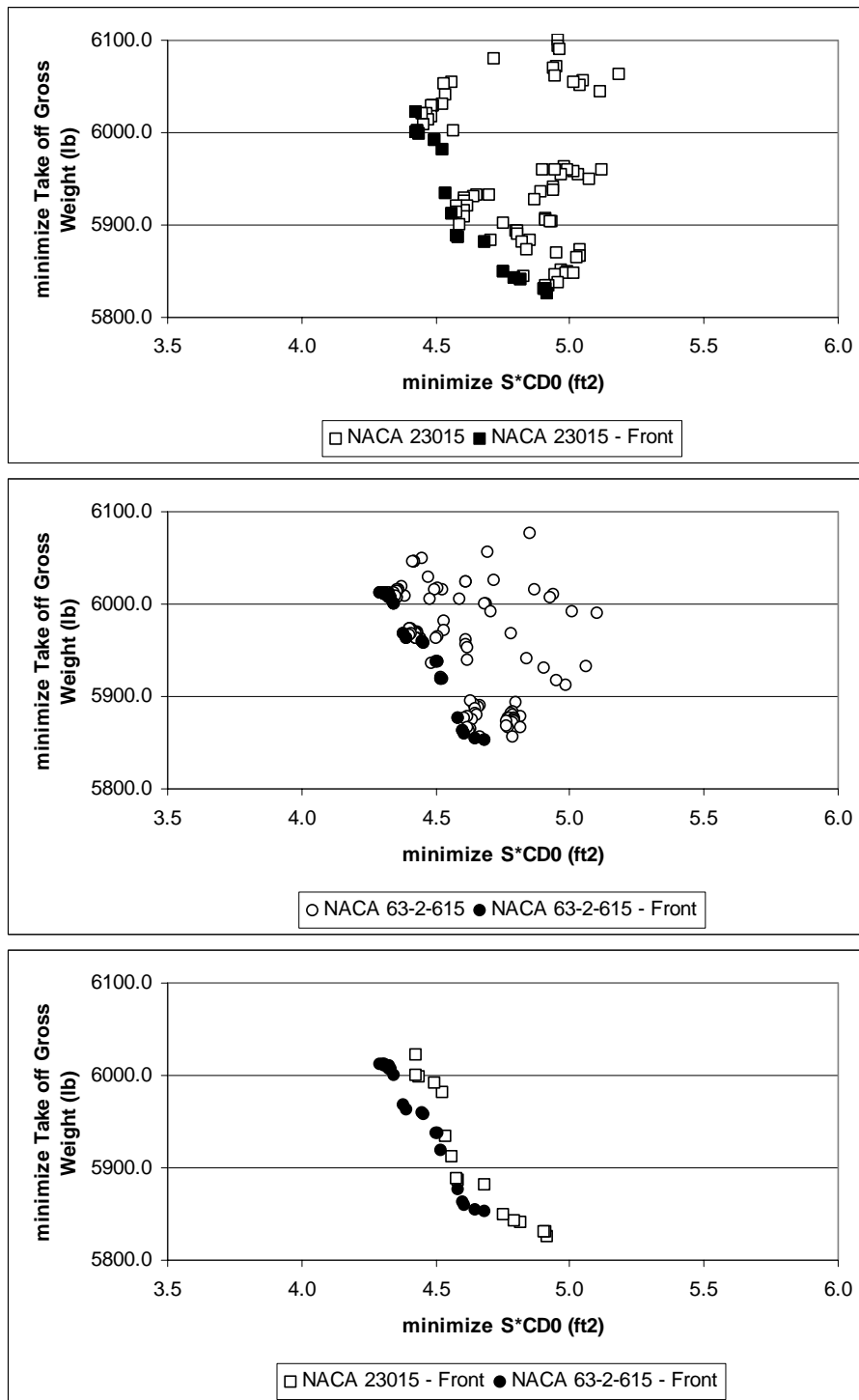


Figure 4.8. Fronts obtained while minimizing take off gross weight and minimizing equivalent flat plate area together

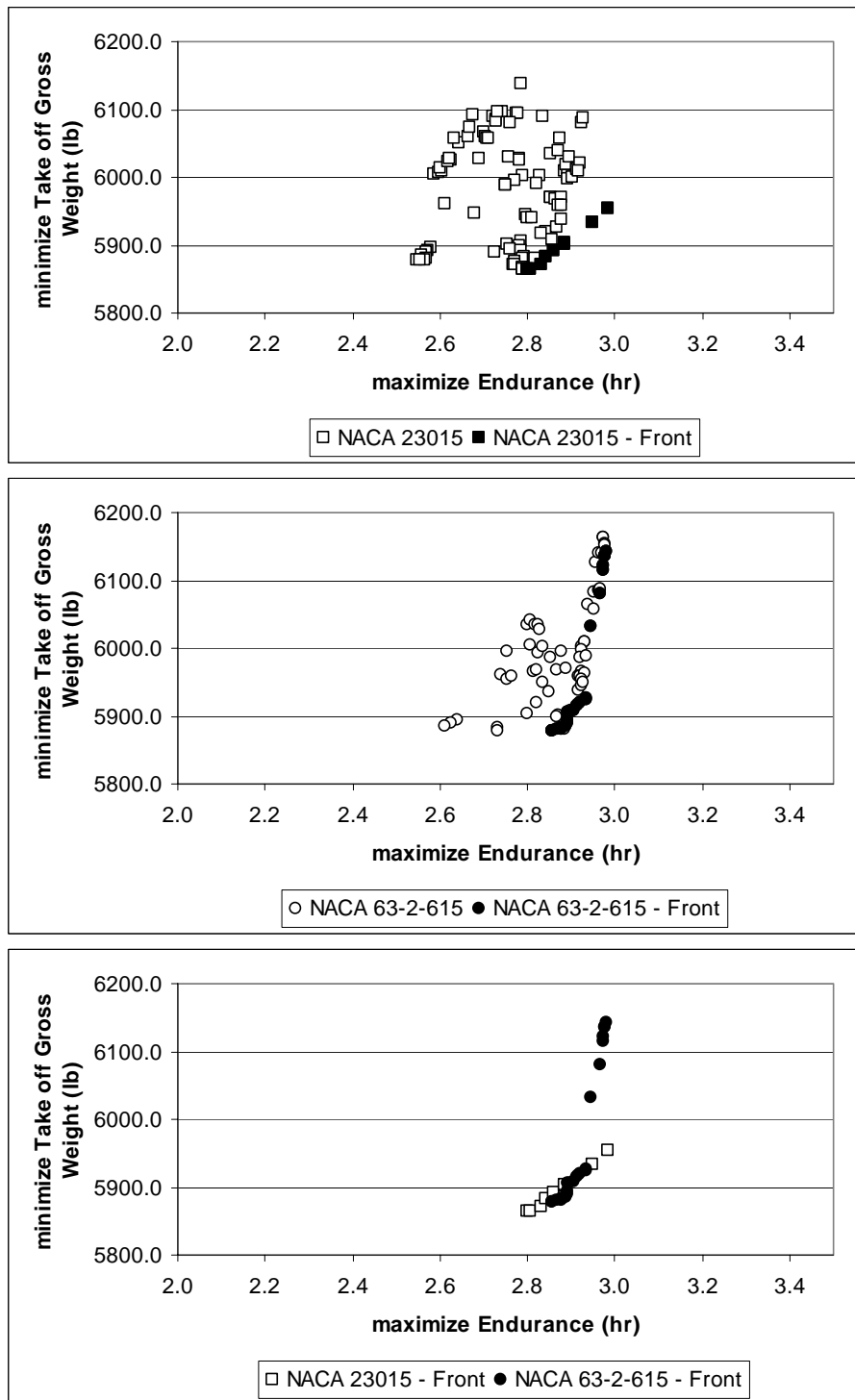


Figure 4.9. Fronts obtained while minimizing take off gross weight and maximizing endurance together

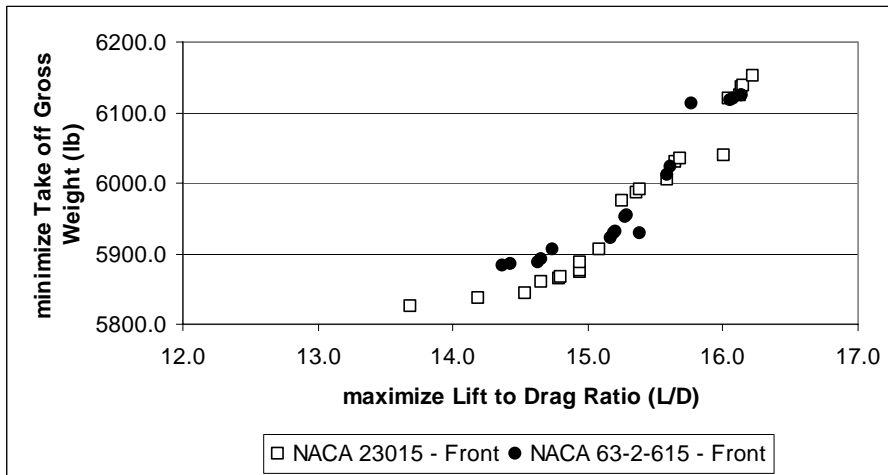
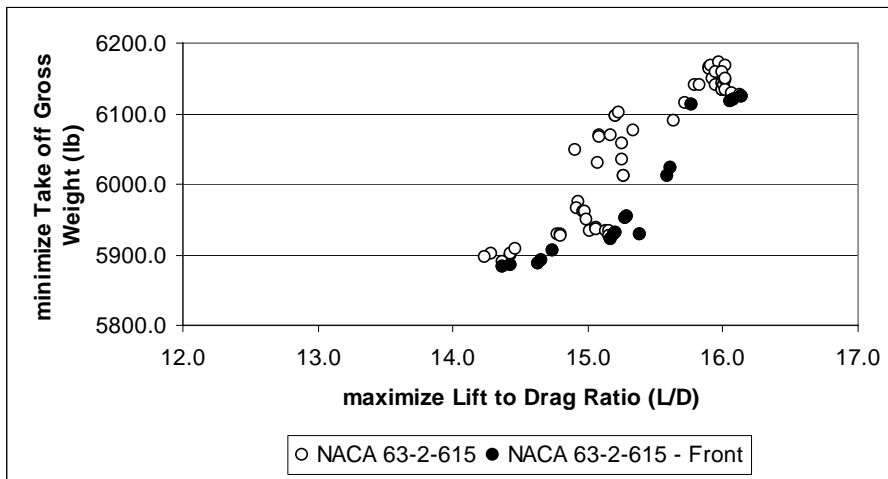
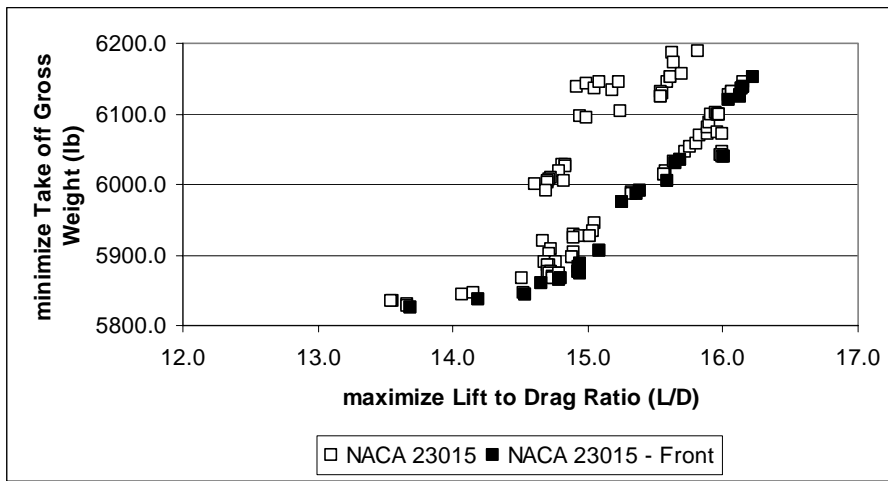


Figure 4.10. Fronts obtained while minimizing take off gross weight and maximizing lift to drag ratio together

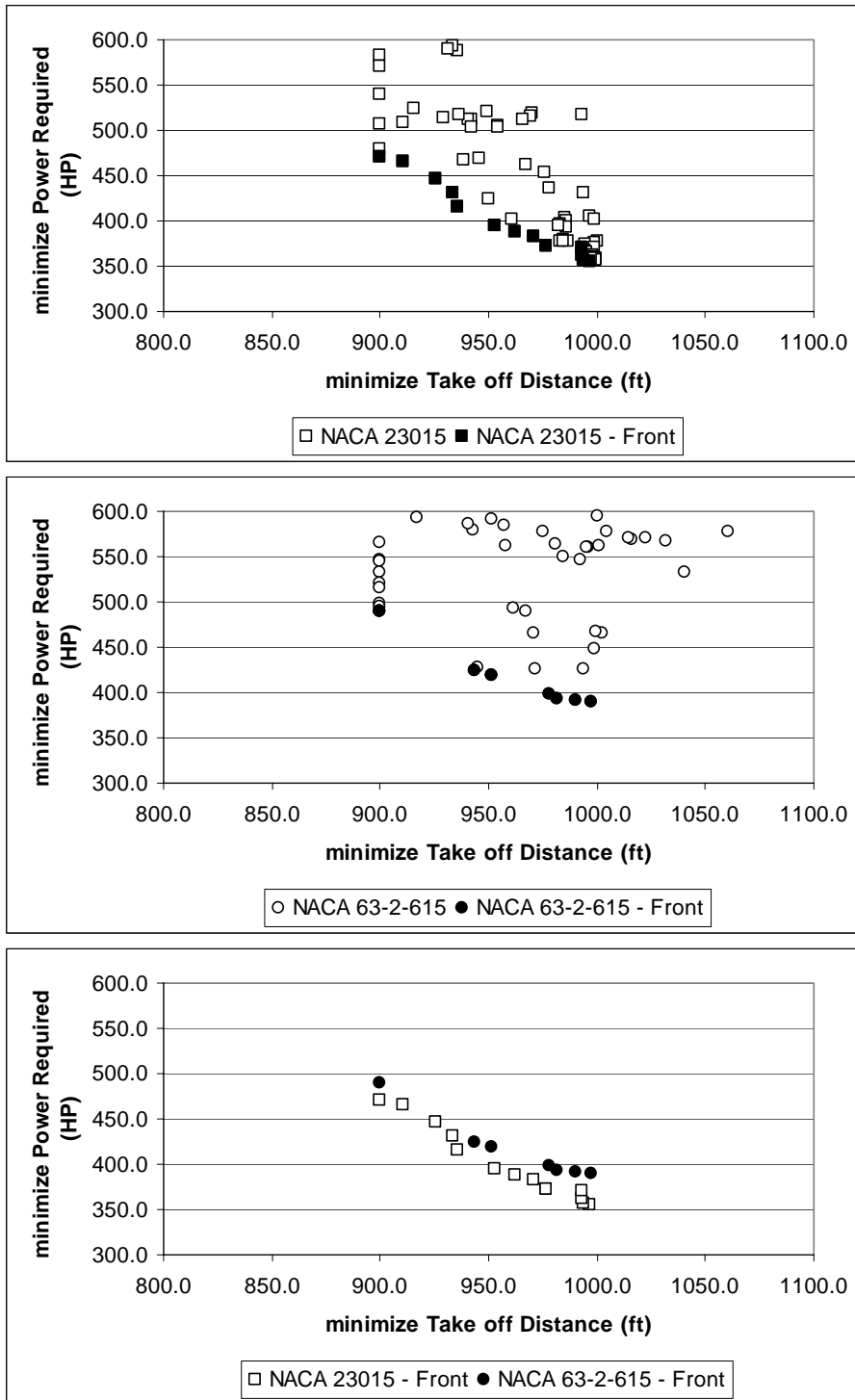


Figure 4.11. Fronts obtained while minimizing take off gross weight and maximizing take off distance together

CHAPTER V

CONCLUSION

5.1. Conclusion

In this thesis, conceptual design of an Agricultural Aerial Robot (AAR) is performed. The proposed robot is envisaged to fly autonomously to carry out the spraying tasks of fields using navigational aids such as GPS, DGPS, GPS aided INS, onboard. It is assumed to be vehicle transportable, capable of take off and landing from unprepared runways. The general configuration will have a tractor engine, with classical low wing configuration and a tail attached to the wings by a twin boom.

A program, called Aircraft Design Program, is written to size the aircraft, determine dimensions and locations of tail surfaces, control surfaces, landing gear, hopper and the fuel tanks. This FORTRAN code includes mathematical models for aerodynamics, structural, and propulsive analysis. Classical aeronautical knowledge is used, with models taken from various references [4, 40, 41 & 46] for aerodynamics, weight and balance, mission and performance analysis leading to fast and efficient for optimization. Thus, the program is capable of carrying out aircraft conceptual design.

While selecting the optimum configuration Multiple Cooling Multi Objective Simulated Annealing algorithm, MC-MOSA, which is shown to be superior to the existing multi objective methods through a number of benchmark problems [5], is

integrated to the conceptual design tool. In this way both single objective and multi objective designs optimization studies are carried out. Since Integration of the optimization model with the ADP is carried out in source codes, it is possible to easily change the design variables, constraints, and objective functions for different design optimization studies.

The baseline configuration is chosen as Turkey's first agricultural aircraft complying with the FAR-23 aviation norms, ZIU. First single objective optimization problems are solved to minimize take off gross weight, maximize endurance, minimize equivalent flat plate area, minimize takeoff difference, and minimize power required. It is shown that each optimization objective yields a different set of aircraft design variables, and it is difficult to assess the best aircraft configuration with many parameters to determine. The problems are also formulated as multi objective optimization problems, to arrive the Pareto optimum fronts. For this purpose a number of bi-objective problems are solved. These are: minimization of take of gross weight together with either of the maximization of hopper volume, minimization of equivalent flat plate area, maximization of endurance, maximization of lift to drag ratio, minimization of take off distance and minimization of required power. These fronts obtained show the range of objectives attainable within the design constraints. Consequently, multi objective optimization is a powerful tool in arriving the best design.

Although only problems with continuous optimization variables are considered in this thesis, it is possible to adapt MC-MOSA to mixed optimization problems, where some parameters are continuous, while others are discrete. This property is especially useful if some components of the aircraft are to be selected off the shelf.

The present capabilities of ADP present only the first step to the development of a conceptual aircraft design tool. In the future more sophisticated models may be added to the program. The integration with the optimization algorithm may be done more

comprehensively, with a user interface to select desired objectives and constraints. For example, for more accurate analysis, flight simulations may be added to estimate fuel consumption throughout the mission profile. Databases may also be included for the selection of off the shelf engines, tires, propellers etc. In this way the accuracy of the design may be improved. It is also possible to add cost estimation models to the program as well.

REFERENCES

- [1] Hürriyet newspaper, “Tarımsal Havacılık Zorda”,
<http://arsiv.hurriyetim.com.tr/tatilpazar/turk/98/10/04/yazarlar/55yaz.htm> , (Last accessed date: August 2005)
- [2] Tarımsal Havacılık, “Zirai Havacılık”, <http://www.tayyareci.com/zirai.asp>, (Last accessed date: August 2005)
- [3] Stanford University, “The Aircraft Design Process”,
<http://adg.stanford.edu/aa241/design/designprocess.html>, (Last accessed date: August 2005).
- [4] John D. Anderson Jr., *Aircraft Performance and Design*, McGraw-Hill, 1999.
- [5] Tekinalp O., Karşlı G., Simulated annealing for the generation of pareto fronts with aerospace applications, *M.S. Thesis, Aeronautical Engineering Department, METU*, Ankara, January 2004
- [6] H. R. Quantick, *Handbook for Agricultural Pilots*, 4th ed., Collins Professional and Technical Books, 1985.
- [7] Aerial Agricultural Association of Australia, “The Need for Aerial Agriculture”,
<http://www.aerialag.com.au/site/comm.asp>, (Last accessed date: August 2005)

- [8] Wong K.C., *Survey of Regional Developments: Civil Applications*, School of Aerospace, Mechanical and Mechatronic Engineering, University of Sydney, 2001
- [9] Tactical Aerospace Group, "Agricultural Spraying", http://www.tacticalaerospacegroup.com/agricultural_spraying.html, (Last accessed date: August 2005)
- [10] Sobieski J., Chopra Inderjit, Multidisciplinary Optimization of Aeronautical Systems, *Journal of Aircraft*, Vol 27, No. 12, pp. 997-998, December 1990
- [11] MacMillin P. E., Golovidov O. B., Mason W. H., Grossman B., and Haftka R. T., An MDO Investigation of the Impact of Practical Constraints on an HSCT Configuration, AIAA 97-0098, 35th Aerospace Sciences Meeting & Exhibit, January 6-9, 1997 / Reno, NV
- [12] Giunta A.A., Aircraft Multidisciplinary Design Optimization Using Design of Experiments Theory and Response Surface Modeling Methods, PHD Thesis, Virginia Polytechnic Institute and State University, Blacksburg, Virginia, May 1997
- [13] Dovi A.R., Wrenn G.A., Aircraft Design for Mission Performance Using Nonlinear Multiobjective Optimization Methods, *Journal of Aircraft*, Vol 27, No. 12, pp. 1043-1049, December 1990
- [14] Cabral L. V., Paglione P., Conceptual Design of Families of Aircraft Using Multi Objective Design Optimization Theory And Genetic Algorithm Techniques, Department of Aeronautical and Mechanical Engineering, Technological Institute of Aeronautics, Brazil,

- [15] Giunta A.A., Golivodov O., Knill D.L., Grossman B., Haftka R.T., Mason W.H., Watson L.T, Multidisciplinary Design Optimization of Advanced Aircraft Configurations, *15th International Conference on Numerical Methods in Fluid Dynamics*, Monterey, CA, June 26, 1996
- [16] Bingöl, M., *Trajectory and Multidisciplinary Design Optimization of Missiles Using Simulated Annealing*, M.S. Thesis, Aeronautical Engineering Department, METU, Ankara, January 2000
- [17] CSEP, “Mathematical Optimization Chapter”,
<http://csep1.phy.ornl.gov/CSEP/MO/MO.html>, (Last accessed date: July 2005)
- [18] Metropolis, N., Rosenbluth, A.W., Rosenbluth, M. N., Teller, A.H. and Teller, E., Equations of State Calculations by Fast Computing Machines, *J. Chem. Phys.* 21, 1087- 1092, 1958.
- [19] Pincus, M., A Monte Carlo Method for the Approximate Solution of Certain Types of Constrained Optimization Problems, *Oper. Res.* 18, 1225-1228, 1970.
- [20] Kirkpatrick, S., Gerlatt, C. D. Jr., and Vecchi, M.P., Optimization by Simulated Annealing, *Science* 220, 671-680, 1983.
- [21] Bélisle C. J. P., Romeijn H. E., Smith R.L., Hide-and-Seek: A Simulated Annealing Algorithm for Global Optimization, *Department of Industrial and Operations Engineering, Technical Report 90-25*, University of Michigan, Ann Arbor, 1990
- [22] Lu, Ping and Khan, Asif, Nonsmooth Trajectory Optimization: An Approach Using Continuous Simulated Annealing, *Journal of Guidance, Control and Dynamics*, Vol.17, No.4, July-August 1994

- [23] Utalay S., *Trajectory and Multidisciplinary Design Optimization of Missiles Using Simulated Annealing*, M.S. Thesis, Aeronautical Engineering Department, METU, Ankara, January 2000
- [24] Tekinalp, O., Utalay S., Simulated Annealing for Missile Trajectory Planning and Multidisciplinary Missile Design Optimization, *AIAA 38th Aerospace Sciences Meeting*, Reno, NY, January 10-13, 2000
- [25] Tekinalp O., Bingöl M., Simulated Annealing for Missile Optimization: Developing Method and Formulation Techniques, *Journal of Guidance, Control, and Dynamics*, 2003 (to appear)
- [26] Ulungu L. E., Teghem J., Fortemps P., Heuristics for multi-objective combinatorial optimization problems by simulated annealing, *MCDM: Theory and Applications*, Sci-tech, Windsor, pp. 269-278, 1995
- [27] Ulungu L. E., Teghem J., Fortemps P. H., Tuyttens D., MOSA method: A tool for solving multi-objective combinatorial optimization problems, *Journal of Multi-Criteria Decision Analysis*, 8, pp. 221-236, 1999
- [28] Tuyttens D., Teghem J., Fortemps P. H., Nieuwenhuyze K. V., Performance of the MOSA method for the bicriteria assignment problem, *Journal of Heuristics*, 6, pp. 295-310, 2000
- [29] Serafini P., Simulated Annealing for multiple objective optimization problems, *Multiple Criteria Decision Making, Expand and Enrich the Domains of Thinking and Application*, Springer Verlag, pp. 283-292, 1994
- [30] Suman B., Simulated annealing-based multi-objective algorithms and their application for system reliability, *Engineering Optimization*, Vol 35, No. 4, pp. 391-416, August 2003

- [31] Ulungu L. E., Teghem J., Ost C., Interactive simulated annealing in a multi-objective framework: application to a industrial problem, *Journal of Operational Research Society*, 49, pp. 1044-1050, 1998
- [32] Czyżak P., Hapke M., Jaskiewicz A., Application of the Pareto-simulated annealing to the multiple criteria shortest path problem, *Technical Report*, Politechnika Poznanska Instytut Informatyki, 1994
- [33] Czyżak P., Jaskiewicz A., Pareto simulated annealing-A metaheuristic technique for multiple objective combinatorial optimization, *Journal of Multi-criteria Decision Analysis*, 7, pp. 34-47, 1998
- [34] Suppattnarm A., Seffen K. A., Parks G. T., Clarkson P. J., Simulated annealing: An alternative approach to true multi-objective optimization, *Engineering Optimization*, 33(1), pp. 59-85, 2000
- [35] Suman B., Simulated annealing-based multi-objective algorithms and their application for system reliability, *Engineering Optimization*, Vol 35, No. 4, pp. 391-416, august 2003
- [36] Kubotani H., Yoshimura K., Performance evaluation of acceptance probability functions for multi-objective SA, *Computers & Operations Research*, 30, pp. 427-442, 2003
- [37] TUSAŞ Aerospace Industries, “Zirai İlaçlama Uçağı (ZİU)”, www.tai.com.tr ZIU Technical Documents, *ZIU_DT*, 19.07.1999, (Last accessed date: June 2005)
- [38] *Jane’s All The World’s Aircraft 2004-2005*, Paul Jackson MRAs.
- [39] Certification Specifications for Normal, Utility, Aerobatic, and Commuter Category Aeroplanes CS-23

- [40] Daniel P. Raymer, *Aircraft Design: A Conceptual Approach*, 2nd ed., AIAA Education Series, American Institute of Aeronautics and Astronautics, Washington, 1992.
- [41] ROSKAM, J., “*Airplane Design, Part I-VII*”, DAR Corporation, 2000.
- [42] Dr. Friedrich Wilhelm Riegels, “*Aerofoil Sections Results from Wind-Tunnel Investigations Theoretical Foundations*”, Butterworths, London, 1961.
- [43] Abbot, Ira H. and Von Doenhoff, Albert E. (1975) *Theory of Wing Sections*, Ruppel Publications, New York, NY.
- [44] Nicolai, Leland M. (1975) *Fundamentals of aircraft Design*, METS Inc, 6520 Kingsland Ct, San Jose, Ca 95120
- [45] Torenbeek, E., “*Synthesis of Subsonic Airplane Design*”, Kluwer Academic Publishers, 1982.
- [46] Francis, J. Hale, *Introduction to Aircraft Performance, Selection and Design*, Wiley, New York, 1984.
- [47] *Advanced Airplane Analysis (AAA) Program, Version 2.5*, DAR Corporation, 2005.

APPENDIX A

AGRICULTURAL AIRCRAFT ZIU

A.1. Characteristics of ZIU

In this section, specifications of ZIU are given.

Table A.1. Fuselage dimensions of ZIU [37]

FUSELAGE	
Length	9.87 m / 32.39 ft
Width	1.30 m / 4.28 ft
Height	3.78 m / 12.41 ft

Table A.2. Wing dimensions of ZIU [37]

WING	
Area	29.78 m ² / 320.55 ft ²
Span	13.86 m / 45.49 ft
Root Chord Length	2.15 m / 7.05 ft
Tip Chord Length	2.15 m / 7.05 ft
Aspect Ratio	6.45
Sweep(Quarter chord)	0.0 deg
Taper ratio	1.0
Incidence	2.0 deg
Dihedral	7.0 deg

Table A.3. Vertical tail dimensions of ZIU [37]

VERTICAL TAIL	
Area	3.07 m ² / 33.05 ft ²
Span	2.13 m / 6.99 ft
Root Chord Length	1.96 m / 6.43 ft
Tip Chord Length	0.936 m / 3.07 ft
Aspect Ratio	1.48
Sweep(Quarter chord)	13.584 deg
Taper ratio	0.465
Incidence	0.0 deg
Dihedral	0.0 deg

Table A.4. Horizontal tail dimensions of ZIU [37]

HORIZONTAL TAIL	
Area	5.30 m ² / 57.05 ft ²
Span	4.41 m / 14.49 ft
Root Chord Length	1.12 m / 3.94 ft
Tip Chord Length	1.12 m / 3.94 ft
Aspect Ratio	3.91
Sweep(Quarter chord)	0.0 deg
Taper ratio	1.0
Incidence	-1.0 deg
Dihedral	0.0 deg

Table A.5. Performance Specifications of ZIU [32]

PERFORMANCE SPECIFICATIONS	
Flight Altitude	3000 ft
Operating Temperature	ISA+16
Take-off ground roll,	275 m / 902.2 ft
Landing distance (from 50 feet altitude, unprepared runway)	500 m / 1640.4 ft
Endurance	Min. 3-4 hours
Range	400 km
Minimum speed	104 km/hr / 94.8 ft/sec
Max. Cruise speed	276.1 km/hr / 251.6 ft/sec
Service Ceiling	16000 ft
Agricultural Applications	1.Spreading (solid) 2.Spraying (liquid)

Table A.6. Engine Specifications of ZIU [37]

ENGINE SPECIFICATIONS	
Single Turbocharged Piston Engine	Orenda OE600-A
Propeller Type	Constant Velocity
Propeller Diameter	106 inch
Number of Blades	3
Take-off Power	600 hp @ 4400 rpm
Max. Continuous Power	500 hp @ 4200 rpm
Weight	691 lb
Specific Fuel Consumption	0.44 lb/hp/hr

Table A.7. Structural Weight Breakdown of ZIU [37]

ITEMS	WEIGHT, kg
Wing	486
Fuselage (inc. firewall + door)	352
Horizontal Tail	63
Vertical Tail	28
Main Landing Gear	247
Tail Landing Gear	11
Structure Total	1186

Table A.8. Basic Empty Weight Breakdown of ZIU [37]

ITEMS	WEIGHT, kg
Structure Total	1186
Power Plant Total	567
Agricultural System Total	118
Fixed Equipment Total	225
Standard Items (oil + tof)	30
Basic Empty Weight	2096

Table A.9. Design Weights of ZIU [37]

WEIGHTS	
Basic Empty Weight (BEW)	2096 kg / 4620.9 lb
Fuel Weight (fuel density: 0.70 kg/lt)	280 kg (400 liters)
Hopper Weight (payload density: 1kg/lt)	1500 kg (1500 liters)
Operational Empty Weight (OEW)	2206 kg / 4863.4 lb
Maximum Zero Fuel Weight (MZFW)	3410 kg / 7517.8 lb
Maximum Take-off Weight (MTOW)	3500 kg / 7718 lb

APPENDIX B

ADP INPUTS AND OUTPUTS

B.1. Multi objective Optimization Program Input File

An example input file for multi objective optimization program is given in Table B.1.

Table B.1. initin.txt file

```
&initialize
p=0.01,
Temperature = 50*10000000.,
fdim = 14,
ffdim = 11,
accuracy_required = 0.0000001,
fe_per_loop = 20000,
loop_factor = 1.,.5,0.25, 10*0.1
x0 = 45.486,6.45,1.0,2.0,0.0,7.0,1.0,0.478,0.0,13.584,3.916,1.492,4.278,350.
xupper = 55, 10.,1.0,3.0,7.0,9.0,1.0,1.0,7.0,15.0,8.26,2.27,4.278,600.0
xlower = 35, 5.5,0.5,0.0,0.0,0.0,0.5,0.5,0.0,0.0,3.404,0.78,3.0,300.0
fmax = 10000000.,
fmin = -10000000.,
stopcriteria = 78000,
ftest = -1000.
weights = 1.0,0.9,0.8,0.7,0.6,0.5,0.4,0.3,0.2,0.1,0.0
penalty_coeff = 0.1, 0.01, 0.01, 0.1,0.1, 0.1, 0.1, 0.1, 1.
/
```

B.2. Pre-assigned Airfoil Variables

Airfoil properties are given as input to the program. They are in text file format. The 'WINGAIRFOIL.txt' file includes NACA 23015 and NACA 63₂615 airfoil properties depending on the airfoil used for the configuration. The 'NACA0012.txt' file includes NACA 0012 airfoil properties. The variables and their values for each airfoil are tabulated in Table 4.4.

B.3. An example output file of ADP

```
Gross Weight(lb)= 5996.298
Empty Weight(lb)= 1882.823
Fuel Weight(lb)= 206.9154
Fuselage weight(lb)= 120.8094
Wing Weight(lb)= 389.1992
Horizontal tail Weight(lb)= 40.56682
Vertical tail Weight(lb)= 17.99928
Power_plant Weight(lb)= 796.2618
Agricultural System Weight(lb)= 260.1451
Hopper_weight(kg)= 1500.000
Hopper_weight(lb)= 3306.930
*****
Wing Span(FT)= 37.63752
Wing Aspect Ratio = 5.581029
Wing Taper Ratio= 0.5206218
Wing Incidence Angle(DEG)= 2.103373
Wing Sweep Angle(DEG)= 4.766098
Wing Dihedral Angle(DEG)= 4.167821
HT Taper Ratio= 0.5445390
VT Taper Ratio= 0.9319651
HT Sweep Angle(DEG)= 6.155717
VT Sweep Angle(DEG)= 9.956239
HT Aspect Ratio = 3.642634
VT Aspect Ratio = 0.8212423
Diameter of Fuselage(FT)= 3.000432
*****
Wing Root Chord Length(FT)= 8.869833
Wing Tip Chord Length(FT)= 4.617829
Wing Mean Aerodynamic Chord(FT)= 6.967239
Spanwise Loc. of Wing Mean Aerodynamic Chord(FT)= 8.420606
Wing Area(FT^2)= 253.8210
*****
Length of Hopper Tank(FT)= 15.28994
Length of Fuselage(FT)= 19.02681
*****
Volume of Fuel Tank(FT^3)= 2.367453
Length of FuelTank(FT)= 0.4769650
Width of Fuel Tank_initial(FT)= 4.257520
Width of Fuel Tank_last(FT)= 4.205791
Height of Fuel Tank_initial(FT)= 0.8869833
Height of Fuel Tank_last(FT)= 0.8762066
*****
Horizontal Tail Area(FT^2)= 46.47211
Horizontal Tail Span(FT)= 13.01080
Horizontal Tail Root Chord Length(FT)= 4.625083
Horizontal Tail Tip Chord Length(FT)= 2.518538
Horizontal Tail Ratio 3.642634
Spanwise Loc. of Horizontal Tail Mean Aero Chord(FT)= 2.932976
Horizontal Tail Mean Aerodynamic Chord Length(FT)= 3.675342
```

Vertical Tail Area(FT^2)= 20.08365
 Vertical Tail Span(FT)= 4.061224
 Vertical Tail Root Chord Length(FT)= 5.119368
 Vertical Tail Tip Chord Length(FT)= 4.771072
 z L. of Horizontal Tail Mean Aerodynamic Chord(FT)= 2.006776
 Vertical Tail Mean Aerodynamic Chord Length(FT)= 4.947265
 Vertical Tail Ratio 0.8212423

 Maximum Lift Coefficient(2d)= 1.700000
 Maximum Lift Coefficient Clean(3d)= 1.524710
 Maximum Lift Coefficient Landing(3d)= 2.340000
 Maximum Lift Coefficient Takeoff(3d)= 1.890000

 Engine arm(FT)= 1.868433
 Hopper tank arm(FT)= 11.38184
 Payload arm(FT)= 11.38184
 Fuselage arm(FT)= 9.852843
 Wing arm(FT)= 1.045086
 Fuel arm(FT)= 1.045086
 Center of Gravity Location(FT)= 9.786266

 Power Requirement for TO Constraint(HP)= 749.6915
 Power Requirement for ROC Constraint(HP)= 382.5215
 Engine Horsepower(HP)= 593.1506
 Power Required for Spraying(HP)= 70.72809
 Power Required for Cruise(HP)= 224.0925
 Height of Engine(FT)= 2.017710
 Width of Engine(FT)= 2.125978
 Length of Engine(FT)= 3.736866
 Engine RPM= 4200.000
 Number of blades= 3.000000
 Propeller Diameter(FT)= 4.945145
 Maximum Forward Velocity of the Airplane(FT/SEC)= 408.0955
 Required Max. Forward Velocity of the Airplane(FT/SEC)= 255.1764

 Power Loading(LB/HP)= 10.10923
 Wing Loading (LB/FT^2) = 23.62412

 Stall Speed(FT/SEC)= 112.8199

 Takeoff Flight Path Radius(FT)= 2753.443
 Takeoff Airborne Distance(FT)= 522.3450
 Takeoff Ground roll(FT)= 477.3235
 Takeoff Distance(FT)= 999.6685
 Liftoff Speed(FT/SEC)= 124.1019

 Landing Flight Path Radius(FT)= 0.0000000E+00
 Landing Airborne Distance(FT)= 954.0850
 Landing Flare Distance(FT)= 0.0000000E+00
 Landing Ground roll(FT)= 569.1024
 Landing Distance(FT)= 1523.188

 Maximum Lift to Drag Ratio= 15.23061

Loiter Lift to Drag Ratio= 13.19010
 Maximum Lift to Drag Ratio for Best Range= 15.23061
 Velocity for Best Range(FT/SEC)= 193.0412
 Range(KM)= 467.8430

 Maximum Lift to Drag Ratio for Best Endurance= 13.19010
 Velocity for Best Endurance(FT/SEC)= 146.4034
 Endurance(HR)= 2.473038

 Instantaneous Turn Rate Load Factor(g)= 4.2038954E-45
 Instantaneous Turn Bank Angle(DEG)= 73.87615
 Instantaneous Turn Rate(DEG/SEC)= 32.20811

 Maximum Load Factor(g)= 3.600347
 Turn Radius(FT)= 164.5762
 Sustained Turn Bank Angle(DEG)= 73.87615
 Sustained Turn Rate(DEG/SEC)= 47.13411
 Serkan-Sustained Turn Rate(DEG/SEC)= 47.13411

 Radius of Turn(FT)= 72.21204
 Maximum Rate of Climb(FT/MIN)= 2579.109

 Hopper Volume(FT^3)= 52.97201
 Reduced Volume Application Rate(LT/FT^2)= 5.000000
 Flow Rate of Spraying(FT^3/SEC)= 8.5708983E-03
 Velocity for Spraying(FT/SEC)= 138.8240
 Endurance for Spraying(SEC)= 6180.450
 Range for Spraying(FT)= 857994.6
 Width of the Field for Spraying(FT)= 3112.529
 Length of the Field for Spraying(FT)= 10375.10
 Area of the Field for Spraying(FT^2)= 3.2292784E+07
 Number of Turns around the Field for Spraying(FT)= 83

 Drag Force Coefficient of Fuselage= 2.1105807E-03
 Drag Force Coefficient of Wing= 8.7450454E-03
 Drag Force Coefficient of Horizontal Tail= 1.2356306E-03
 Drag Force Coefficient of Vertical Tail= 1.7976431E-04
 Drag Force Coefficient of Landing Gear= 1.2012262E-02
 Miscellaneous Drag Force Coefficient of Engine= 4.6737699E-04
 Total Parasitic Drag Coeff. for Clean Configuration= 1.6668247E-02
 Oswalds Efficiency= 0.8821315
 Coeff. appears in Drag Polar for Clean Configuration= 6.465695E-02
 Total Parasitic Drag Coeff. with Landing Gear= 2.5497446E-02

 Wing Loading for Takeoff (LB/FT^2)= 23.62412
 Wing Loading for Landing (LB/FT^2)= 21.74319
 Wing Loading for Cruise (LB/FT^2)= 22.48252
 Wing Loading for Loiter (LB/FT^2)= 22.39794
 W_S_FOM (LB/FT^2)= 23.62412
 HP_W(HP/LB)= 9.8919459E-02
 AR_FOM= 5.581029
 Em= 15.23061
 W_b (LB/FT)= 159.3171

SCD0 (FT^2)= 4.230752
GFOM= 211.6440
Best_mileage (FT/LB) = 9079.895
Maximum_range (FT)= 1878770.
Maximum_payloadrange (LB-FT)= 6.2129608E+09
Best-range airspeed (FT/SEC) = 208.8468
Minimum_fuelflowrate (LB/HR)= 72.86720
Maximum_endurance (HR) = 2.839623
Fastest_airspeed (FT/SEC) = 364.2686
Minimum_takeoffrun (FT) = 765.4821
Maximum_ceiling (FT) = 33114.87
Steepest_climbangle (DEG)= 2.088120
Maximum_rateofclimb (FPM)= 1913.983
Minimum_time to service ceiling = 9.558348
Minimum_time to 50 FT = 2.6134243E-02
Maximum_loadfactor (g_s)= 2.397124
Fastest_turningrate (DEG/SEC)= 31.33411
Tightest_turn (FT)= 84.56689

APPENDIX C

AGRICULTURAL TERMS

C.1. Agricultural Definitions

The term ‘reduced volume application’ covers ULV (ultra low volume) and VLV (very low volume) pesticide applications. Generally, HV (high volume) is a term which usually indicates that the crop is wetted over most of its surface. MV (medium volume) is a term which usually indicates that a proportion of the crop surface is totally wetted. The term LV (low volume) is also widely used for aerial spraying in the range 5-50 liters/ha. These terms have been defined as follows [6].

Table C.1. Agricultural definitions [6]

Category	Bushes and trees	Ground crops
ULV	< 5	< 5
VLV	> 5 – 200 liters/ha	> 5 – 50 liters/ha
LV	> 200 – 500 liters/ha	> 50 – 200 liters/ha
MV	> 500 – 1000 liters/ha	> 200 – 700 liters/ha
HV	> 1000 liters/ha	> 700 liters/ha

APPENDIX D

COMPETITOR STUDY

D.1. Competitor Study

Starting a new design the information about the aircrafts of the same type that are the competitors are needed. This database at hand is used as an initial point to start the analysis. This study includes a competitor database.

In this research, the aircrafts are agricultural type, single piston propeller engine aircrafts. The existing aircrafts in the world that match these criteria are found in Ref. [4, 38].

The databases for 32 aircrafts from all over the world that match the stated criteria are tabulated in the following pages.

Table D.1. Competitor database

	AT-502B	ZLIN Z 37T AGRO TURBO	PZL Mielec M-15	AEROSTAR AG-6	PZL-106BT TURBO-KRUK	TRANSAVIA SKYFARMER T-300A
MAX.TAKE-OFF WEIGHT [kg]	4309	2260	5750	1500	3500	1925
DIMENSIONS						
GENERAL						
Fuselage frontal area [m ²]	1.646	1.295	1.005	1.604	N/A	N/A
Length overall [m]	9.91	10.46	13.135	7.45	10.24	6.35
Height overall[m]	2.99	3.505	5.339	3.415	3.82	2.79
Fuselage max.width [m]	1.513	1.7	1.272	1.404	N/A	0.97
Fuselage max.height [m]	1.56	1.159	1.78	1.456	N/A	N/A
WING						
Wing Span [m]	15.85	13.63	Up: 22.33 Lower: 16.428	Up: 10.56 Lower: 10.26	15	11.98
Wing Root Chord [m]	1.83	2.39	2.53	1.3	2.16	1.76
Wing Tip Chord [m]	1.83	1.224	1.08	1.3	2.16	1.27
Wing AR	8.7	7	12	8.58	7.1	6.8

Table D.2. Competitor database (continued)

	AT-502B	ZLIN Z 37T AGRO TURBO	PZL Mielec M-15	AEROSTAR AG-6	PZL-106BT TURBO-KRUK	TRANSAVIA SKYFARMER T-300A
Wing Root Incidence [deg]	N/A	3	N/A	N/A	6 ° 6'	upper:3°30' lower:4
Wing Tip Incidence [deg]	N/A	0	N/A	N/A	6 ° 6'	upper:3°30' lower:4
Root Airfoil Profile	N/A	NACA 33015	N/A	N/A	NACA 2415	NACA23012
Tip Airfoil Profile	N/A	NACA 44012	N/A	N/A	NACA 2415	NACA23012
Root t/c Ratio [%]	N/A	15%	N/A	N/A	15%	12%
Tip t/c Ratio [%]	N/A	12%	N/A	N/A	15%	12%
Wing Position [m](from nose of fuselage)	3.2	2.76	4.1	1.82	N/A	N/A
Wing LE Sweep [deg]	0	0	7	0	0	N/A
Wing Sweep at c/4 [deg]	0	0	7	0	6 (SWEEPBACK)	N/A
Wing Dihedral [deg]	4	7	6	N/A	4	1°30'
Wing Area (Gross) [m ²]	28.99	26.69	67.9	26	32.18	27.31
HORIZONTAL TAIL						
Horizontal Tail Span [m]	5.22	5.743	6.36	3.796	5.41	2.13
Horizontal Tail Root Chord [m]	1.01	0.923	1.812	1.144	1.5	N/A

Table D.3. Competitor database (continued)

	AT-502B	ZLIN Z 37T AGRO TURBO	PZL Mielec M-15	AEROSTAR AG-6	PZL-106BT TURBO-KRUK	TRANSAVIA SKYFARMER T-300A
Horizontal Tail Tip Chord [m]	1.01	1.303	1.812	0.572	1.2	N/A
Horizontal Tail AR	5.17	5.16	3.45	4.07	N/A	N/A
Horizontal Tail Incidence [deg]	N/A	N/A	N/A	N/A	N/A	N/A
Horizontal Tail Position [m] (from nose of fuselage)	8.244	8.797	11.325	5.824	N/A	N/A
Horizontal Tail LE Sweep [deg]	0	7	0	5	N/A	N/A
Horizontal Tail Dihedral [deg]	0	N/A	0	0	N/A	N/A
Horizontal Tail Area [m ²]	5.27	6.392	10.0	3.54	5.94	3.9
VERTICAL TAIL						
Vertical tail span[m]	1.328	1.304	3.2	1.82	1.98	N/A
Vertical tail chord tip[m]	0.914	0.76	1.63	0.468	1.2	N/A
Vertical tail chord root[m]	1.832	1.629	1.36	1.872	1.98	N/A
Vertical tail AR	0.969	1.1	2.27	2.12	1.25	N/A
Vertical tail LE sweep[deg]	23	17	15	35	N/A	N/A

Table D.4. Competitor database (continued)

	AT-502B	ZLIN Z 37T AGRO TURBO	PZL Mielec M-15	AEROSTAR AG-6	PZL-106BT TURBO-KRUK	TRANSAVIA SKYFARMER T-300A
Vertical tail area[m ²]	1.82	1.558	4.51	1.56	3.14	N/A
CONTROL SURFACES						
AILERON						
Aileron area (incl.tabs)	2.78	2.428	9.03	1.28(Upper wing))	N/A	1.67
Aileron chord ratio	25.0%	29.0%	25.0%	23.0%	N/A	N/A
Ailerons Locations(n.d. w.r.t.wing)	Chordwise:75%,100%	Chordwise: 71%,100 %	Chordwise: 75 % ,100%	Chordwise: 78.43%,100%	N/A	N/A
(body, wing L.E %0)	Spanwise: 50.3%,89%	Spanwise: 63.5%,100%	Spanwise: 56%,95.7%	Spanwise: 54.41%,91.6%	N/A	N/A
ELEVATOR						
Elevator Area (incl. tabs) [m ²]	2.77	3.008	4.08	1.94	N/A	1.3
Elevator Chord Ratio	%50	Root:44.7% Tip:47.1%	45%	Root:45% Tip:43%	N/A	N/A

Table D.5. Competitor database (continued)

	AT-502B	ZLIN Z 37T AGRO TURBO	PZL Mielec M-15	AEROSTAR AG-6	PZL-106BT TURBO-KRUK	TRANSAVIA SKYFARMER T-300A
RUDDER						
S_r =Rudder Area [m ²] (Including Tabs)	1.3	1.054	4	0.936	N/A	0.56
R_r =Rudder Chord Ratio (c _r /c)	34.10%	Root:56.7% Tip:57.1%	50%	Root:40% Tip:40%	N/A	N/A
Z_r =Rudder Location [-] (fraction of vertical tail span; from top)	0%,100%	0%,100%	13.3%,100%	0%,100%	N/A	N/A
FLAP						
Flap Area(m ²)	One side : 1.16	4.37	4.99	–	1.34(one side)	1.67
Flap Chord Ratio	20.0%	20.5%	23.3%	–	N/A	N/A
Flap Span Ratio	21.0%	27.8%	55.7%	–	N/A	N/A
Flap Locations(n.d. w.r.t.wing)	Chordwise:75%,100%	Chordwise: 79.5%,100%	Chordwise: 76.6%,100%	–	N/A	N/A
(Body,L.E of wing %0)	Spanwise:8.3%,51.9%	Spanwise:0% ,64.3%	Spanwise:0%,56%	–	N/A	N/A

Table D.6. Competitor database (continued)

	AT-502B	ZLIN Z 37T AGRO TURBO	PZL Mielec M-15	AEROSTAR AG-6	PZL-106BT TURBO-KRUK	TRANSAVIA SKYFARMER T-300A
PERFORMANCE						
Vs (kts) & condition (clean, TO, LD)	At 3629 kg flaps up:72	flaps up:48	flaps up:60.5	power off	at SL	flaps up:47/52
	flaps down:59	flaps down :42	Flaps down :48	60	49	flaps down :39/50
TOFL (SL, ISA) (ft)	At AUW of 3629kg,with PT6A - 15AG : 775 ft	870	1247	755	755 (with agricultural equipment)	1080
LFL (SL, ISA) (ft)	N/A	985	624	657	427	270 (LIGHT WEIGHT)
Rate of Climb (AEO) (fpm)	AUW of 4309 kg with PT6A-15AG :760 with PT6A-34AG :925	827	1280 (atS/L)	690 (at S/L)	1180	514 (at S/L)
Service Ceiling(ft)	N/A	N/A	N/A	13425	N/A	12500
Ferry Range (nm)	538	N/A	N/A	280	N/A	N/A
Working Speed(km/h)	193-233	145-165 km/h	86-95 kts	150-175	150-170	N/A
Max.Cruising Speed (km/h)	253	190 (at 500 m)	200	175	N/A	188 (75% power)
T-O Speed	N/A	N/A	N/A	N/A	N/A	N/A
Landing Speed	N/A	N/A	N/A	N/A	N/A	N/A

Table D.7. Competitor database (continued)

	ICA IAR-827A	AERO BOERO 260 Ag	WTA (PIPER)PA-36 NEW BRAVE	SUKHOI Su-38	M-18 DROMADER	M-21 DROMADER
MAX.TAKE-OFF WEIGHT [kg]	2800	1350	Normal:1769 Res:2177	1800	Far23:4200 Cam8:4700	3300
DIMENSIONS						
GENERAL						
Fuselage frontal area	0.973	0.652	1.441	1.164	2.392	N/A
Length overall [m]	8.8	7.3	8.38	7.235	9.47	9.48
Height overall[m]	2.6	2.04	2.29	2.97	3.7	3.11
Fuselage max.width [m]	1.16	0.904	1.092	0.974	1.193	N/A
Fuselage max.height [m]	1.3	0.852	1.29	0.99	1.3	N/A
WING						
Wing Span [m]	14	10.9	11.82	11.345	17.7	10.51
Wing Root Chord [m]	1.92	1.61	2.03	2.055	2.286	N/A
Wing Tip Chord [m]	1.92	1.61	1.75	1.75	2.286	N/A
Wing AR	6.7	6.77	6.7	5.7	7.8	6.5

Table D.8. Competitor database (continued)

	ICA IAR-827A	AERO BOERO 260 Ag	WTA (PIPER)PA-36 NEW BRAVE	SUKHOI Su-38	M-18 DROMADER	M-21 DROMADER
Wing Root Incidence [deg]	N/A	3	2° 30'	2	3	N/A
Wing Tip Incidence [deg]	N/A	0	0° 30'	2	3	N/A
Root Airfoil Profile	NACA 23015	NACA 23012 (MODIFIED)	NACA 63-618	N/A	NACA 4416	NACA 4416
Tip Airfoil Profile	NACA 23015	NACA 23012 (MODIFIED)	NACA 63-618	N/A	NACA 4412	NACA 4412
Root t/c Ratio [%]	15%	12%	18%	N/A	16%	16%
Tip t/c Ratio [%]	15%	12%	18%	N/A	12%	12%
Wing Position [m](from nose of fuselage)	2.23	1.993	1.664	1.962	2.16	N/A
Wing LE Sweep [deg]	0	0	0	0	0	N/A
Wing Sweep at c/4 [deg]	0	0	0	0	0	N/A
Wing Dihedral [deg]	6 (FROM ROOTS)	3 (FROM ROOTS)	6	3	1°25'/ 6 (on outer panels)	N/A
Wing Area (Gross) [m ²]	29.4	17.55	20.96	22.53	40	32.6
HORIZONTAL TAIL						
Horizontal Tail Span [m]	4.52	3.263	4.01	4.773	5.5	5.6
Horizontal Tail Root Chord [m]	1.12	1.145	1.115	1.352	1.31	N/A

Table D.9. Competitor database (continued)

	ICA IAR-827A	AERO BOERO 260 Ag	WTA (PIPER)PA-36 NEW BRAVE	SUKHOI Su-38	M-18 DROMADER	M-21 DROMADER
Horizontal Tail Tip Chord [m]	1.12	0.509	0.776	1.352	1.31	N/A
Horizontal Tail AR	4.03	3.42	7.58	3.53	4.2	N/A
Horizontal Tail Incidence [deg]	N/A	N/A	N/A	N/A	N/A	N/A
Horizontal Tail Position [m] (from nose of fuselage)	7.16	5.215	6.596	5.93	7.83	N/A
Horizontal Tail LE Sweep [deg]	0	8	10	0	0	N/A
Horizontal Tail Dihedral [deg]	0	0	0	0	N/A	N/A
Horizontal Tail Area [m ²]	5.06	3.113	2.11	6.45	7.2	3.86
VERTICAL TAIL						
Vertical tail span[m]	1.26	1.012	1.746	1.663	1.75	N/A
Vertical tail chord tip[m]	0.79	0.509	0.679	0.698	0.74	N/A
Vertical tail chord root[m]	1.8	1.272	2.134	1.657	1.7	N/A
Vertical tail AR	0.96	1.14	1.75	1.41	1.16	N/A
Vertical tail LE sweep[deg]	30	40	50	26	22	N/A

Table D.10. Competitor database (continued)

	ICA IAR-827A	AERO BOERO 260 Ag	WTA (PIPER)PA-36 NEW BRAVE	SUKHOI Su-38	M-18 DROMADER	M-21 DROMADER
Vertical tail area[m ²]	1.65	0.901	1.75	1.958	2.65	N/A
CONTROL SURFACES						
AILERON						
Aileron area (incl.tabs)	1.78	1.172	2.01	2.198	3.84	3.84
Aileron chord ratio	21.3%	15.8%	30.0%	21.8%	27.0%	N/A
Ailerons Locations(n.d. w.r.t.wing)	Chordwise:78.7%, 100%	Chordwise:79.4%, 100%	Chordwise:69.4%, 100%	Chordwise:75.6%, 100%	Chordwise:73%, 100%	N/A
(body, wing L.E %0)	Spanwise:61.8%, 83.6%	Spanwise:%51.2,%94	Spanwise:52.72%, 92.26%	Spanwise:55.2%, 100%	Spanwise:57.8%, 92.4%	N/A
ELEVATOR						
Elevator Area (incl. tabs) [m ²]	2.42	2.064	1.92	4.67	3.914	3.42
Elevator Chord Ratio	47.30%	Root:48.1% Tip:45%	Root:62.5% Tip:50%	Root:42% Tip:100%	%28.4	N/A

Table D.11. Competitor database (continued)

	ICA IAR-827A	AERO BOERO 260 Ag	WTA (PIPER)PA-36 NEW BRAVE	SUKHOI Su-38	M-18 DROMADER	M-21 DROMADER
RUDDER						
S_r =Rudder Area [m ²] (Including Tabs)	0,78	0,44	0,9	1,088	0,9	1,44
R_r =Rudder Chord Ratio (c _r /c)	Root:45% Tip:52%	Root:28.3% Tip:50.1%	60%	Root:44.7% Tip:81.2%	Root:40% Tip:46%	N/A
Z_r =Rudder Location [-] (fraction of vertical tail span; from top)	0%,100%	0%,100%	0%,100%	0%,100%	34.1%,100%	0%,100%
FLAP						
Flap Area(m ²)	1.21	1.574	0.92(one side)	1.030(one side)	5.69	2.78
Flap Chord Ratio	18.3%	%22.4	20.0%	21.8%	%28.5	N/A
Flap Span Ratio	%49.1	40.0%	42.5%	41.8%	%50.5	N/A
Flap Locations(n.d. w.r.t.wing)	Chordwise:82%,100%	Chordwise: 75.8%,100%	Chordwise: 77.8%,100%	Chordwise: 75.6%, 100%	Chordwise: 72%,100%	N/A
(Body,L.E of wing %0)	Spanwise:12.7%,61.8 %	Spanwise:%9.9,%47.6	Spanwise:8.7%,51.75 %	Spanwise:0%, %55.2	Spanwise:%13,%58 .5	N/A

Table D.12. Competitor database (continued)

	ICA IAR-827A	AERO BOERO 260 Ag	WTA (PIPER)PA-36 NEW BRAVE	SUKHOI Su-38	M-18 DROMADER	M-21 DROMADER
PERFORMANCE						
Vs (kts) & condition (clean, TO, LD)	power off	flaps down	flaps up:63	N/A	flaps up:69	flaps up:65
	flaps 10 ⁰ 60	engine idling 46	flaps down :58	N/A	flaps down :59	flaps down :59
TOFL (SL, ISA) (ft)	328	280(TO 15m)	715	395	275m	N/A
LFL (SL, ISA) (ft)	492	270(FROM 15m)	740	920	330	1805
Rate of Climb (AEO) (fpm)	690 (at S/L)	1180 (at S/L)	1051	1180(atS/L)	340 m/min 1115 ft/min	985 (at S/L)
Service Ceiling(ft)	14775	18375	N/A	11800	6500	13125
Ferry Range (nm)	N/A	N/A	465	432	520 km	323 (no reserve)
Working Speed(km/h)	78.97 kts	N/A	N/A	N/A	92-102.5 kts	155 - 180 km / h
Max.Cruising Speed (km/h)	193	N/A	240 (75% power)	220 (at S/L)	190	N/A
T-O Speed	N/A	N/A	N/A	140 km/h	N/A	N/A
Landing Speed	N/A	N/A	N/A	150 km/h	N/A	N/A

Table D.13. Competitor database (continued)

	EMB 202	M-21 DROMADER	PZL - 106B KRUK	FU-24-954	AGRICOPTEROS SCAMP MODEL B
MAX.TAKE-OFF WEIGHT [kg]	1500	3300	3000	2463	428
DIMENSIONS					
GENERAL					
Fuselage frontal area	1.09	N/A	1.014	1.419	N/A
Length overall [m]	7.43	9.48	9.25	9.7	4.37
Height overall[m]	2.2	3.11	3.32	4.158	1.73
Fuselage max.width [m]	0.93	N/A	1.375	1.14	N/A
Fuselage max.height [m]	1.048	N/A	1.24	1.716	N/A
WING					
Wing Span [m]	11.69	10.51	14.9	12.81	5.94
Wing Root Chord [m]	1.71	N/A	1.9	2.13	0.91
Wing Tip Chord [m]	1.71	N/A	1.9	2.13	0.91
Wing AR	6.9	6.5	6.9	6	6.52

Table D.14. Competitor database (continued)

	EMB 202	M-21 DROMADER	PZL - 106B KRUK	FU-24-954	AGRICOPTEROS SCAMP MODEL B
Wing Root Incidence [deg]	3	N/A	6° 6'	2	N/A
Wing Tip Incidence [deg]	3	N/A	6° 6'	2	N/A
Root Airfoil Profile	NACA 23015	NACA 4416	NACA 2415	NACA 4415	NACA 23012
Tip Airfoil Profile	NACA 23015	NACA 4412	NACA 2415	NACA 4415	NACA 23012
Root t/c Ratio [%]	15%	16%	15%	15%	12%
Tip t/c Ratio [%]	15%	12%	15%	15%	12%
Wing Position [m](from nose of fuselage)	2.078	N/A	1.76	2.57	N/A
Wing LE Sweep [deg]	0	N/A	5	0	N/A
Wing Sweep at c/4 [deg]	0	N/A	1	0	N/A
Wing Dihedral [deg]	7	N/A	4	8 (only outhter)	N/A
Wing Area (Gross) [m ²]	19.94	32.6	32.18	27.31	10.82
HORIZONTAL TAIL					
Horizontal Tail Span [m]	3.73	5.6	5.5	4.17	1.98
Horizontal Tail Root Chord [m]	0.88	N/A	1.43	1.02	N/A

Table D.15. Competitor database (continued)

	EMB 202	M-21 DROMADER	PZL - 106B KRUK	FU-24-954	AGRICOPTEROS SCAMP MODEL B
Horizontal Tail Tip Chord [m]	0.88	N/A	1.105	1.02	N/A
Horizontal Tail AR	4.24	N/A	6.8	4.08	N/A
Horizontal Tail Incidence [deg]	N/A	N/A	N/A	N/A	N/A
Horizontal Tail Position [m] (from nose of fuselage)	6.308	N/A	7.345	8.63	N/A
Horizontal Tail LE Sweep [deg]	0	N/A	5	0	N/A
Horizontal Tail Dihedral [deg]	0	N/A	3	0	N/A
Horizontal Tail Area [m ²]	3.17	3.86	4.4	4.25	N/A
VERTICAL TAIL					
Vertical tail span[m]	1.508	N/A	1.325	1.72	N/A
Vertical tail chord tip[m]	0.782	N/A	1.17	0.91	N/A
Vertical tail chord root[m]	1.663	N/A	1.85	1.5	N/A
Vertical tail AR	1.23	N/A	1.61	1.42	N/A
Vertical tail LE sweep[deg]	24	N/A	40	15	N/A

Table D.16. Competitor database (continued)

	EMB 202	M-21 DROMADER	PZL - 106B KRUK	FU-24-954	AGRICOPTEROS SCAMP MODEL B
Vertical tail area[m ²]	1,844	N/A	1,09	2,07	N/A
CONTROL SURFACES					
AILERON					
Aileron area (incl.tabs)	1,222	3,84	2,46	1,82	N/A
Aileron chord ratio	18,7%	N/A	23,0%	19,7%	N/A
Ailerons Locations(n.d. w.r.t.wing)	Chordwise:80%,100%	N/A	Chordwise. 75%,100%	Chordwise: 79%,100%	N/A
(body, wing L.E %0)	Spanwise:58.6%,89.7 %	N/A	Spanwise: 52.8%,95%	Spanwise: 63%,100%	N/A
ELEVATOR					
Elevator Area (incl. tabs) [m ²]	1.681	3.42	4.22	3.08	N/A
Elevator Chord Ratio	%61.1	N/A	Root:0.40% Tip: 0.48%	79%	N/A

Table D.17. Competitor database (continued)

	EMB 202	M-21 DROMADER	PZL - 106B KRUK	FU-24-954	AGRICOPTEROS SCAMP MODEL B
RUDDER					
S_r =Rudder Area [m ²] (Including Tabs)	0.146	1.44	1.62	0.64	N/A
R_r =Rudder Chord Ratio (c_r/c)	Root:38.2% Tip:37.5%	N/A	44%	Root:32% Tip:23%	N/A
Z_r =Rudder Location [-] (fraction of vertical tail span; from top)	0%.100%	0%.100%	0%.100%	0%.100%	N/A
FLAP					
Flap Area(m ²)	2.3	2.78	2.42	3.16	N/A
Flap Chord Ratio	18.7%	N/A	23.0%	15.7%	N/A
Flap Span Ratio	24.8(half wing)%	N/A	50.0%	62.5%	N/A
Flap Locations(n.d. w.r.t.wing)	Chordwise:80%,100%	N/A	Chordwise: 78.12%,100%	Chordwise: 88.8%,100%	N/A
(Body,L.E of wing %0)	Spanwise:0%,58.2%	N/A	Spanwise: 8.29%,50.69%	Spanwise: 0%,62.5%	N/A

Table D.18. Competitor database (continued)

	EMB 202	M-21 DROMADER	PZL - 106B KRUK	FU-24-954	AGRICOPTEROS SCAMP MODEL B
PERFORMANCE					
Vs (kts) & condition (clean, TO, LD)	flaps up:56	flaps up:65	at SL	flaps up:55	43,5
	flaps 30 ⁰ :50	flaps down :59	49	flaps down :49	-
TOFL (SL, ISA) (ft)	655	N/A	656(BR) 394(BS)	N/A	N/A
LFL (SL, ISA) (ft)	505	1805	525 (BR) (BS)	680	500
Rate of Climb (AEO) (fpm)	930	985 (at S/L)	748(BR) 1220(BS) (at S/L)	920 (at S/L)	N/A
Service Ceiling(ft)	11380	13125	N/A	16000	8500(TESTED) 12500(ESTIMATE D)
Ferry Range (nm)	506	323 (no reserve)	540 (BS) 593 (BR)	N/A	N/A
Working Speed(km/h)	N/A	155 - 180 km / h	150-160 km / h (BR) 160 km / h (BS)	212 km/h	N/A
Max.Cruising Speed (km/h)	213	N/A	N/A	209 km/h	140
T-O Speed	N/A	N/A	N/A	N/A	N/A
Landing Speed	N/A	N/A	N/A	N/A	N/A

Figure D.1. Tabulation of agricultural aircraft, [6]

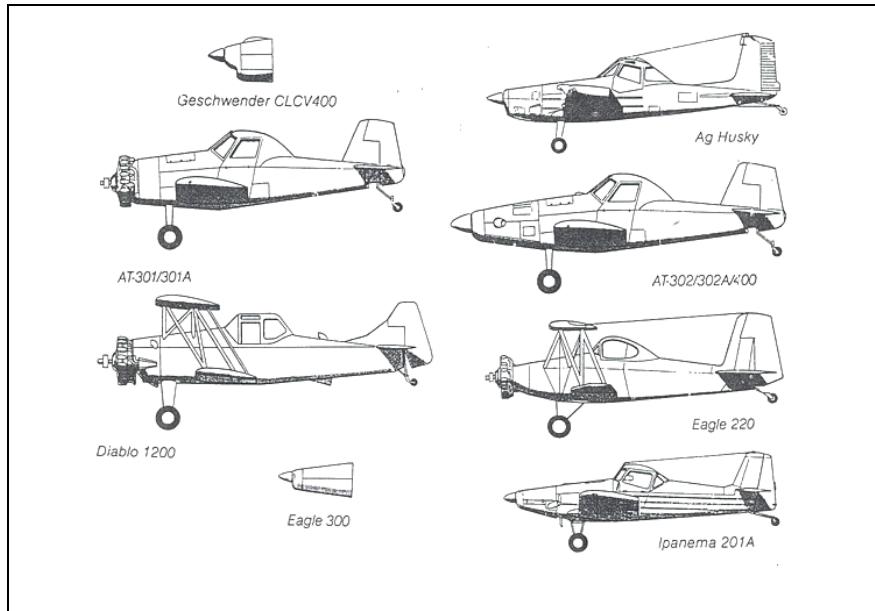


Figure D.2 Tabulation of agricultural aircraft (continued), [6]

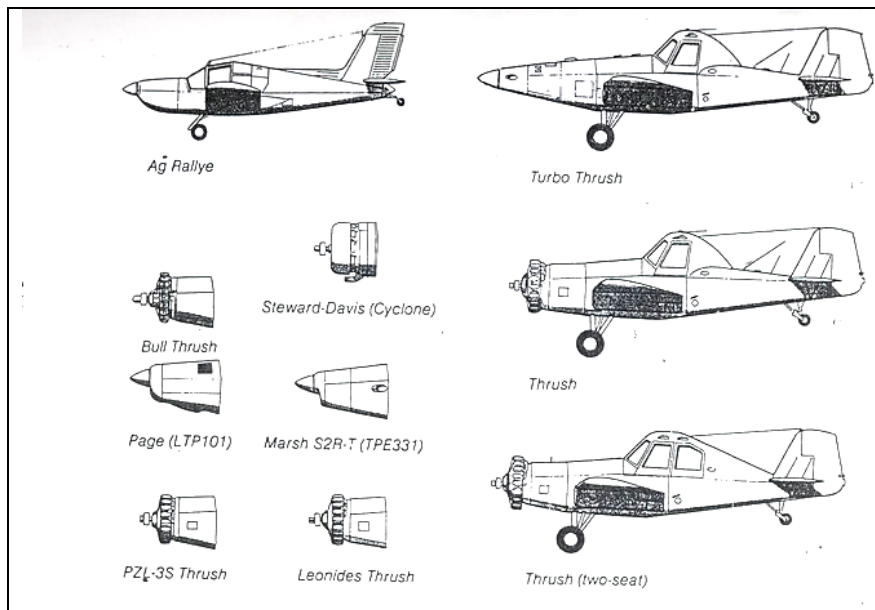


Figure D.3. Tabulation of agricultural aircraft (continued), [6]

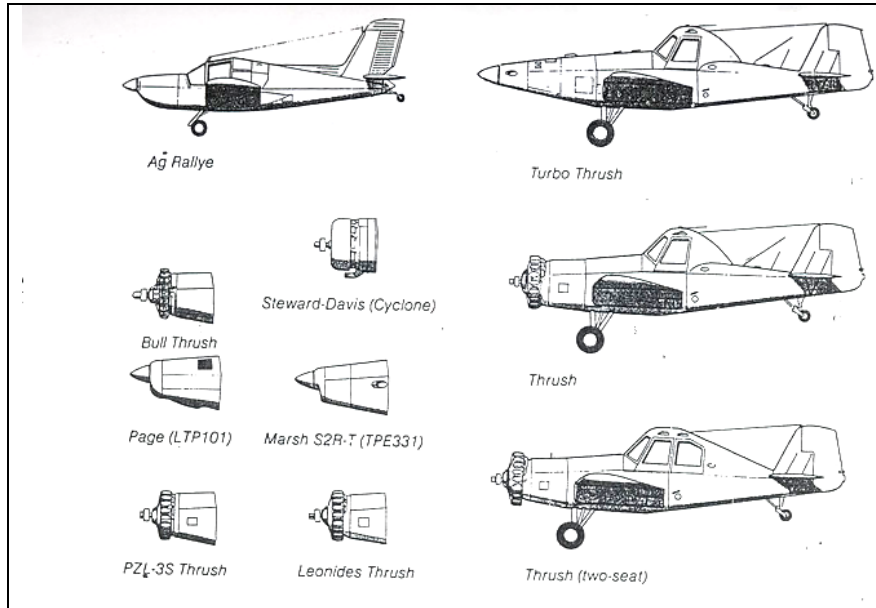


Figure D.4. Tabulation of agricultural aircraft (continued), [6]

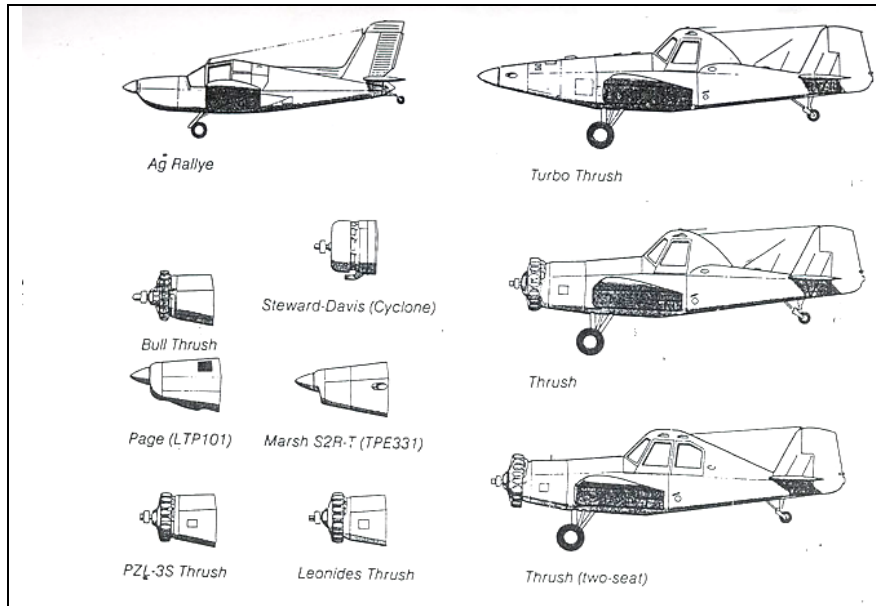


Table D.19. Tabulation of agricultural aircraft, [6]

Type	Manufacturer	Engine	Span	Gross weight	Disposable weight	Hopper capacity	Price
Ag Husky	Cessna Aircraft Wichita, Kansas 67201, U.S.A.	Continental TS10-520T 310 b.h.p. at 2700 r.p.m.	41 ft 8 in 12.7 m	4400 lb 1966 kg	2078 lb 943 kg	280 U.S. gal. 1060 l	\$79 900
Ag Truck	Cessna	Continental IO-520-D 300 b.h.p. at 2850 r.p.m. (take off) 285 b.h.p. at 2700 r.p.m. (max. continuous)	41 ft 8 in 12.7 m	4200 lb 1905 kg	1970 lb 894 kg	280 U.S. gal. 1060 l	\$71 200
AT-301	Air Tractor, P.O. Box 485 Olney, Texas 76374, U.S.A.	Pratt & Whitney R1340, 600 h.p.	45 ft 13.7 m	6900 lb 3130 kg	3250 lb 1473 kg	320 U.S. gal. 1211 l	\$81 500
AT-301A	Air Tractor	Pratt & Whitney R1340, 600 h.p.	45 ft 13.7 m	7300 lb 3311 kg	3450 lb 1565 kg	350 U.S. gal. 1325 l	\$83 500
AT-302	Air Tractor	Avco Lycoming LTP101 600 s.h.p.	45 ft 13.7 m	6600 lb 2994 kg	3350 lb 1522 kg	320 U.S. gal. 1211 l	on request
AT-400	Air Tractor	Pratt & Whitney PT6A-15AG 680 s.h.p.	45 ft 13.7 m	7800 lb 3538 kg	4250 lb 1928 kg	400 U.S. gal. 1514 l	\$187 500
Diablo 1200	Emair, Hangar 38, Industrial Airpark, Harlingen, Texas 78550, U.S.A.	Wright Cyclone R1820 1200 h.p.	41 ft 8 in 12.7 m	8400 lb 3810 kg	4000 lb 1814 kg	475 U.S. gal. 1798 l	on request
Eagle 220	Eagle Aircraft, Box 4127, Boise, Idaho 83704, U.S.A.	Continental W-670-6N 200 h.p.	55 ft 16.8 m	5400 lb 2450 kg	2750 lb 1247 kg	250 U.S. gal. 945 l	\$81 495
Eagle 300	Eagle	Lycoming IO-540-M1B5D 300 h.p.	55 ft 16.8 m	5400 lb 2450 kg	2750 lb 1247 kg	250 U.S. gal. 945 l	\$96 450
Ipanema 201A	Embraer, P.O. Box 343 12,200 Sao José dos Campos, Sao Paulo, Brazil	Avco Lycoming IO-540-K1FSD	38 ft 4 in 11.7 m	3968 lb 1800 kg	1841 lb 835 kg	180 U.S. gal. 680 l	\$91 030

Table D.20. Tabulation of agricultural aircraft, [6]

Type	Manufacturer	Engine	Span	Gross weight	Disposable weight	Hopper capacity	Price
Thrush	Ayres Corporation, P.O. Box 3090, Albany, Georgia 31706, U.S.A.	Pratt & Whitney R1340, 600 h.p.	44 ft 4 in 13.5 m	6900 lb 3130 kg	3200 lb 1450 kg	400 U.S. gal. 1514 l	\$116 500
Turbo Thrush (500 gal)	Ayres	PT6A-34AG 750 h.p. or PT6A-15AG 680 h.p.	44 ft 5 in 13.5 m	8500 lb 3855 kg	4600 lb 2086 kg	500 U.S. gal. 1893 l	\$259 000 \$228 500
Turbo Thrush (400 gal)	Ayres	PT6A-34AG 750 h.p. or PT6A-15AG 680 h.p. or PT6A-11AG 500 h.p.	44 ft 5 in 13.5 m	8200 lb 3719 kg	—	400 U.S. gal. 1514 l	\$251 500 \$221 000 \$209 500
PZL Thrush	Ayres	PZL-3S 600 h.p.	44 ft 4 in 13.5 m	6900 lb 3132 kg	—	400 U.S. gal. 1514 l	\$122 500
Bull Thrush	Ayres	Wright R-1820 1200 h.p.	44 ft 5 in 13.5 m	10000 lb 4536 kg	—	510 U.S. gal. 1930 l	\$145 500
Leo-Thrush	R. W. Harker, 40 Pont St, London S.W.1, U.K.	Alvis Leonides 550 h.p.	44 ft 4 in 13.5 m	6900 lb 3130 kg	3200 lb 1450 kg	400 U.S. gal. 1514 l	\$18 000 (engine)
S2R-T	Marsh Aviation, 5060 East Faldon Drive, Mesa, Arizona 85205, U.S.A.	TPE 331-1-101	44 ft 4 in 13.5 m	9200 lb 4173 kg	—	400/500 U.S. gal. 1515/1893 l	on request
Cyclone	Stewart-Davis, 3200 Cherry Ave., Long Beach, California 90807, U.S.A.	Wright R-1820 1200 h.p.	44 ft 4 in 13.5 m	6903 lb 3130 kg	3200 lb 1450 kg	600 U.S. gal. 2273 l	on request
Page	Page Industries, Box 191, Yukon, Oklahoma 73099, U.S.A.	Avco Lycoming LTP 101, 600 s.h.p.	44 ft 4 in 13.5 m	6900 lb 3130 kg	3200 lb 1450 kg	400 U.S. gal. 1514 l	on request
Ag Rallye	Aérospatiale (Socata) BP38, 65001, Tarbes, France	Avco Lycoming O-540 235 h.p.	31 ft 11 in 9.7 m	2980 lb 1350 kg	1450 lb 655 kg	153 U.S. gal. 579 l	on request

Table D.21. Tabulation of agricultural aircraft, [6]

Type	Manufacturer	Engine	Span	Gross weight	Disposable weight	Hopper capacity	Price
Super Ag-Cat B	Schweiger Aircraft, Box 147, Elmira, NY 14902, U.S.A.	Pratt & Whitney R985 450 s.h.p. or R1340 600 s.h.p.	42 ft 12.9 m	6075 lb 2758 kg	— —	400 U.S. gal. 1514 l	\$121 995
Leo Cat	R.W. Harker, 40 Pont St, London S.W.1, U.K.	Alvis Leonides 550 h.p.	42 ft 3 in 12.9 m	6075 lb 2756 kg	3000 lb 1360 kg	300 U.S. gal. 1136 l	\$18 000 (engine)
Marsh/Gulfstream C164-C-T	Marsh Aviation, 5060 East Faldon Drive, Mesa, Arizona 85205, U.S.A.	Garrett TPE 331-1-101	42 ft 2 in 12.9 m	9000 lb 4082 kg	—	500 U.S. gal. 1892 l	on request
Frakes Turbo	Frakes Aviation, Route 3, Box 229B, Cleburne, Texas 76031, U.S.A.	Pratt & Whitney PT6A-34AG 750 s.h.p. (derated 540 s.h.p.)	42 ft 3 in 12.9 m	8500 lb 3856 kg	5150 lb 2336 kg	500 U.S. gal. 1893 l	on request
Stage II	Stage II, 3013 Airport Avenue, Santa Monica, California 90405, U.S.A.	Liquid cooled V8 450 h.p.	42 ft 3 in 12.9 m	6075 lb 2758 kg	3075 lb 1393 kg	300 U.S. gal. 1136 l	on request
Page	Page Industries, Box 191, Yukon, Oklahoma 73099, U.S.A.	Avco Lycoming LTP 101, 620 s.h.p.	42 ft 3 in 12.9 m	6075 lb 2756 kg	3475 lb 1568 kg	300 U.S. gal. 1136 l	on request
King-Cat	Mid-Continent Aircraft, Hayti, Missouri 63851, U.S.A.	Wright Cyclone R1820, 1200 h.p.	42 ft 3 in 12.9 m	8500 lb 3856 kg	— —	500 U.S. gal. 1893 l	\$152 000
NDN 6 Fieldmaster	NDN Aircraft, Isle of Wight Airport, Sandown, Isle of Wight, U.K.	Pratt & Whitney PT6A-34AG 750 s.h.p.	50 ft 3 in 15.3 m	8500 lb 3856 kg	3500 lb 1588 kg	698 U.S. gal. 2642 l	\$400 000
PL-12 Airtruk	Transavia, 73 Station Road, Seven Hills, NSW 2147, Australia	R-R Continental IO-520-D flat 6	39 ft 4 in 12 m	4090 lb 1855 kg	1850 lb 839 kg	83 Imp gal. 379 l	on request
T-300 Skyfarmer	Transavia	Avco-Lycoming IO-540-K145	39 ft 4 in 12 m	4090 lb 1855 kg	3800 lb 1723 kg	83 Imp gal. 379 l	on request
FU24-954	New Zealand Aerospace, Hamilton Airport, N.Z.	Avco Lycoming IO-720, 400 h.p.	42 ft 12.8 m	5430 lb 2463 kg	2420 lb 1100 kg	276 U.S. gal. 1045 l	on request
Cresco 600	New Zealand Aerospace	Avco Lycoming LTP101, 600 s.h.p.	42 ft 12.8 m	7000 lb 3175 kg	4005 lb 1817 kg	450 U.S. gal. 1705 l	on request

Table D.22. Tabulation of agricultural aircraft, [6]

Type	Manufacturer	Engine	Span	Gross weight	Disposable weight	Hopper capacity	Price
Pawnee D	Piper Aircraft, Lockhaven, Pa 17745, U.S.A.	Avco Lycoming IO-540, 235 h.p.	36 ft 2 in 11 m	2900 lb 1316 kg	1301 lb 544 kg	150 U.S. gal. 572 l	\$53 180
Brave 300	Piper Aircraft	Avco Lycoming IO-540, 300 h.p.	38 ft 10 in 11.8 m	4400 lb 1996 kg	2202 lb 999 kg	225 U.S. gal. 852 l	\$74 740
Brave 375	Piper Aircraft	Avco Lycoming IO-720, 375 h.p.	38 ft 10 in 11.8 m	4800 lb 2177 kg	2335 lb 1059 kg	275 U.S. gal. 1041 l	\$99 860
Kruk	PZL-Warszawa, 02-256 Warsaw-Okecle, Al Krakowska, 100/114, Poland	Pezetel PZL-35 600 h.p.	48 ft 6 in 14.8 m	6614 lb 3000 kg	2205 lb 1000 kg	370 U.S. gal. 1400 l	on request
Turbo Kruk	PZL-Warszawa	PT6A-34AG	48 ft 6 in 14.8 m	6614 lb 3000 kg	2645 lb 1200 kg	370 U.S. gal. 1400 l	on request
M-15	PZL-Mielec ul. Ludowego Polskie- A1-25, go 3, 39-301 Mielec, Poland	Ivchenko	73 ft 6 in 22.4 m	12676 lb 5750 kg	4850 lb 2200 kg	766 U.S. gal. 2900 l	on request
M-18 Dromader	PZL-Mielec	Pezetel ASZ-621R 1000 h.p.	58 ft 1 in 17.7 m	9259 lb 4200 kg	3307 lb 1500 kg	660 U.S. gal. 2500 l	\$145 000
620	Weatherley Aviation, 2304 San Felipe Road, Hollister, Calif. 95023, U.S.A.	Pratt & Whitney R985, 450 h.p.	41 ft 12.5 m	5800 lb 2640 kg	3000 lb 1360 kg	335 U.S. gal. 1270 l	\$74 000
620TP	Weatherley Aviation	PT6A-11AG	41 ft 12.5 m	5800 lb 2640 kg	3000 lb 1360 kg	335 U.S. gal. 1270 l	\$156 000